The Dissertation Committee for Charmaine Yvonne Brown Certifies that this is the approved version of the following dissertation:

THE CELLULAR AND MOLECULAR MECHANISMS UNDERLYING VENTRAL MIDLINE PATTERNING AND MORPHOGENESIS IN THE AMNIOTE MIDBRAIN

Committee:

Seema Agarwala, Supervisor

Johann Eberhart

Lauren Ehrlich

Jeff Gross

Steve Vokes

THE CELLULAR AND MOLECULAR MECHANISMS UNDERLYING VENTRAL MIDLINE PATTERNING AND MORPHOGENESIS IN THE AMNIOTE MIDBRAIN

by

Charmaine Yvonne Brown, B.S.

Dissertation

Presented to the Faculty of the Graduate School of

The University of Texas at Austin

in Partial Fulfillment

of the Requirements

for the Degree of

Doctor of Philosophy

The University of Texas at Austin

August 2015

Dedication

This is dedicated to my parents, Mark and Iris, who have loved and supported me through the ups and downs, and to my grandparents, Chet and Joyce, without whom I wouldn't be where I am today.

THE CELLULAR AND MOLECULAR MECHANISMS UNDERLYING VENTRAL MIDLINE PATTERNING AND MORPHOGENESIS IN THE AMNIOTE MIDBRAIN

Charmaine Yvonne Brown, Ph.D.

The University of Texas at Austin, 2015

Supervisor: Seema Agarwala

The floorplate (FP) is located at the ventral midline of the developing neural tube, and is involved in patterning and specification of ventral and dorsal cell fates. The FP has long been known to pattern ventral cell fates via secretion of Sonic Hedgehog (SHH). However, the mechanism by which the FP is specified is controversial due to species variations where SHH is differentially required for FP specification in fish and mouse. In Chapter 3, we show that, similar to the fish, the amniote anterior neural plate can be divided into medial (MFP) and lateral (LFP) subdivisions which differentially require SHH and FOXA2 for their specification, and that FOXA2, but not SHH, is sufficient to induce the entire midbrain FP pattern. In addition, we show that all three midbrain signaling centers are physically continuous and interconvertible, with their specification depending on SHH.

Prior to the expression of SHH protein, the ventral midline undergoes a morphogenetic event called median hinge point (MHP) formation which buckles the flat neural plate and lifts the neural folds which ultimately fuse into a cylindrical neural tube. Previous studies in the lab have shown that Bone Morphogenetic Proteins (BMP)

modulate HP formation. HP formation involves dynamic cell-shape changes, which result in HP cells becoming wedge-shaped. Multiple mechanisms (constriction of the adherens belt via cytoskeletal and junctional remodeling, and polarized endocytosis) have been proposed to explain this shape change. However, they do not explain how reduction in apical area can be achieved in the amniote neural plate where cells are bipolar and only slender processes contact the apical surface in non-mitotic cells. In Chapter 4, we develop an early electroporation technique which is used in Chapter 5 to visualize HP formation in real time as part of a novel 3D explant system. Our results suggest that BMP attenuation regulates cell cycle progression by increasing the duration of G1 and S phases, and causes a subset of cells to prematurely exit the cell cycle and undergo sub-apical G2-M transition, similar to what is seen in the MHP where there is reduced mitotic index and cells undergo mitosis sub-apically.

Table of Contents

List of Tables xi

List of Figures xii

Chapter 1: Introduction 1

Neurulation 1

HP formation 3

Apical Constriction 3

Interkinetic Nuclear Migration 5

Mitotic Entry 7

BMP signaling 8

BMP Signaling Cascade 9

Floorplate Specification 11

MFP versus LFP specification 12

Chapter 2: Materials and Methods 14

Chick Embryos 14

Egg Windowing 14

In Ovo Electroporation 14

Early Electroporation (HH4-6) 14

Late Electroporation (HH9-10) 16

Constructs 16

Timelapse Experiments 18

Explant 18

Imaging 18

Cell cycle phase calculations 18

Cleavage angle 19

Immunofluorescent Staining 21

Collection and preparation 21

Cryosectioning 22
Immunofluorescent staining 22
Coverslipping 23
Imaging 23
In Situ Hybridization 23
Riboprobes 23
Embryo preparation 24
Hybridization 25
Post-hybridization 25
Color Reaction 25
Second color reaction 25
Quantitative Analysis 26
Mitotic localization 26
Chapter 3: A novel role for FOXA2 and SHH in organizing midbrain signaling centers 27
Introduction 27
Results 31
Differential gene expression in medial and lateral FP 31
SHH is sufficient for LFP, but not MFP induction in the midbrain 34
SHH is necessary for midbrain MFP and LFP specification 37
FOXA2 induces the full midbrain FP program via HH-dependent and independent mechanisms 41
FOXA2, but not SHH, is sufficient for specifying the full spinal FP program 44
SHH and FOXA2 regulate the specification of all midbrain signaling centers 46
The midbrain–hindbrain boundary 46
The roof plate 48
Discussion 50
The role of *FOXA2* and *SHH* in FP specification 50

The role of SHH and FOXA2 in regulating midbrain's signaling centers 55
The midbrain–hindbrain boundary 56
Chapter 4: A simple technique for early in vivo electroporation of E1 chick embryos 58
Introduction.....58
Experimental Procedures and Results.....60
Electrode Assembly 60
In Ovo Electroporation 61
Efficacy of Electroporation.....64
Controlling the Size and Location of the Electroporation 64
Cell Fate Specification Is Not Affected by E1 Electroporations 66
Early Electroporations Do Not Affect Midbrain Size or Morphology 66
Cell Proliferation Is Not Affected by Early Electroporations.....69
Cell Death and Early Electroporations 69
Discussion.....69
Chapter 5: Bone Morphogenetic Proteins (BMPs) regulate neural tube closure by cell cycle dependent mechanisms: a 4D time-lapse analysis.....73
Introduction.....73
Results.....75
WT MHP cells exhibit decreased and sub-apical mitosis.....75
Ectopic hinge points induced by BMP blockade display reduced mitotic index and sub-apical mitosis similar to the endogenous MHP ...76
Explant system allows real time analysis of cell behaviors during MHP formation.....78
BMP signaling alters mitotic localization and cleavage angle, not mitotic duration 81
BMP signaling regulates G1 duration.....84
BMP blockade regulates S phase duration.....86
BMP signaling results in premature exit of G2 in a subset of cells.....86
Discussion.....89

Cell-cell variability 89
Apical constriction versus basal nuclear localization 91
Subapical mitosis may result from regulation of cell polarity 92
Chapter 6: Future Directions 93
Introduction 93
FOXA2-BMP-TGFβ interactions 93
Nuclear versus cytoplasmic role of FOXA2 94
The Cellular basis of HP formation 95
Identification of pSMAD interacting partners 95
Role of nuclear localization in HP formation 96
Cell cycle manipulations 97
Electroporation Alternatives 98
Chapter 7: Conclusions 100
References 102

List of Tables

Table 2.1 Subcloning paradigms for expression vectors 17

Table 3.1 Summary of gene expression patterns identifying the midbrain signaling centers. 33

List of Figures

Figure 1.1 Neural plate bends and fuses to go from a flat sheet to a cylindrical neural tube. 2

Figure 1.2 Neural progenitors undergo interkinetic nuclear migration 6

Figure 1.3 BMP signaling cascade 10

Figure 2.1 Constructs used to define cell cycle phases 20

Figure 3.1 Gene expression patterns distinguish the midbrain MFP and LFP. ..32

Figure 3.2 SHH misexpression is sufficient for LFP, but not MFP induction. ..35

Figure 3.3 SHH is necessary for MFP induction. 39

Figure 3.4 Foxa2 is necessary and sufficient for midbrain FP specification. 42

Figure 3.5 FOXA2 is sufficient for MFP and LFP induction in the spinal cord. 45

Figure 3.6 SHH and FOXA2 regulate the signaling centers of the midbrain. ...47

Figure 3.7 FOXA2 and SHH regulate roof plate specification 49

Figure 3.8 Cartoon summarizing the role of SHH and FOXA2 in patterning the MFP, MHB and RP. 51

Figure 4.1 The experimental setup for early electroporations. 62

Figure 4.2 Early electroporations can be varied in size and location and do not affect cell fate specification 65

Figure 4.3 Early electroporations do not affect the size of the embryo, midbrain size and morphology 67

Figure 4.4 Early electroporations do not affect cell proliferation 68

Figure 4.5 The rate of apoptosis does not differ between control, early and late electroporated midbrains 70

Figure 5.1 BMP blockade mimics MHP behaviors 77

Figure 5.2 3D explant culture paradigm and HP formation in vitro 79
Figure 5.2 3D explant culture paradigm and HP formation in vitro 80
Figure 5.3 BMP signaling regulates mitotic cleavage angle but not mitotic duration 82
Figure 5.3 BMP signaling regulates mitotic cleavage angle but not mitotic duration. 83
Figure 5.4 BMP blockade increases G1 duration. 85
Figure 5.5 BMP blockade increases S phase duration. 87
Figure 5.6 BMP causes a subset of cells to prematurely exit G2 resulting in subapical mitosis. 88
Figure 5.7 BMP blockade induces basal nuclear migration by increasing G1 and S phases. 90

Chapter 1: Introduction

NEURULATION

During neurulation, neurectoderm is initially induced by the node (the primary tissue organizer) as a flat epithelial sheet (Figure 1.1A; Darnell et al., 1999; Streit and Stern, 1999; Streit et al., 1995). This sheet then undergoes several complex shape changes in order to roll up and fuse along the dorsal midline to become a cylindrical neural tube (NT; Portch and Barson, 1974; Schoenwolf and Smith, 1990; Schoenwolf and Franks, 1984; Smith, 1997). The exact shape changes required for NT closure vary along the anterior-posterior axis of the neural tube, however one of the earliest events at all axial levels is the formation of a hinge point at the ventral midline (Schoenwolf and Smith, 1990). This median hinge point (MHP) buckles the neural plate and lifts the lateral neural folds (Figure 1.1B; Schoenwolf and Smith, 1990; Schoenwolf and Franks, 1984). In the chick, MHP formation begins at Hamburger Hamilton (HH) stage 4 and the hinge becomes deeper and more exaggerated through HH7 which brings the neural folds progressively closer (Schoenwolf and Smith, 1990; Schoenwolf and Franks, 1984; Schoenwolf, 1985).

At anterior regions of the neural plate, there is a second hinging event in the lateral neural plate. This hinging occurs in pairs with one on either neural fold and are located at the junction between the neurectoderm and the overlying surface epithelium (Schoenwolf and Smith, 1990; Ybot-Gonzalez et al., 2002). These dorsolateral hinge points (DLHP) pivot the neural folds inward, allowing them to come in close proximity and ultimately fuse (Figure 1.1C-D). At more posterior axial levels (spinal cord), true DLHPs do not form. Instead, the MHP folds the NP in half so the lateral sides of the NP

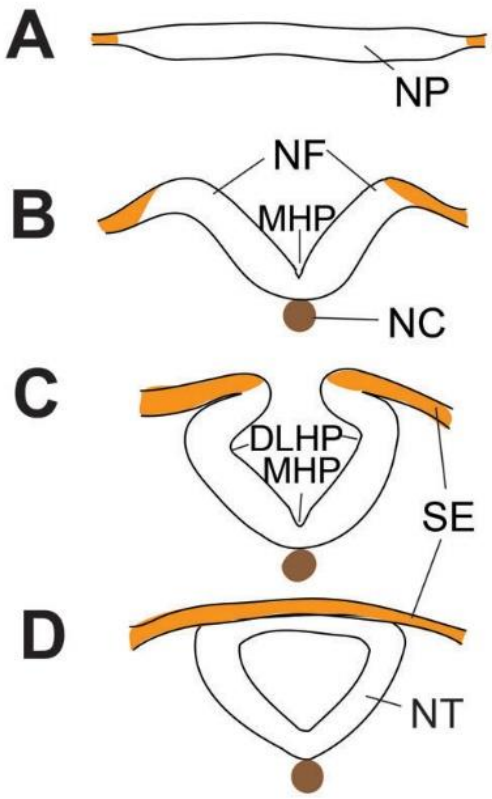

Figure 1.1 Neural plate bends and fuses to go from a flat sheet to a cylindrical neural tube.

A) Neuroepithelium is specified as a flat epithelial sheet. B) Neural plate buckles at the midline to elevate the neural folds. C) A second hinging event in lateral neural plate turns the folds inward where they become apposed. D) The neural folds fuse along the dorsal midline resulting in a continuous neural tube with overlying surface ectoderm (NP: neural plate; NF: neural fold; MHP: median hinge point; NC: notochord; DLHP: dorsolateral hinge point; SE: surface ectoderm; NT: neural tube) (Eom et al., 2013)

are apposed with almost no intervening lumen, permitting fusion to occur across the dorsal midline (Schoenwolf and Smith, 1990). Defects in HP formation or NT fusion lead to NT closure defects which are among the most prevalent birth defects, affecting approximately 1-5/1000 pregnancies (Copp et al., 2003; Grosse et al., 2005). Common neural tube defects include spina bifida (failure of posterior neural tube closure) anencephaly (failure of anterior neural tube closure) and craniorachischisis (failure of both anterior and posterior neural tube closure). These defects can range in severity, however, the anencephaly and craniorachischisis phenotypes are lethal (Copp et al., 2003).

HP FORMATION

Hinge points are formed by the orchestration of polarized cell movements and shape changes, including apical constriction and basal localization of nuclei, which is referred to in classic literature as basal nuclear migration (Colas and Schoenwolf, 2001). Although the gross morphological behaviors associated with hinge point formation are fairly well characterized, the cell and molecular bases of how these behaviors are executed are not well understood.

APICAL CONSTRICTION

Apical constriction is the reduction of apical surface area. The reduction of apical surface with respect to the basal surface results in cell wedging which is thought to be important for hinge point formation (Haigo et al., 2003; Hildebrand, 2005; Nishimura and Takeichi, 2008). There is evidence that this apical constriction is actin cytoskeleton dependent. These studies suggest that Shroom3 (an adherens junction scaffolding protein) recruits Rho kinase (ROCK) to the adherens junctions where it phosphorylates and

activates myosin II and leads to constriction of the adherens belt (Haigo et al., 2003; Hildebrand, 2005; Nishimura and Takeichi, 2008). Another possible mechanism that has recently been proposed is that planar cell polarity (PCP)-dependent junctional remodeling associated with convergent extension results in constriction of the apical surface. This model suggests that as cells undergo convergent extension, they exchange junctional neighbors, and these junctional exchanges result in a reduction of apical surface area (Nishimura et al., 2012). As the tissue undergoes convergent extension, cells move directionally to narrow and lengthen the tissue. This process involves directed cell intercalations. As cells move medially, toward the ventral midline, they intercalate between the cells that occupy that space, leading to a decrease in tissue width and an increasing in tissue length (Copp et al., 2003; Keller, 2002; Wallingford et al., 2002). This cell intercalation results in the reduction and ultimately elimination of previously established cell-cell junctions, which leads to a reduction in the apical surface area of the ventral midline cells (Nishimura et al., 2012).

These models adequately explain the role of apical constriction in forming wedge shaped HP cells in tissues such as the frog neurepithelium which is specified as a cuboidal bilayered epithelium. However, the chick neurepithelium is pseudostratified by HH7 when the MHP is still forming, and cells are bipolar with cell processes that extend to the apical and basal surfaces (Baye and Link, 2007; Sauer, 1935; Sauer and Walker, 1959). These cells undergo interkinetic nuclear migration (IKNM), during which the nucleus moves along the apicobasal axis as it progresses through the cell cycle (Kosodo, 2012; Kosodo and Huttner, 2009; Kosodo et al., 2011; Leung et al., 2011; Sauer, 1935; Schoenwolf and Smith, 1990a; Smith and Schoenwolf, 1987). Mitotic nuclei are localized to the apical surface, while G1, S and G2 phase nuclei are located throughout the

apicobasal thickness of the tissue (Figure 1.2; Baye and Link, 2007; Guthrie et al., 1991). Since the cell body/nucleus is the widest part of the cell, localization of the nucleus away from the apical surface, as a consequence of IKNM, can result in an decrease in apical surface area. Thus, basal nuclear translocation via cell cycle-dependent IKNM has resulted in controversy in the field as to the contribution of apical constriction (via actin based mechanisms) versus basal nuclear localization in hinge point formation because the apical processes of bipolar cells may be so fine that their constriction is unlikely to substantially reduce apical surface area. In this scenario, it is possible that only the constriction of apically localized mitotic cells can contribute to the decrease in apical surface area. Thus, hinge point formation in pseudostratified tissues is likely to occur as a consequence of basal nuclear localization rather than actomyosin constriction.

INTERKINETIC NUCLEAR MIGRATION

As discussed above, progenitor cells of the neuroepithelium are bipolar with a pseudostratified organization which undergo IKNM as they proceed through the cell cycle (Figure 1.2; Baye and Link, 2007; Sauer, 1935; Sauer and Walker, 1959; Smith and Schoenwolf, 1987). Multiple mechanisms for how the nucleus moves during IKNM have been proposed, but it is generally accepted in the field that basal to apical translocation during G2 requires the microtubule-dependent mechanisms (Gambello et al., 2003; Hebbar et al., 2008; Tsai et al., 2005). The minus ends of microtubules attach to the apically localized centrosomes, and evidence suggests that the cell nucleus is moved along these microtubules via dynein motor proteins (Cappello et al., 2011; Kosodo, 2012; Norden et al., 2009; Tsai et al., 2005). Lis1 and NudC, members of the dynein motor complex, are required for the G2 movement of the nucleus to the apical surface for mitosis. Disruption of Lis1 has been shown to inhibit this apical migration and results in

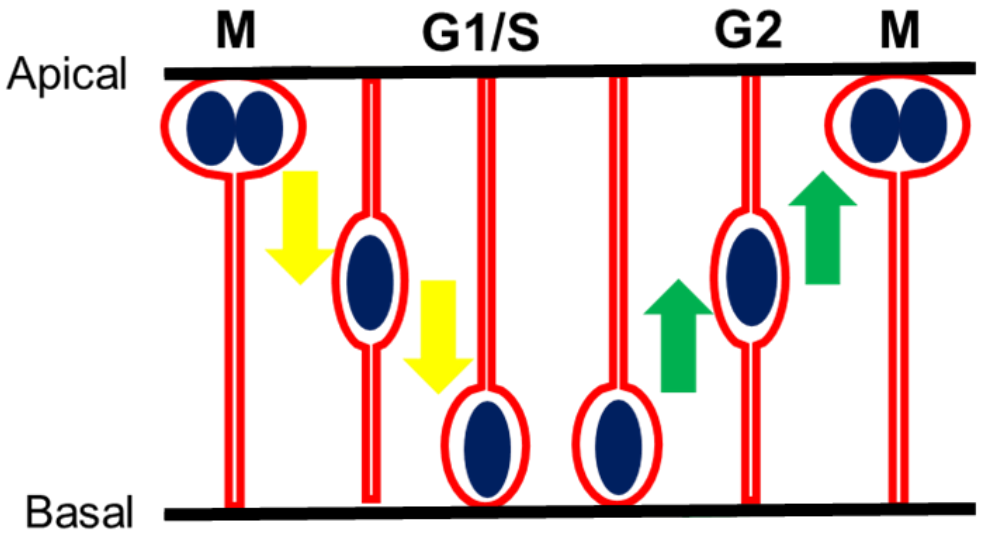

Figure 1.2 Neural progenitors undergo interkinetic nuclear migration

Mitosis (M) occurs at the apical surface. The nucleus then moves basally in G1 phase before returning to the apical surface during G2 where the cell rounds for mitosis.

nuclei being basally localized (Assadi et al., 2003; Cappello et al., 2011; Faulkner et al., 2000; Gambello et al., 2003; Hebbar et al., 2008; Smith et al., 2000; Tsai et al., 2005).

Although there is significant evidence suggesting that microtubule-based dynein motors move the nucleus to the apical surface, the mechanism by which the nucleus moves basally is a bit more controversial (Baye and Link, 2008; Kosodo, 2012; Kosodo et al., 2011; Tsai et al., 2010). Some evidence in the rat brain suggests that apical to basal migration is mediated by an unconventional kinesin motor protein called KIF1a (Tsai et al., 2010). Similar to dynein, kinesins are motor proteins that move cargo along mictrotubules (Hirokawa et al., 2010). Knockdown of KIF1a via siRNA results in the inhibition of basal migration and a resulting apical localization of nuclei (Tsai et al., 2010).

Another proposed mechanism of apical to basal nuclear translocation is stochastic movement (Kosodo et al., 2011; Leung et al., 2011). This model suggests that while the basal to apical nuclear movement is achieved via active cytoskeletal mechanisms, the post-mitotic apical to basal movement is achieved via passive displacements due to mitotic nuclear crowding at the apical surface. As cells move apically, there simply isn't enough space for all of the nuclei. Therefore, the cells which have already completed mitosis are pushed basally to make room (Kosodo et al., 2011; Leung et al., 2011).

MITOTIC ENTRY

Centrosomes are located at the apical surface where they anchor the cilium, and it has long been known that the centrosomes are critical for mitotic entry (Dubreuil et al., 2007; Hinds and Ruffett, 1971; Smart, 1972). A cascade of proteins which are localized at the centrosome trigger mitosis by activating the cyclin B/CDK1 complex, and it was therefore presumed that the centrosomes trigger mitosis once the nuclei reach the apical

surface (Hirota et al., 2003; Jackman et al., 2003). However, evidence suggests that cells may enter prophase prior to arriving at the apical surface (Hinds and Ruffett, 1971; Sauer, 1936). Recent studies have shown that the centrosomes actually leave the apical surface prior to the nucleus arriving. The centrosomes dissociate from the cilium and migrate basally to meet the nucleus during late G2. Once the centrosomes contact the nucleus, the nuclear envelope begins to breakdown and the cell enters mitosis (Cappello et al., 2006; Imai et al., 2006; Spear and Erickson, 2012).

Since centrosomal/nuclear membrae interaction initiates mitosis, studies have shown that mislocalization of centrosomes results in subapical mitosis. One mechanism by which centrosomes may be mislocalized is via downregulation of apical junctional polarity proteins and a resulting displacement of centrosomes from the apical surface (Imai et al., 2006; Liu et al., 2010; Tamai et al., 2007). When the centrosome arrives at the nucleus, the nuclear envelope begins to breakdown and the cell proceeds into mitosis subapically (Cappello et al., 2006; Imai et al., 2006).

BMP SIGNALING

Bone Morphogenetic Proteins (BMP) signaling is involved in a variety of developmental processes, including the HP formation (Burstyn-Cohen et al., 2004; Eom et al., 2011, 2012; Oshimori and Fuchs, 2012; Postigo, 2003). Recent studies in the lab have shown that HP formation is mediated by BMP signaling, with BMP blockade inducing ectopic hinge points and exaggerating the MHP and BMP overexpression resulting in flattening of the MHP (Eom et al., 2011, 2012).

BMP signaling is regulated along the mediolateral axis of the neural plate where there is low BMP signaling in the MHP and increasing amounts of BMP signaling in more lateral tissues (Eom et al., 2011, 2012). However, interestingly, BMP signaling is

modulated in a cell cycle dependent manner. Mitotic cells exhibit high levels of BMP signaling (as evidenced by high pSMAD1,5,8) while cells in other phases of the cell cycle have relatively low BMP signaling activation by comparison (Eom et al., 2011, 2012). In addition, BMP signaling has also been shown to regulate cell cycle kinetics. For example, BMP blockade in neural crest cells has been shown to block the G1 to S transition (Burstyn-Cohen and Kalcheim, 2002; Burstyn-Cohen et al., 2004). In addition, BMP misexpression has been shown to decrease the number of BrdU+ nuclei after pulse labeling (Ille et al., 2007). This lends support to our hypothesis that BMP signaling may regulate cell cycle progression in the neural plate and thereby induce basal nuclear migration via the resulting shift in IKNM.

BMP SIGNALING CASCADE

Canonical BMP signaling initiates with the binding of BMP ligand to type II transmembrane seronine threonine kinase receptors (BMPRIIB, ACTRIIA and ACTRIIB). The type II receptor then forms a heterodimer and phosphorylates type I receptors (ALK2, BMPR1A and BMPR1B). Upon activation, type I receptors phosphorylate downstream receptor Smads (Smad 1, 5, or 8) which then bind to Smad 4. This pSmad1,5,8-Smad4 complex translocates into the nucleus to regulate gene transcription (Figure 1.3; Liu and Niswander, 2005).

BMP signaling can be negatively regulated by multiple mechanisms. The first is via extracellular antagonists. Noggin, Chordin and Follistatin, known BMP antagonists, bind to the BMP ligand and inhibit its ability to interact with the BMP receptors, thus effectively inhibiting BMP signaling (Figure 1.3; Nakamura et al., 1990). Another mechanism of BMP regulation is via inhibitory Smads (Smad6). Smad6 is able to inhibit the phosphorylation of Smad 1,5,8 thereby preventing their interaction with Smad4,

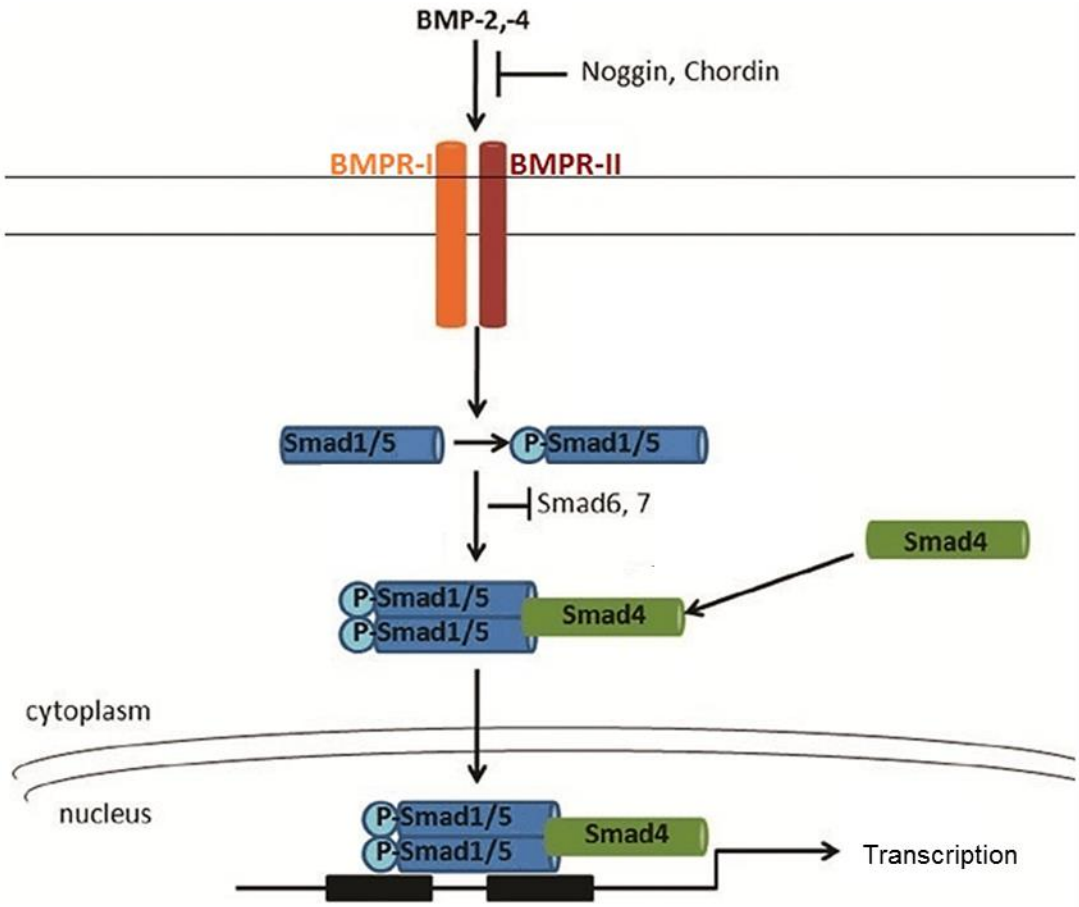

Figure 1.3 BMP signaling cascade

BMP ligands bind to type II BMP receptor which phosphorylates and forms a heterodimer with type I receptors which leads to phosphorylation of receptor Smads (Smad 1,5,8). Activated receptor Smads bind to Smad4 and enter the nucleus to regulate transcription. The BMP signaling pathway can be regulated by extracellular molecules (Noggin, Chordin) or downstream by Smad 6,7. Adapted from Vrijens et al., 2013.

which, in turn, inhibits nuclear translocation and the resulting transcriptional regulation (Figure 1.4; Imamura et al., 1997).

FLOORPLATE SPECIFICATION

As discussed above, the ventral midline of the neural plate is important for the morphogenetic shaping of the neural tube. However this area is also the site of the floorplate (FP) which is a secondary organizer and plays a critical role in NT patterning. The midbrain has 3 main signaling centers which are involved in patterning and morphogenesis of the midbrain; FP, roof plate (RP) and midbrain hindbrain boundary (MHB). The Sonic Hedgehog (SHH) secreting FP is known to be involved in the specification of ventral cell fates (Kingsbury, 1920; Placzek and Briscoe, 2005; Strähle et al., 2004). However, there is controversy in the field as to the extent to which SHH is involved in FP specification. This is, in large part, due to complications caused by species variations (Placzek and Briscoe, 2005). The classic model for FP specification in the amniote involves SHH secretion from the notochord, which activates effectors in the overlying neurectoderm and auto-induces SHH expression in the presumptive FP (Dodd, 1998). This model is supported by notochord transplant experiments which show that the notochord is sufficient to induce FP in naïve neurectoderm. In addition, mutant mouse studies utilizing mice which lack functional SHH, GLI2 or SMO (SHH signaling components) showed that without SHH signaling, FP is not specified. Conversely, when patched1 (a negative SHH regulator) is mutated, there is a significant enlargement of the FP (Ang and Rossant, 1994; Bai et al., 2004; Chiang et al., 1996; Goodrich, 1997; Matise et al., 1998; Weinstein et al., 1994; Wijgerde et al., 2002).

MFP VERSUS LFP SPECIFICATION

In zebrafish, FP has been subdivided into medial (MFP) and lateral (LFP) subdivisions. SHH pathway mutants in zebrafish provide evidence that SHH is only required in the LFP and is not required for the specification or maintenance of MFP (Schauerte et al., 1998). However, mutants in the Nodal pathway suggest that MFP induction is Nodal dependent (Odenthal et al., 2000; Strähle et al., 1996). Interestingly, the lack of MFP phenotype in the Nodal mutants can be rescued by FOXA2, a winged/helix transcription factor, which is a target of Nodal signaling and activates SHH signaling (Norton et al., 2005; Rastegar et al., 2002; Strahle et al., 1993). Therefore, this suggests a model where Nodal signaling activates FOXA2 in the MFP, which in turn induces SHH signaling and specifies LFP.

Evidence in the chick suggests that FP in the amniote may also be partitioned into MFP and LFP subdivision based on cell type, gene expression patterns. Studies have shown that a portion of the FP is composed of cells that have migrated from the node or area a (the region anterior to the node). These cells have been shown to exclusively colonize the medial portion of the FP, suggesting that this area may be unique from the rest of the FP (Charrier et al., 2002; Schoenwolf and Sheard, 1990). In addition, the chick spinal cord shows MFP and LFP subdivisions based on gene expression. For example, a MFP region expresses *SHH* and *FOXA2*, but lacks *SOX1* expression. Conversely, there is a LFP region that shows *SHH*, *SOX1* and *NKX2.2* expression (Charrier et al., 2002). In this model system, SHH misexpression has been shown to be insufficient to induce MFP (Catala et al., 2000; Charrier et al., 2002). However, notochord transplant experiments are sufficient to induce the entire FP program. This suggests that there are other notochord

derived factors besides SHH that specify MFP (Catala et al., 2000; Charrier et al., 2002; Gray and Dale, 2010).

One possible factor could be the FOXA2 which is known to upregulate SHH and has been shown to be capable of inducing MFP in the fish (Rastegar et al., 2002; Strahle et al., 1993). However, FOXA2 has been shown to be induced by SHH as well as the ability to induce SHH. Due to the reciprocal nature of this interaction, it is difficult to determine the distinct functions of these molecules (Altaba et al., 1995). Although most FP studies in the chick have been performed in the spinal cord, examination of SHH and FOXA2 in the midbrain indicated that these proteins do indeed reciprocally induce one another, and they are expressed in overlapping, though not identical patterns (Agarwala et al., 2001; Altaba et al., 1995). The potential partition of MFP and LFP in the anterior NT and the roles of SHH and FOXA2 in the specification of these FP subdivisions are explained in Chapter 3.

Chapter 2: Materials and Methods

CHICK EMBRYOS

Fertilized leghorn (*Gallus gallus)* eggs (Ideal Poultry, TX; Texas A&M University, Department of Poultry Science, TX) were incubated in a forced draught humidified chamber (G.Q.F. Mfg. Co.) at 38°C until the desired stage was reached. Embryos were staged according to the criteria defined by Hamburger and Hamilton (Hamburger and Hamilton, 1951).

EGG WINDOWING

Eggs were windowed to facilitate electroporation procedures by creating working distance between the embryo, which localizes to the top of the yolk, and the overlying shell. Eggs were incubated on their sides (on the long axis of the egg), and a scalpel was used to drill two small holes in the shell; one on the top and one on the small side of the egg. 2-2.5mL of albumin was removed from the lateral hole with a 10mL syringe fitted with an 18 gauge needle. Eggs were then re-sealed with polyethylene or standard packaging tape (3M, TX). Eggs were either windowed 4-5 hours after the start of incubation or just before electroporation for early electroporations, and windowed 1 day prior to use (at E1) for late electroporations.

IN OVO ELECTROPORATION

Early Electroporation (HH4-6)

In ovo electroporations were performed at HH4-6 according to published protocols (Brown et al., 2012a, 2012b). Specifically, the egg was cut open with scissors and 2-3 drops of Ringer's solution was placed on top of the embryo to help prevent the embryo from drying out during the procedure. Then, approximately 20µL of 1% India ink

(Pelikan, Hamburg, Germany) in Ringer's solution was injected underneath the embryo using a 1mL syringe fitted with a 30-gauge needle which was bent at a 130˚ angle. This allowed for greater contrast and visualization of the embryo. Those embryos that appeared abnormal in any way were discarded at this stage. Those embryos that appeared normal were re-irrigated with 10 drops of Ringer's solution. This provides sufficient liquid to ensure good electrical conduction in subsequent electroporation steps. Next, forceps were used to make a small incision in the vitelline membrane to allow access to the embryo. It is important that this incision was made in the area opaca so as not to injure the underlying embryo. The plasmid DNA of interest was injected through this incision.

Plasmid DNA was isolated via maxi prep DNA isolation kit (Origene Technologies, Inc, MD) and resuspended in double distilled water. Plasmid DNA of the appropriate volume was mixed with 0.1% Fast Green (Sigma, MO) and double distilled water to reach the appropriate concentration required or each construct (1-5µg/µl). The addition of Fast Green allowed the DNA to be easily visible during injection. The DNA solution was front-loaded into a pulled glass capillary tube (Sigma, MO) using a picospritzer (WPI Instruments, FL). Front-filling requires the solution to pass through the small opening at the tip of the glass pipe which helps to eliminate large particles and contaminants which are not able to pass through the small opening. The glass pipet was slipped through the incision in the vitelline membrane and into the space between the membrane and the embryo. The picospritzer was used to inject an amount of DNA (50-300 nl) sufficient to cover the entire area of interest (presumptive midbrain) into the space overlying this area.

Working quickly so that the DNA did not diffuse, the positive electrode was inserted through the area opaca via the vitelline membrane incision and the tip of the electrode was placed underneath the presumptive midbrain while the rest of the electrode curved down, away from the embryo. The negative electrode was positioned directly above the presumptive midbrain with the <1mm of the tip inserted into the Ringer's solution overlying the embryo. It is specifically important to ensure that the electrodes do not touch one another or touch the embryo as this will cause tissue damage and likely embryo death. Once the electrodes are in position, a series of electrical pulses were applied via an ECM 830 Electro Square Porator (BTX Genetronic) under the following parameters: 5 Volts, 3 pulses, 50ms pulse length, 100ms intervals. The hole in the egg was then taped closed with electrical tape.

Late Electroporation (HH9-10)

Eggs were opened and India ink was injected as described above. Those embryos at appeared morphologically normal were irrigated with an additional 5 drops of Ringer's solution. Then forceps were used to remove the vitelline membrane from the region of interest (the midbrain). DNA was prepared as described above and injected into the lumen of the midbrain. The negative electrode was then inserted so that the tip of the electrode was in the middle of the lumen. The positive electrode was placed outside the embryo, approximately 100μm away from the negative electrode. Exact electrode placement was altered based on the intended location and breadth of the electroporation.

Constructs

Expression vectors were subcloned via standard techniques (Table 2.1)

Vector Name	Backbone Vector	Vector Cuts	Starting Insert Vector	Insert Cuts	Ligation Type
Efx-IRES-RFP	Efx-IRES-EGFP	MscI NotI	Efx-dsRed	EcoRV	Blunt
Efx-IRES-mRFP	Efx-IRES-EGFP	MscI NotI	Efx-mRFP	EcoRV	Blunt
Efx-IRES-mGFP	Efx-IRES-EGFP	MscI NotI	Efx-mGFP	EcoRV	Blunt
Efx-Noggin-IRES-mRFP	Efx-IRES-mRFP	EcoRI	Efx-mRFP	EcoRI	Sticky
Efx-Noggin-IRES-mGFP	Efx-IRES-mGFP	EcoRI	Efx-mGFP	EcoRI	Sticky

Table 2.1 Subcloning paradigms for expression vectors

TIMELAPSE EXPERIMENTS

Explant

Embryos were electroporated at HH5-7 and explanted at HH9-11. All steps were performed on ice. Embryos were collected in Ringer's solution and sagittal cuts were made in the midbrain and posterior to the MHB to remove the midbrain while leaving the RP, FP and MHB signaling centers intact. Midbrain explants were placed in Leibovitz L-15 media (Life Technologies) with 10% FBS, PenStrep and Fungizone until ready to be placed in agarose. Explants were not kept in L-15 media for longer than 10min.

Once several explants were extracted, they were transferred to 1% low melting point agarose in Neurobasal (NB; Life Technologies) held at 39˚C. Agarose plus explants were kept at 39˚C for 2-3 min to allow agarose to penetrate into the lumen of the explant. Explants were then transferred into a 35mm glass bottom culture dish and oriented with midbrain pressed against the glass. The culture dish was placed on ice for 10min to allow agarose to solidify. Then NB was added to cover the agarose and explants and incubated at 37˚C with 5% CO2 for at least 2 hours prior to imaging.

Imaging

Timelapse images were taken on an Olympus IX51 spinning disc confocal microscope and captured with Slide Book Pro. Images were taken with a 40X or 60X objective and taken at 2 min or 10min intervals. Microscope was equipped with an environmental chamber set to 37˚C and 5% CO2. Each z-plane was 1μm in thickness.

Cell cycle phase calculations

To determine the duration of mitosis, cells were electroporated with mGFP or Noggin along with Importin-RFP (Figure 2.1A-A''). Images were taken at 2 min

intervals. Mitosis was said to have begun when Importin-RFP is no longer visible, indicating nuclear envelope break down (Figure 2.1A''), and end when two daughter cells (separated by mGFP-labeled membrane) are visible and the Importin-RFP labeled nuclear envelope begins to reform, indicating cytokinesis has occurred.

To determine the duration of G1, cells were electroporated with mRFP or Noggin along with PCNA-GFP (Figure 2.1B-B'''). The start of G1 was defined as the first visualization of PCNA-GFP after cytokinesis (Figure 2.1B) and the end of G1 was considered the visualization of PCNA-GFP puncta, which indicates the beginning of S phase (Figure 2.1B'; Leonhardt, 2000; Leung et al., 2011).

To determine the duration of S phase, cells were electroporated with mRFP or Noggin along with PCNA-GFP to visualize S phase. S phase was considered to start when PCNA-GFP puncta become visible (Figure 2.1B') and end when puncta are no longer present (Figure 2.1B'"; Leonhardt, 2000; Leung et al., 2011).

To determine the duration of G1 phase, cells were electroporated with mRFP or Noggin along with PCNA-GFP. G2 was considered to start when PCNA-GFP puncta were no longer visible (Figure 2.1B''') and end when PCNA-GFP expression disappeared and the cell rounded for mitosis (Leonhardt, 2000; Leung et al., 2011).

Cleavage angle

Cleavage angle in WT HH4-7 neural plates were determined in static images where mitotic nuclei were immunostained with PHH3 and nuclei were counterstained with DAPI. Cleavage angle was only measured in mitotic cells where the chromatids had separated and a clear demarcation between the newly forming daughter nuclei could be determined. In these cells, a line was drawn tangent to the the apical surface, and a

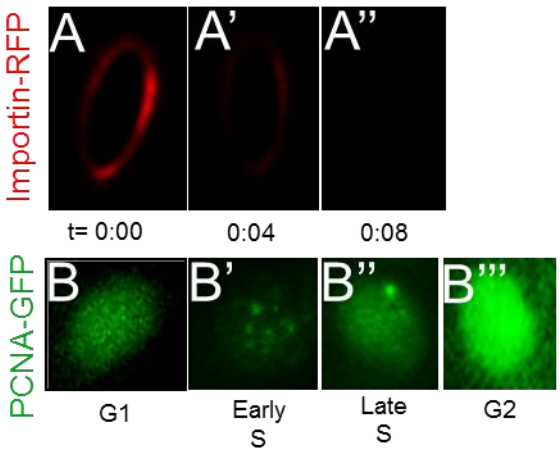

Figure 2.1 Constructs used to define cell cycle phases

A-A'') The Importin-RFP labeled nuclear envelope breaks down as the cell enters mitosis. B-B''') PCNA-GFP was used to define G1/S/G2 transitions. The PCNA is destribued throughout the nucleus is G1 (B), becomes punctate in S (B'), the puncta become larger and fewer in late S (B'') and returns to being distributed throughout in G2 (B''').

second line was drawn along the cleavage plane The angle of intersection of these two lines were used to represent cleavage angle.

Cleavage angle in control and Noggin electroporated tissues was determined in timelapse. At the beginning of cytokinesis (the first time point where membrane could be seen between the forming daughter nuclei) a line was drawn along the apical surface, and a second line was drawn along the cleavage plane. The angle of intersection of these two lines were used to represent cleavage angle.

IMMUNOFLUORESCENT STAINING

Collection and preparation

Embryos were collected in PBS and fixed on ice in 4% PFA for 15min to 1hr, depending on the age of the embryo. After fixation, the embryos were placed in 30% sucrose in PBS and agitated on a rocker until the tissue sunk to the bottom of the vial (approximately 30min to 1hr). If embryos had been previously electroporated, they were screened for fluorescence at this stage, and only those which had been electroporated in the proper area were kept. Those embryos which were kept, were then trimmed at the forebrain and hindbrain, leaving only the midbrain. Forceps or a plastic transfer pipet (Sarstedt) were used to move the tissue into an EM mold (VWR) filled approximately 8mm high with OCT (VWR). Tissue was swirled to help dissipate any remaining sucrose PBS solution and allowed to equilibrate in the OCT for 5-10min. Tissue was then positioned in the center of the mold with dorsal side up and anterior and posterior labeled on the mold. Once the embryo was properly positioned, the EM mold was frozen in a dry ice, ethanol slurry. The frozen blocks were then stored at -80^{o}C until sectioned.

Cryosectioning

Frozen blocks were removed from the EM molds and trimmed around the embedded tissue. The trimmed block was then mounted onto a cryostat stage using OCT with anterior facing up (away from the stage). Sections were taken at 14μm and mounted onto charged glass slides (Superfrost) Slides were then placed in slide mailers at -20^{o}C or -80^{o}C for storage.

Immunofluorescent staining

All wash steps consisted of adding solution to a slide mailer and placing the mailer upright on a rocker for the duration of the wash. Slides were washed three times for 10min each in 3% PBSTx (Triton X-100 (Sigma, MO) in 1X PBS). Slides were then outlined with a PAP pen (RPI) and covered with blocking solution. Blocking solution is made of 5% Goat Serum) and 2% BSA) in PBSTx. Slides were blocked for 1hr at room temperature or overnight at 4°C. After blocking, the slides were incubated in primary antibody solution. Antibodies were diluted 1:50 to 1:1000 in half concentrated blocking solution and slides were incubated for 1hr at room temperature or overnight at 4°C.

Following primary antibody incubation, slides were washed 3 times for 10min in PBSTx and then incubated in secondary antibody solution. This and all subsequent steps were performed in foil wrapped mailers and incubation boxes to reduce exposure to light. Alexa conjugated secondary antibodies were diluted 1:250 in half concentrated blocking solution. Slides were incubated in a humidified chamber for 1hr. After secondary incubation, slides were washed 2 times for 10 min each in PBSTx then in 1:20,000 DAPI (in PBSTx for 10min followed by 3 additional 10 min washes in PBSTx.

Coverslipping

After immunofluorescent staining, approximately 20µl of Pro-long Gold (Invitrogen) mounting media was added to each slide. A coverslip was then carefully placed on each slide, avoiding air bubbles. The slides were allowed to dry for 5-10min, then nail polish was used to seal the edges of the coverslip. Slides were allowed to dry for 15 min and were then were directly imaged or placed in -20°C for storage.

Imaging

Immunofluorescent images were taken on an Olympus IX51 spinning disc confocal microscope and captured with Slide Book Pro. Images were taken with 10X, 20X, 40X, 60X and 100X objective lenses.

IN SITU HYBRIDIZATION

Embryos were collected in PBS and fixed in 4% PFA at 4°C overnight or up to one week. DIG or FL conjugated riboprobes were made from chick cDNA for each of the genes of interest. One and two color wholemount in situ hybridizations were conducted according to established protocols (Agarwala et al., 2001).

Riboprobes

20ug of template DNA plasmid were digested with the appropriate restriction enzyme overnight and spiked with additional enzyme for 1hour before proceeding. Cut plasmid was phenol chloroform extracted and resuspended in 20ul of DEPC-H_2O. Templates were either used promptly or stored at -20˚C.

The prepared templates were used to make DIG or Fl labeled riboprobes according to the following recipe:

4ul 5X transcription buffer (Promega)

2ul 100mM DTT

1ul RNase Inhibitor (Pharmacia)

2ul 10X nucleotide mix (DIG or Fluorscein labelled)

2ul appropriate RNA polymerase (T3, T7 or Sp6)

1ug of template DNA

? ul of DEPC-H_2O to equal 20ul total volume

Reaction mixture was incubated at 37˚C for 2hrs and then DNA was removed with 2.5ul DNase for 30min.

DIG labeled probes were precipitated with 4M LiCl in EtOH for 20min at -20˚C, then washed in 70% EtOH and resuspended in 100ul DEPC-H_2O. FL labeled probes were precipitated with 7.8M NH_4Acetate in Isopropanol for 20min at -20˚C, then washed in 70% isopropanol and resuspended in 20ul DEPC-H_2O. A second round of precipitation was performed and then the pellet was resuspended in 100ul DEPC-H_2O. Probes were stored at -20˚C until use.

Embryo preparation

Embryos were collected in PBS and fixed in 4% PFA at 4°C overnight or up to one week. Further dissection (if necessary) as performed on day 2. Embryos were dehydrated in 10min serial Methanol PBS-Tween20 (Sigma) washes and stored at -20˚C overnight. The embryos were then re-hydrated in 10min serial methanol-PBS-Tween20 washes. After rehydration, the embryos were bleached in 6% hydrogen peroxide-PBS-Tween20 for 60min. The peroxide was removed by 2 PBS-Tween20 washes and then embryos were washed in detergent mix for a total 90min. Embryos were post-fixed in 0.2% gluteraldehyde, 1% Tween20 in 4% PFA for 20min. Post-fix was removed in PBS-

Tween20 washes, then embryos were placed in 5ml pre-hybridization solution and stored at -20˚C until use.

Hybridization

Embryos in pre-hybridization solution were heated at 72˚C for 1hr before adding 0.5-2ug of riboprobe, then incubated overnight for hybridization to occur.

Post-hybridization

Following hybridization, embryos were washed 4 times in pre-heated Solution X (50% formamide, 2XSSC, 1%SDS in H_2O) for a total of 3hrs then switched to TBST (1X TBS, 1% Tween20). After several TBST washes, embryos were incubated in TBST with 10% heat inactivated lamb serum for 2 hours before adding pre-absorbed DIG or FL antibody and incubating overnight at 4˚C. Antibodies were used at approximately 1:500 to 1:8000 dilution. After antibody incubation, unbound antibody was removed with overnight TBST washes.

Color Reaction

Embryos were transferred into NTMT (100mM TrisHCL, 100mM NaCl, 50mM MgCl, 1% Tween 20) and washed several times. They were then incubated in NTMT with NBT and BCIP. Embryos were checked frequently at the beginning of the color reaction (every 10-15min) and then less frequently if color developed slowly. When the desired level of color was reached, the reaction as stopped by several TBST washes.

Second color reaction

After the first color reaction, the antibody was stripped from the embryos with 3 30min washes with SolutionX at 72˚C, then blocked in 10% lamb serum in TBST and incubated with pre-absorbed antibody as previously described. After overnight antibody

incubation, embryos were washed overnight in TBST. Embryos were switched to NTMT for the color reaction and incubated in NTMT with BCIP and N,N-dymethylformamide. When desired level of color was reached, the reaction was stopped with several washes in TE buffer. Embryos were then stored indefinitely in 10% formaldehyde in PBS at 4˚C.

QUANTITATIVE ANALYSIS

Static analyses were performed with ImageJ software.

Mitotic localization

Tissue was collected and processed for PHH3 immunohistochemistry. The midbrain tissue was then imaged at 40X magnification. All PHH3+/EGFP+ cells in a field of view were counted, and the mean and standard deviation was calculated. A student's T-test was used to calculate significant differences between EGFP controls and BMP4, or Noggin electroporated manipulations. The location of these PHH3+/EGFP+ cells was also studied. For this analysis, the distance from the apical most end of the nucleus to the apical surface was measured.

Chapter 3: A novel role for FOXA2 and SHH in organizing midbrain signaling centers[1]

INTRODUCTION

During development, the ventral midline of the vertebrate neural tube is occupied by the FP, which secretes SHH and plays a critical role in cell fate specification and axon guidance (Kingsbury, 1920; Placzek and Briscoe, 2005; Strähle et al., 2004). Despite 100 years of study, questions remain unanswered with regard to the embryonic origin, specification and function of the FP across species and axial levels of the neural tube (Placzek and Briscoe, 2005).

The simplest functional organization of the FP to have emerged is its partition into medial (MFP) and lateral (LFP) subdivisions (Odenthal et al., 2000; Schauerte et al., 1998). These divisions are well established in the anamniote and avian spinal FP where the MFP and LFP differ from each other in their embryonic origin, and more controversially, in their dependence upon HH signaling (Charrier et al., 2002; Odenthal et al., 2000; Peyrot et al., 2011; Placzek and Briscoe, 2005; Strähle et al., 2004). HH signaling is required in the fish for specification of the neurectoderm-derived LFP, while the node-derived MFP depends upon Nodal signaling for its induction (Hatta et al., 1991; Odenthal et al., 2000; Schauerte et al., 1998; Strähle et al., 2004). However, these results are complicated by a requirement for HH signaling in the maintenance of MFP at later

---

[1] Bayly, R.D.*, Brown, C.Y.*, Agarwala, S., 2012. A novel role for FOXA2 and SHH in organizing midbrain signaling centers. Dev. Biol. 369, 32–42.
*These authors contributed equally to this publication.

R.D. Bayly performed the experiments identifying MFP and LFP expression patterns and the roles of FOXA2 and SHH in FP specification.

C.Y. Brown performed the experiments examining the roles of FOXA2 and SHH in MHB and RP, the interconvertability of signaling centers, and all explant experiments.

stages and by the presence of residual FP cells in the nodal (cyclops) mutant (Odenthal et al., 2000; Ribes et al., 2010).

Gene expression patterns also support a partition of the mouse FP into medial and lateral subdivisions (Odenthal et al., 2000). However, the entire FP disappears following the loss of HH signaling, leaving unanswered the question of whether these subregions differentially require HH signaling for maintenance and/or induction as they do in the fish (Chiang et al., 1996; Fogel et al., 2008; Odenthal et al., 2000).

The chick spinal FP also displays node and neurectoderm-derived MFP and LFP subdivisions (Catala et al., 2000; Charrier et al., 2002). Here, SHH misexpression cannot induce an ectopic MFP, while notochord transplants readily do so via unidentified mechanisms (Catala et al., 2000; Charrier et al., 2002; Gray and Dale, 2010). More recent studies have suggested that early and transient exposure to SHH is capable of inducing a FP in all species, including the bird, fish and mouse (Ribes et al., 2010). But whether SHH is necessary and sufficient for the full FP program has not been addressed.

Even less is known about the specification of anterior (midbrain, rostral hindbrain) FP, which is distinct from the spinal FP in some respects (Patten et al., 2003; Placzek and Briscoe, 2005). For example, in addition to contributions from the node and neurectoderm, the chick anterior FP is also colonized by a unique population of cells emerging from “area a”, a region anterior to Hensen's node (Patten et al., 2003; Schoenwolf and Sheard, 1990). Interestingly, “area a” explants can be induced to a FP fate in the absence of the notochord by a brief exposure to prechordal plate-derived SHH and Nodal activity (Patten et al., 2003). But whether the anterior FP cell-types are organized into medial and lateral subdivisions and whether they differentially utilize HH and Nodal signaling is not known.

This question has recently acquired significance with the identification of an MFP-like ventral midline region as the predominant source of midbrain dopaminergic (mDA) neurons, which help regulate voluntary movements and the reward-reinforcement circuitry of the brain (Bayly et al., 2007; Blaess et al., 2011; Joksimovic et al., 2009; Ono et al., 2007). Recent work, including ours, suggests that HH signaling may not be necessary for patterning this MFP-like region (Hynes et al., 2000; Kittappa et al., 2007; Lin et al., 2009; Ye et al., 1998). Instead, some studies have reported that the winged helix transcription factor FOXA2 may be a more potent inducer of mDA progenitors than SHH (Kittappa et al., 2007; Lin et al., 2009; Norton et al., 2005; Ribes et al., 2010; Sasaki and Hogan, 1994).

Since SHH and FOXA2 transcriptionally upregulate each other, the differences between their inductive abilities are not well understood (Kittappa et al., 2007; Sasaki et al., 1997). FP studies in the fish suggest that FOXA2 activity can be regulated by, and interacts with, both the SHH and TGFß/Nodal signaling cascades (Strähle et al., 2004). However, the role of FOXA2 in fish FP specification is complicated by several observations. Although FOXA2 can rescue the MFP in the fish nodal (cyclops) mutant, nodal-dependent induction of FP occurs in the absence of FOXA2 (Norton et al., 2005; Rastegar et al., 2002). Despite its ability to induce the fish MFP, FOXA2 mutants display relatively mild phenotypes consisting mainly of a failure of the FP to fully differentiate (Norton et al., 2005). Although these observations suggest a role for FOXA2 in elaborating, rather than inducing the fish FP, they may also reflect functional redundancy among Foxa2 homologs. This idea is supported by the concurrent downregulation of Foxa2 and Foxa3 in the fish, which results in a complete loss of node-derived structures, including the notochord and MFP (Dal-Pra et al., 2011). An identical phenotype is seen

in Foxa2−/− mutant mice where the absence of the node and notochord also precludes FP specification (Ang and Rossant, 1994; Norton et al., 2005).

Although conditional Foxa2 or Foxa1/2 knockouts targeting the ventral midbrain have been created in mice, they are not informative because they disrupt FOXA1/2 activity around E9, when ventral midbrain specification is well (Bayly et al., 2007; Blaess et al., 2006; Ferri et al., 2007; Fogel et al., 2008; Lin et al., 2009; Perez-Balaguer et al., 2009). Thus, the precise requirement for SHH and FOXA2 in FP specification remains poorly understood.

In this study, we have approached this problem by comparing the role of *SHH* and *FOXA2* in midbrain and spinal FP specification in the chick, a species in which *FOXA1* or *FOXA3* genes have not been identified. We show that the midbrain FP can be clearly distinguished into MFP and LFP according to multiple criteria. Early manipulations of *SHH* and *FOXA2* exclusively targeted to the neural plate suggest that *SHH* is not sufficient to induce the MFP in either the midbrain or spinal cord. By contrast, *FOXA2* is necessary and sufficient for full MFP and LFP specification and does so via HH-dependent and independent mechanisms.

Notably, we show for the first time that the midbrain signaling centers express a common set of genes, and can take on each other's' identities in a SHH-dependent manner. Thus, by regulating the identity of orthogonal signaling centers, MFP signals direct 3-dimensional patterning in the midbrain and hindbrain.

RESULTS

Differential gene expression in medial and lateral FP

We first determined whether the midbrain FP could be divided into medial and lateral divisions by differential gene expression (Odenthal et al., 2000; Placzek and Briscoe, 2005; Strähle et al., 2004). *SHH, FOXA2, LMX1B* and Bone morphogenetic protein 7 (*BMP7*) mRNAs were expressed in the presumptive midbrain FP by H&H 4 and continued to be expressed there until at least E6 (Fig. 3.1A–I; Aglyamova and Agarwala, 2007; Altaba et al., 1995; Echelard et al., 1993; Hamburger and Hamilton, 1951; Lawson et al., 2001; Yuan and Schoenwolf, 1999). By H&H 13, a *SHH+/FOXA2+/LMX1B*-negative/*BMP7*-negative territory emerged rostrally to surround the *SHH+/FOXA2+/LMX1B+/BMP7+* FP (Fig. 1E; Aglyamova and Agarwala, 2007). This lateral region expanded caudally toward the MHB, so that it fully encompassed the medial region between late E3–E6 (Fig. 3.1F, G). Based on gene expression and additional criteria described below, these FP territories were identified as MFP and LFP (Odenthal et al., 2000).

Several other markers, e.g., *LMX1A, DISP1, MN-CAD* and Chordin, were also expressed in the MFP and distinguished it from the LFP (Fig. 3.1H, I; data not shown). Their expression patterns were dynamic and some occupied narrower domains than the *LMX1B* territory, especially at later ages (Fig. 3.1H, I; data not shown). A closer examination also showed that the expression of *SHH, FOXA2, DISP1* and *LMX1B* in MFP cells was mosaic, suggesting that the subarchitecture of the MFP may be more complex than outlined here (Fig. 3.1H; data not shown). However, since our perturbations did not differentially affect the MFP markers identified above, we treated the MFP as one entity in this study.

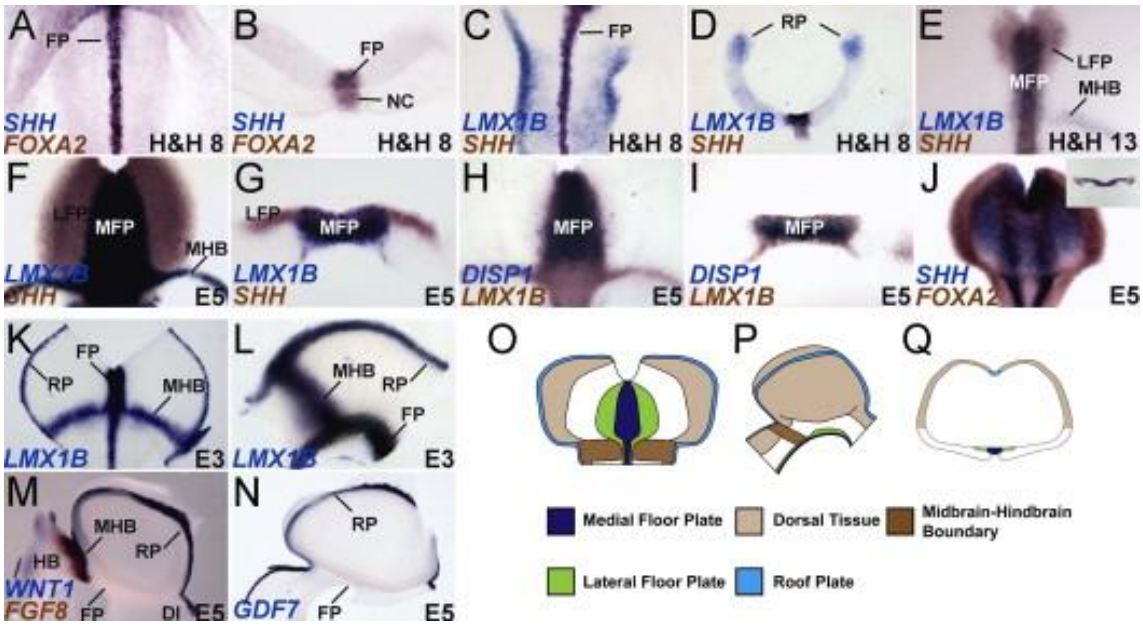

Figure 3.1 Gene expression patterns distinguish the midbrain MFP and LFP.

(A)–(J) *SHH*, *FOXA2*, *LMX1B* and*DISP1* expression in the FP. **(**A): Whole embryo, top-down view; (B), (D), (G), (I), inset (J): cross-sections; (C), (E), (F), (H), (J): flattened wholemounts (open book preparation, rostral to the top and ventricular surface facing the viewer). (K)–(N). Overlapping and specific gene expression patterns in midbrain signaling centers. Flattened wholemount (K) and sagittal (L)–(N) views displaying physically contiguous*LMX1B* expression in the MFP, RP and MHB (K), (L), the exclusive expression of *FGF8* in the MHB (M) and of *GDF7* in RP (N). Note that *WNT1* is expressed in the RP and MHB, but not FP. (O)–(Q) Cartoons displaying the 3-dimensional spatial relationships among the midbrain signaling centers. (O): flattened wholemount; (P): sagittal view, rostral to the right; (Q): cross-section.

Lateral floor plate	SHH	FOXA2								
Medial floor plate	SHH	FOXA2	*DISP1*	*MN-CAD*	*LMX1A*	LMX1B	BMP7			
Midbrain-hindbrain boundary						LMX1B	BMP7	WNT1	FGF8	
Roof plate						LMX1B	BMP7	WNT1		GDF7

Table 3.1 Summary of gene expression patterns identifying the midbrain signaling centers.

Unique identifiers for each signaling center are in italics.

We were unable to find markers that uniquely and stably identify the LFP for the duration of our experiments. This included *NKX2.2* expression, which labeled regions outside the FP (data not shown). The midbrain LFP was therefore identified by the combined presence of *SHH* and *FOXA2* and the absence of *LMX1A, LMX1B, DISP1, MN-CAD* and *BMP7* (Fig. 3.1E–J; Table 1; data not shown).

Interestingly, the MFP, RP and MHB all expressed *BMP7* and *LMX1B* and were physically contiguous (Fig. 3.1K, L). However, *LMX1A, DISP1* and *MN-CAD* were expressed exclusively in the MFP, while *FGF8* and *GDF7* were expressed exclusively in the MHB and the RP, respectively (Fig. 3.1H, I, M, N; data not shown). These markers permitted us to unequivocally distinguish the midbrain signaling centers from each other in later experiments (Table 3.1). These data are summarized in Fig. 3.1O–Q.

SHH is sufficient for LFP, but not MFP induction in the midbrain

SHH misexpression can induce *SHH* and *FOXA2*, both generic markers of the FP, but whether it can induce both midbrain MFP and LFP is not known (Agarwala and Ragsdale, 2002; Agarwala et al., 2001). Unlike controls, SHH misexpression (1–5 μg/μl) non-autonomously converted large swaths of midbrain into *SHH+/FOXA2+/LMX1B*-negative/*DISP1*-negative LFP (Fig. 3.2A; Agarwala and Ragsdale, 2002 and Agarwala et al., 2001). However, *SHH* misexpression could only induce MFP markers (*DISP1, LMX1B, BMP7, MN-CAD*) along the MHB and nowhere else in the midbrain (Fig. 3.2A–C).

Spinal cord studies have suggested that FP induction is accomplished by early and transient HH signaling prior to somitogenesis (Patten et al., 2003; Ribes et al., 2010). To determine the precise times during which early HH activity might occur in the midbrain, we examined early *SHH* gene and protein expression. Surprisingly, although *SHH*

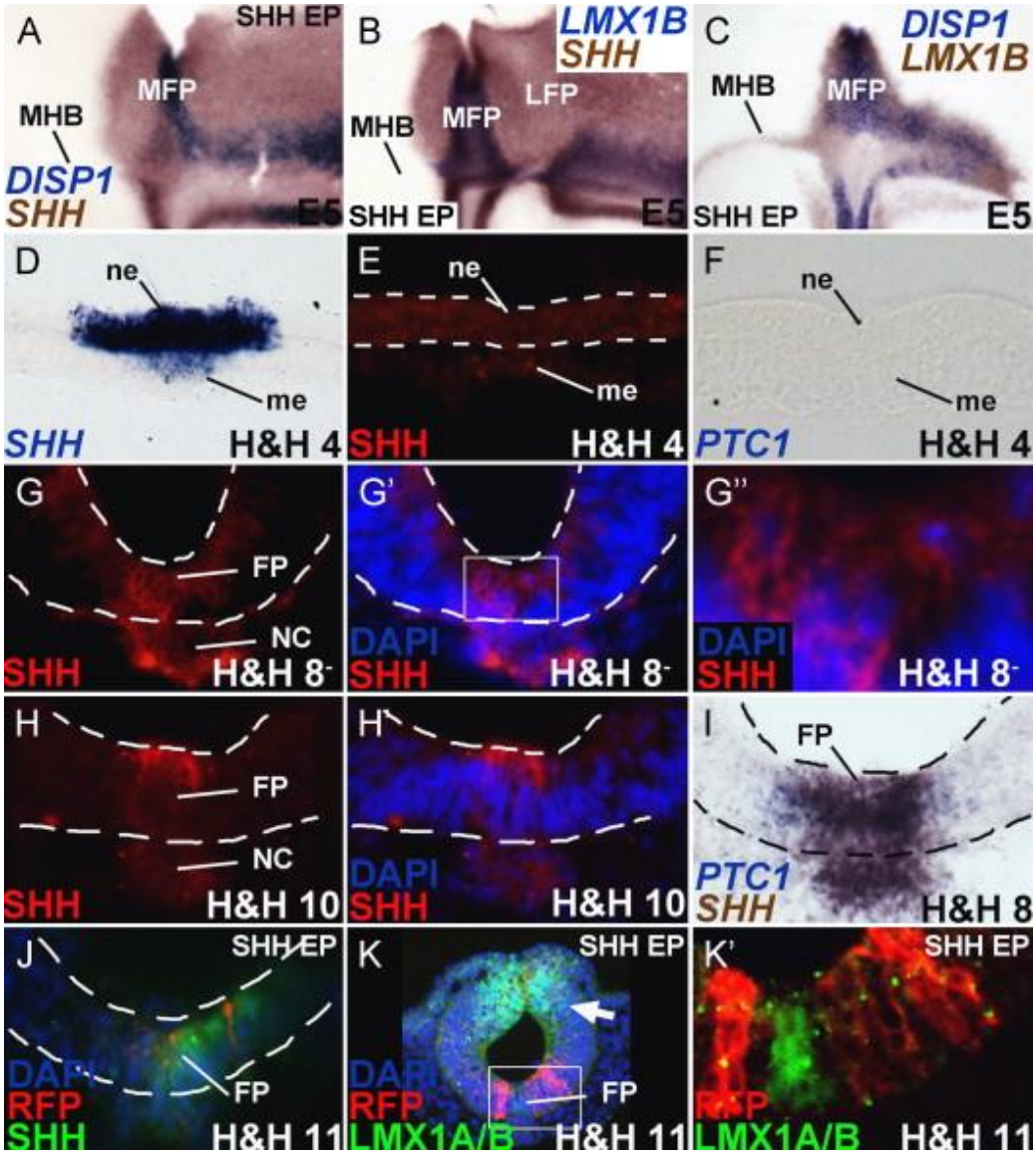

Figure 3.2 SHH misexpression is sufficient for LFP, but not MFP induction.

Figure 3.2 SHH misexpression is sufficient for LFP, but not MFP induction.

(A)–(C), flattened wholemounts, oriented as in Fig. 1 (C); (D)–(K′), cross-sections). (A)–(C) Unilateral *SHH* misexpression is sufficient to convert the entire right half of the midbrain into *SHH*+ LFP (A), (B), but can only specify an*LMX1B*+/*DISP1*+/*SHH*+ MFP along the MHB (A)–(C). (D)–(F) *SHH* mRNA (D) but no SHH protein (E) or*PTC1* transcripts (F) at H&H 4. Sections in (D)–(F) are drawn from presumptive neural plate anterior to Hensen's node. (G)–(H′) SHH protein (red) at H&H 8^{-} (G)–(G″) and H&H 10 (H)–(H′). (G′) and (G″) show the micrograph in (G) with DAPI staining. The boxed area in (G′) is magnified in (G″) to show a SHH+ cell (arrowhead) and a SHH-negative cell (arrow). (H′) shows the image in H with DAPI staining. (I) *SHH* and*PTC1* mRNA at H&H 8. (J), (K′) H&H 4–6 *SHH*-ires-*RFP* electroporation (red) is sufficient for ectopic, non-autonomous SHH ((J), green) induction and dorsal LMX1A/B suppression (arrow, (K)), but it is not sufficient for LMX1A/B (green) induction ventrally (K), (K′). Boxed area in (K) is magnified in (K′) to show the absence of LMX1A/B induction in or around SHH -ires-RFP+ cells. Please note that the sections shown in (G)–(K′) are drawn from the rostrocaudal midpoint of the midbrain.

transcripts were detected as early as H&H 3, no SHH protein or HH receptors (PTC1, PTC2, HHIP) were detected in the axial midline at this time (Fig. 3.2D–F; Aglyamova and Agarwala, 2007; Lawson et al., 2001; Pearse et al., 2001). Modest levels of SHH protein were first detected in the cytoplasm of most FP and notochord cells at H&H 8−, although some cells remained SHH-negative at this time (Fig. 3.2G–G″). SHH expression became stronger by H&H 10 and resembled that of the spinal cord, with strong, cytoplasmic expression along the apical surface of FP cells Fig. 3.2H, H′; Chamberlain et al., 2008). Robust and transient expression of *PTC1* and *GLI1* was seen at the ventral midline between H&H 8− to <H&H 10, with more lateral expression seen at later ages (Fig. 3.2I; Aglyamova and Agarwala, 2007). Together these data defined a narrow window of time during which HH signaling might accomplish midbrain FP induction.

We used a novel early electroporation paradigm to misexpress *SHH-ires-RFP* between H&H 4–6 to obtain robust SHH misexpression by H&H 7, immediately prior to the onset of endogenous SHH protein expression (Brown et al., 2012a, 2012b; Eom et al., 2011, 2012). Interestingly, while SHH misexpression at this time readily induced ectopic SHH expression and suppressed dorsal expression of *LMX1A/B*, it failed to induce an *LMX1A/B+/SHH+* MFP (Fig. 3.2J–K′). Thus, early HH activity is not sufficient for midbrain MFP induction, although it is sufficient for LFP induction and suppression of dorsal midbrain fates.

SHH is necessary for midbrain MFP and LFP specification

To determine whether HH signaling was necessary for the specification of the MFP, we misexpressed Ptc1Δloop2, a dominant negative regulator of HH signaling, between H&H 7–10 when HH signaling is critically required for midbrain cell fate specification (Fig. 3.2G–I; Bayly et al., 2007). Bilateral misexpression of *Ptc1Δloop2*

resulted in a robust disruption of the LFP while leaving *LMX1B* expression in the MFP largely unperturbed (Fig. 3.3A, B; Bayly et al., 2007).

Despite the lack of evidence of an HH signaling cascade prior to H&H 8−, it was possible that low, undetectable levels of early HH activity occurred along the ventral midline and were required for midbrain MFP specification (Ribes et al., 2010). In previous work, we noted that high embryonic lethality was associated with *Ptc1Δloop2* electroporations, and despite robust misexpression throughout the midbrain, only a small number of *Ptc1Δloop2*+ cells were found in the ventral midline (Bayly et al., 2007). Possible reasons for this include the differential cell-affinities of HH+ and HH-negative cells, but exclude (Bayly et al., 2007; Lawrence, 1997; Rodriguez and Basler, 1997; Wijgerde et al., 2002).

To obtain more ubiquitous HH blockade at early stages, we therefore exposed early whole embryo explants to cyclopamine, a fast-acting inhibitor of HH signaling (Incardona et al., 1998). Although we initially divided the explants into 3 age groups (H&H 3–5, 6–7, 8–9), these data were pooled since all explants displayed similar FP phenotypes in response to cyclopamine. Bath application of 100 μM cyclopamine for 24 h in H&H 3–9 explants successfully reduced or abolished the expression of HH pathway/target genes, *PTC1, DISP1* and *FOXA2* (Fig. 3.3C–F′; Incardona et al., 1998). However, cyclopamine treatment did not affect *LMX1B* expression at the ventral midline (n=16/18; Fig. 3.3C–D′; Pearse et al., 2001). Together, the gain and loss of function experiments reported above suggest that regardless of the age of manipulation, HH activity was necessary, but not sufficient for the full execution of the MFP program.

Since the RP, FP and MHB all express *LMX1B*, we next asked whether the *LMX1B* expressing ventral midline retained FP identity following HH blockade (Fig.

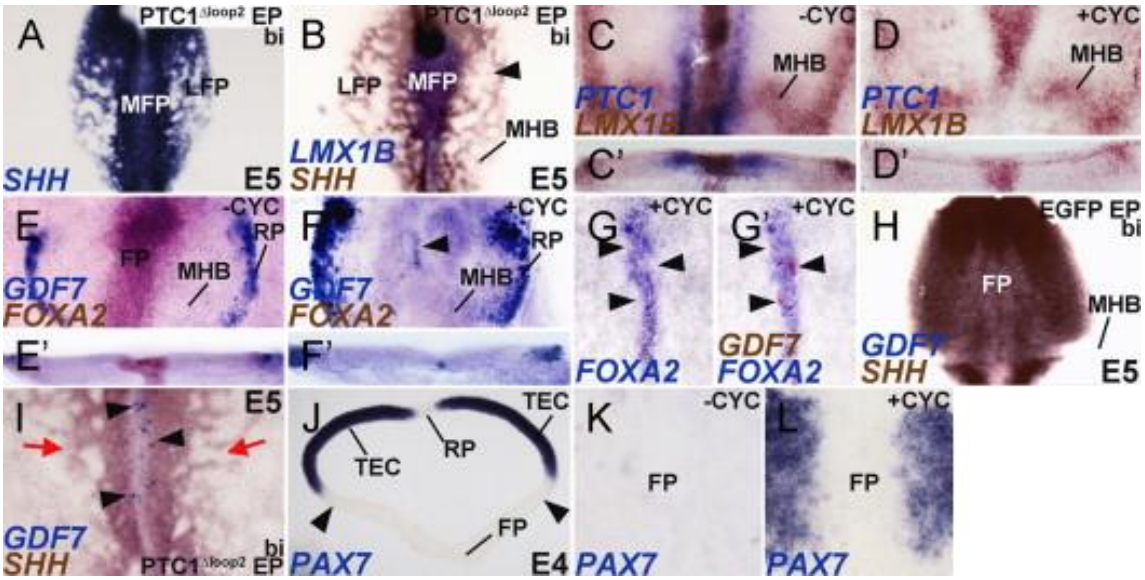

Figure 3.3 SHH is necessary for MFP induction.

(A)–(B) Broad, bilateral misexpression of *PTC1*$^{\Delta}$*loop2* disrupts the*SHH*+/*LMX1B*-negative LFP ((B), arrowhead), but does not affect the *SHH*+/*LMX1B*+ MFP. Control for 3B can be seen in Fig. 4 (E). (C), (D) H&H 3 explants treated with either vehicle (–CYC) or cyclopamine (+CYC) for 24 h demonstrate that HH blockade suppresses *PTC1* expression in LFP, but does not affect*LMX1B* expression in the MFP. (C′), (D′) Cross-sections of the wholemounts shown in (C) and (D). (E), (E′) Control explants in flattened wholemount (E) and cross-sectional (E′) view displaying *GDF7* (RP) and*FOXA2* (FP) expression. (F), F′) Cyclopamine treated explants displaying the loss of *FOXA2* and the ectopic induction of *GDF7* at the ventral midline (arrowhead). Note that compared to E, E′, the roof plate (RP) expression of GDF7 is expanded in F, F′. (G), (G′) Cyclopamine treated explants with mild HH blockade showing ectopic expression of *GDF7* (arrowheads) in the ventral midline whereever *FOXA2*expression is abolished. Note that (G) and (G′) show the same explant before and after *GDF7* staining. Control for (G), (G′) is shown in Fig. (E). (H) Control brain demonstrating that *GDF7* is not expressed in the*SHH*+ FP or MHB. See also, 1N; 7G, (H) for controls. (I) Bilateral HH blockade results in a disruption of the LFP (red arrows) and a conversion of the MFP into *GDF7*+ RP (arrowheads). (J) Midbrain cross-section demonstrating that *PAX7* expression is absent from the RP and ventral midbrain, but present throughout dorsal midbrain (TEC). (K), (L) Control (K) and cyclopamine treated explants (L) shown in wholemount view demonstrating that the ventral expansion of *PAX7* into ventral midbrain (K) excludes the ventral midline. The *PAX7*-negative region between the arrowheads in (J) was flattened in (K), (L).

3.1K, L; data not shown; Chizhikov and Millen, 2004). To our surprise, the cyclopamine-treated explants displayed ectopic *GDF7* expression in ventral midline cells in which *FOXA2* expression had been abolished, suggesting that some FP cells acquired ectopic RP identity in the absence of HH signaling (Fig. 3.3E–G′). Ptc1Δloop2 electroporations at H&H 7–11 provided additional evidence for the conversion of some FP cells into *GDF7*+ RP cells (Fig. 3.3H, I; arrowheads in 3I). With the exception of *GDF7*, exclusive RP markers that were not also expressed in other midbrain signaling centers were not available (Fig. 3.1K–Q; Table 1). However, the ectopic ventral midline expression of *WNT1* (which is expressed in the RP and MHB, but not the avian FP; Fig. 3.1M; Fig. 3.7D) and *WNT1+/GDF7+* cells in the ventral midline following Ptc1Δloop2 electroporations further confirmed the transformation of FP cells into RP identity (Fig. 3.6H, I-J).

To determine whether the ectopic ventral midline expression of *GDF7* represented a specific conversion of the MFP to the RP or a generic ventral to dorsal conversion in the absence of HH activity, we examined *PAX7* expression, which is absent in the ventral midbrain as well as RP, but otherwise present throughout the dorsal midbrain (Fig. 3.3J). Interestingly, cyclopamine treatment resulted in ectopic *PAX7* expression throughout ventral midbrain except for the *LMX1B*+ region along the ventral midline (Fig. 3.3K, L). The presence of *GDF7+/WNT1+/LMX1B+/PAX7*-negative cells in the MFP demonstrated that in the absence of HH signaling, the ventral midline of the midbrain was specified as RP rather than as MFP. Taken together, these results show that HH signaling is necessary, but not sufficient to execute the full midbrain MFP program (Charrier et al., 2002; Peyrot et al., 2011; Ribes et al., 2010).

FOXA2 induces the full midbrain FP program via HH-dependent and independent mechanisms

FOXA2 is necessary and sufficient to induce MFP and LFP in ventral midbrain. Unlike *SHH*, *FOXA2* mRNA and protein expression are seen at the axial midline of the embryo at H&H 2, prior to the activation HH signaling (Fig. 3.4A, B; Fig. 2E, G; Ruiz i Altaba et al., 1993). Given our limited understanding of *FOXA2* function in regionalizing the amniote FP, we asked whether *FOXA2* might induce midbrain MFP (Ang and Rossant, 1994; Norton et al., 2005; Ribes et al., 2010; Sasaki and Hogan, 1993, 1994; Strähle et al., 2004). Interestingly *FOXA2* electroporations early (H&H 4–6) or late (H&H 7–11) non-autonomously converted ventral midbrain into FP (Fig. 3.4C; D, inset 3.4D). Unlike *SHH* however, *FOXA2* was sufficient to induce both LFP and MFP markers throughout the midbrain and not just along the MHB (Fig. 3.4C–F; Fig. 3.2A–C). Conversely, dominant negative *FOXA2* (dnFOXA2) and *FOXA2* RNAi electroporations between H&H 4–11 prevented the induction of both the MFP and the LFP (Fig. 3.4G, H; control for 3.4H is shown in Fig. 3.4K).

FOXA2 cannot ventralize the FP without turning on *SHH*. We next determined the extent to which the *FOXA2*-mediated induction of MFP depended upon HH signaling. Joint electroporations of *FOXA2* and *Ptc1Δloop2* mimicked *FOXA2* misexpression by inducing *LMX1B* expression throughout ventral midbrain, demonstrating that *LMX1B* induction by *FOXA2* is HH-independent (Fig. 3.4I, J). However, in contrast to *FOXA2* misexpression alone, ectopic *LMX1B*+ puncta induced by FOXA2/Ptc1Δloop2 co-electroporations also expressed *GDF7*, an exclusive marker of midbrain RP (Fig. 3.4I, J, arrowheads). Thus, following joint *FOXA2* misexpression and *HH* blockade, cells ectopically expressing *LMX1B* adopt a RP, rather than a FP identity.

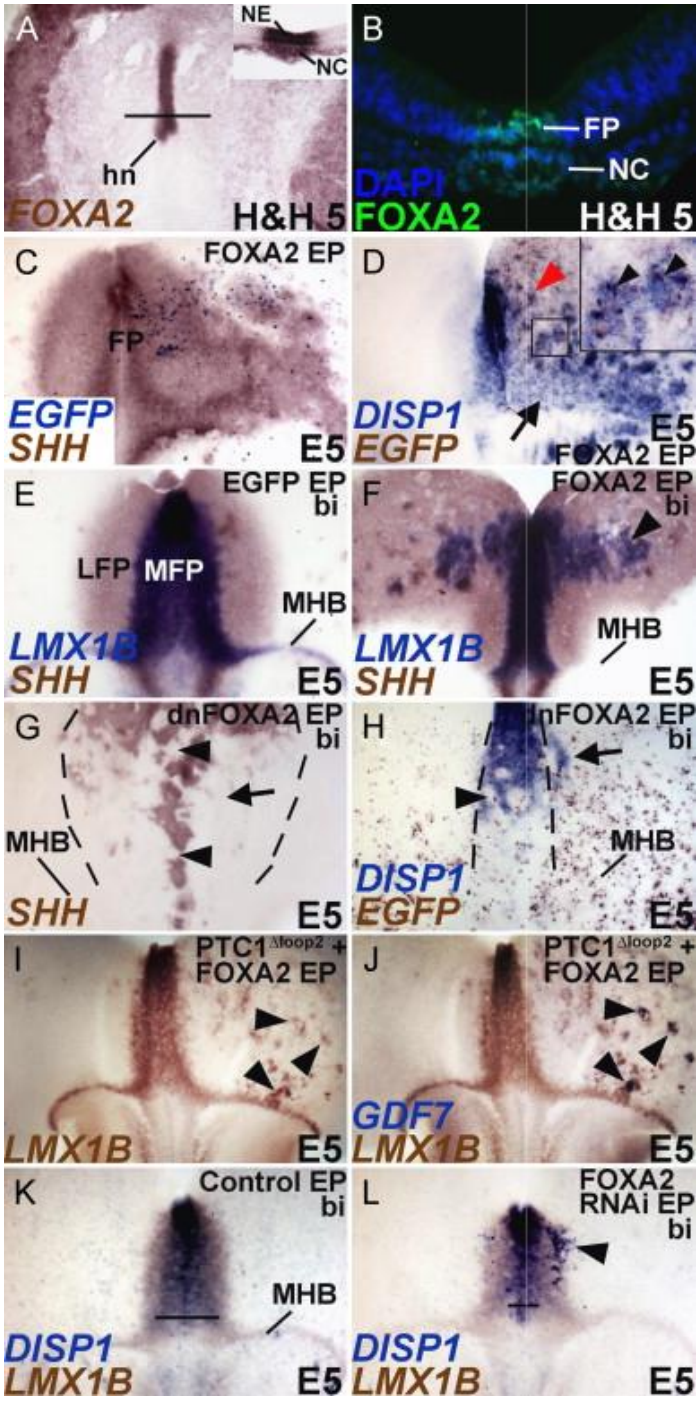

Figure 3.4 Foxa2 is necessary and sufficient for midbrain FP specification.

Figure 3.4 Foxa2 is necessary and sufficient for midbrain FP specification.

(A), (B) *FOXA2* mRNA (A), inset (A) and protein (B) are expressed in the axial midline of the embryo by H&H 5, prior to HH signaling. (A): Whole embryo, top down view. Inset, (A): Section taken from this embryo at the level indicated by the black line. (C) Unilateral misexpression of *FOXA2-ires-EGFP* (right) is sufficient to non-autonomously upregulate*SHH*. (D) Unilateral misexpression of *FOXA2-ires-EGFP* (right) results in *DISP1* upregulation both along (arrow) and away (red arrowhead) from the MHB. Boxed region in (D) is magnified in the inset to demonstrate the non-autonomous induction of *DISP1* (blue) by FOXA2-ires-EGFP (brown) misexpressing cells. (E), (F). EGFP (E) and bilateral *FOXA2* misexpression (F) demonstrating that ectopic *FOXA2* can induce an *LMX1B*+/*SHH*+ MFP away from the MHB (arrowhead, (F)). ((G), (H)) Bilateral *dnFOXA2*electroporation (identified by EGFP detection in (H)) is sufficient to block LFP (arrow, (G)) and MFP (arrowheads, (G), (H)) induction. Arrow in (H) points to the non-cell autonomous expansion of *DISP* following *FOXA2* knockdown. (I),(J)Unilateral *PTC1Δloop2* and *FOXA2* co-electroporation demonstrates that *FOXA2*-mediated induction of *LMX1B* is HH-independent. Note that the cells ectopically inducing *LMX1B* also express *GDF7* and adopt a RP fate (arrowheads) in the absence of HH. The same wholemount is displayed in G and H before and after *GDF7* detection. (K), (L) Compared to controls (K), FOXA2 RNAi results in the suppression of MFP (compare the lines in (K) and (L), marking the mediolateral extent of *DISP1*) as well as the ectopic induction of MFP in lateral midbrain (arrowhead, (L))

We conclude that *FOXA2* is necessary for midbrain MFP and LFP induction, and is necessary and sufficient to induce MFP-specific genes in the absence of SHH. By contrast, HH activity is required for inducing HH-pathway genes (*DISP1, PTC1, FOXA2*), without which the ventral midline cannot acquire a specific MFP identity (Fig. 3.3C–I). Thus the HH pathway is required for LFP specification and the ventralization of the MFP, while HH-dependent and independent activities of *FOXA2* are required for the execution of the full midbrain FP program.

FOXA2 is necessary to restrict MFP induction to the ventral midline of the midbrain. A HH-dependent lateral expansion of netrin1 and nkx2.2a is seen in fish foxa2 (monorail) mutants, suggesting a role for *FOXA2* in limiting HH activity laterally and preventing the lateral expansion of FP (Norton et al., 2005). In agreement with these observations, dnFOXA2 and FOXA2 RNAi-electroporated midbrains demonstrated a non-autonomous induction of MFP in lateral midbrain (n=8; arrow, Fig. 3.4H, arrowhead, Fig. 3.4L). Interestingly, such non-autonomous induction of the MFP was not seen in embryos electroporated with *Ptc1Δloop2*, suggesting that it was likely to be HH-dependent (Fig. 3.3B). Thus, in addition to its role in inducing the MFP and LFP, *FOXA2* also plays a role in restricting the MFP domain to the ventral midline of the midbrain, as suggested by mouse Foxa2 enhancer analyses and fish foxa2 mutants (Norton et al., 2005; Sasaki et al., 1997).

FOXA2, but not SHH, is sufficient for specifying the full spinal FP program

In the chick spinal cord, a notochord transplant can induce a complete FP, while ectopic SHH can only induce the LFP (Charrier et al., 2002). Since FOXA2 is expressed in the spinal FP and notochord, we next asked whether SHH and FOXA2 might play different roles in spinal FP specification as they do in the midbrain. Like the midbrain,

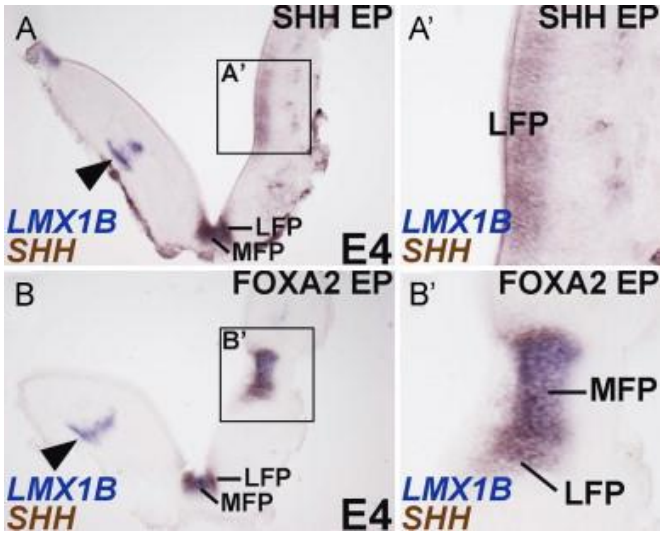

Figure 3.5 FOXA2 is sufficient for MFP and LFP induction in the spinal cord.

Boxed areas in (A) and (B) are magnified in (A′) and (B′), respectively. (A), (A′) Unilateral *SHH* misexpression (right side) is sufficient to induce a *SHH*+ LFP (boxed area, (A); (A′), but fails to induce a *SHH*+/*LMX1B*+ MFP. (B), (B′) *FOXA2*misexpression (right side) in the spinal cord is sufficient to induce both the MFP and LFP (boxed area, (B); (B′), accompanied by a FP-like morphology. Note that unlike the control side (arrowheads, (A), (B) *FOXA2*and *SHH* both suppress *LMX1B*+ dorsal dI5 interneurons.

we noted the presence of an *LMX1B+/SHH+ MFP* and *LMX1B*-negative/*SHH+* LFP in the spinal cord (Fig. 3.5A). Unilateral electroporation of *SHH* in the H&H 10 rostral spinal cord suppressed dorsal fates (e.g., dI5 interneurons, arrowhead; Fig. 3.5A, A′) and readily induced ectopic *LMX1B*-negative/*SHH+* LFP (Fig. 3.5A, A′). However, it did notinduce an *LMX1B+/SHH+* MFP (n=10/10; Fig. 3.5A, A′). By contrast, *FOXA2* misexpression induced both ectopic MFP and LFP, in addition to recapitulating the characteristic FP morphology (Fig. 3.5B, B′). Taken together, our observations suggest that *FOXA2*, but not *SHH*, is sufficient to execute the entire FP program in the midbrain and spinal cord.

SHH and FOXA2 regulate the specification of all midbrain signaling centers

The midbrain–hindbrain boundary

In Fig. 2 and Fig. 4, we demonstrated that ectopic *SHH* and *FOXA2* can induce an MFP along the MHB, although how this occurs was not explored (Figs. 3.2A C; 3.4D). *FOXA2* or *SHH*-mediated induction of MFP markers along the MHB resulted in a concurrent suppression of the MHB markers, *FGF8* and *WNT1* (Fig. 3.6A, B). To determine whether a functional MFP formed along the MHB, we asked whether the ectopic MFP provided axon guidance cues, a known function of the FP (Charron et al., 2003). Immuno-labeling by phosphorylated-SMAD 1/5/8 (a readout of canonical BMP signaling) allows for the identification of multiple axon trajectories in the midbrain, either attracted or repelled by FP signals (Fig. 3.6C; Fedtsova et al., 2008). Interestingly, *FOXA2*-mediated induction of the MFP along the MHB resulted in a complete recapitulation of axon trajectories seen at the MFP, while repressing those seen at the

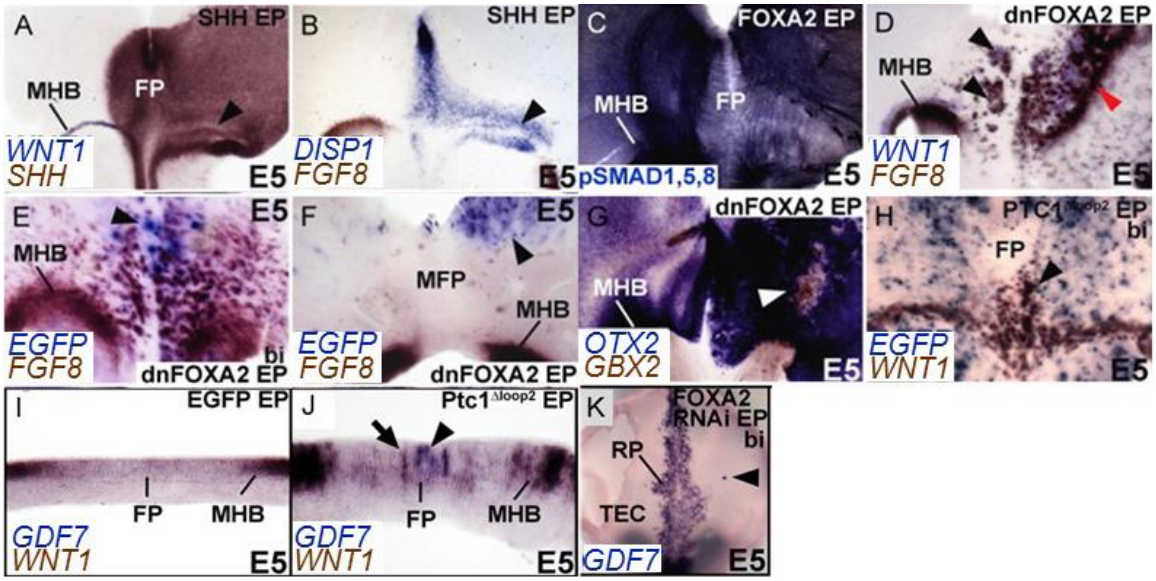

Figure 3.6 SHH and FOXA2 regulate the signaling centers of the midbrain.

(A), (B) Unilateral *SHH* misexpression (right side) induces the MFP (*DISP1*+/*SHH*+) while concurrently suppressing MHB (*FGF8*+, *WNT1*+) fates (arrowheads, (A), (B). (C) *FOXA2* misexpression converts the MHB (right side) into an ectopic MFP, which recapitulates the endogenous MFP pattern of axons, identified by phosphorylated-SMAD 1/5/8 (visualized via whole mount immunohistochemistry). (D) dnFOXA2 misexpression can convert the FP into MHB (arrowheads). Note also that the MHB is expanded and shifted rostrally (red arrowhead) on the right, most likely due to ectopic hindbrain induction caudal to it (See also Fig. 6 (G). (E), (F) Ectopic MHB can only be induced by dnFOXA2 misexpression within the *FOXA2*+ FP (arrowhead, (E)) and not outside it (arrowhead, (F)). (G) dnFOXA2 suppresses *OTX2*+midbrain fate and upregulates *GBX2*+ hindbrain fates (arrowhead). (H) Bilateral HH blockade also results in the conversion of caudal MFP into MHB (arrowhead). (I, J) Unlike EGFP-electroporated controls (I), Ptc1Δloop2-electroporated brains (J) display ectopically induced *GDF7+/WNT1*+ RP cells (blue + brown, arrowhead) and *WNT1+/GDF7*- negative MHB cells (brown, arrow) along the ventral midline. (K) Top down view of RP demonstrating that compared to EGFP-electroporated controls (see Fig. 3.7A), the RP is expanded as a consequence of *FOXA2* (arrowhead) downregulation in ventral midbrain.

MHB (Fig. 3.6C, right side). Thus, *FOXA2* and *SHH* suppress the MHB program and convert it into a functional MFP, which can redirect axon trajectories.

By contrast, dnFOXA2 resulted in a massive induction of *WNT1* and *FGF8*, converting the FP into MHB and the midbrain into hindbrain (black arrowheads, Fig. 3.6D, E and red arrowhead, Fig. 3.6D; see also Fig. 3.6G; (Agarwala and Ragsdale, 2002; Liu et al., 1999). We noted that this MHB induction was non-autonomous, but required that the dnFOXA2 electroporations were targeted to the ventral midline (Fig. 3.6E, F). By contrast, no induction of FGF8 occurred when dnFOXA2 was misexpressed outside the *FOXA2* domain (Fig. 3.6F). We conclude that the non-autonomous induction of *WNT1* and *FGF8* throughout the midbrain was an indirect consequence of converting the MFP into the MHB and of expanding the endogenous MHB.

FGF8 misexpression is known to convert the midbrain into hindbrain by inducing *GBX2* (Liu et al., 1999). Indeed, dnFOXA2 cell-autonomously upregulated *GBX2* and suppressed *OTX2*, converting midbrain into hindbrain, while non-autonomously upregulating *OTX2* (Fig. 3.6G; data not shown). HH blockade by PTC1Δloop2 replicated the effects of dnFOXA2 and also converted the MFP into MHB (Fig. 3.6H; Bayly et al., 2007). Together, these data suggest that FOXA2 and HH signaling are involved in determining whether a midbrain signaling center will take on MHB or MFP fates.

The roof plate

We showed above that HH mediated-ventralization of the midbrain determined whether the *LMX1B*+ ventral midline expressed MFP or RP fates (Fig. 3.3E–I; Fogel et al., 2008). We explored the inter-convertibility of MFP and RP further with *SHH* gain and loss of function experiments. Ventral *SHH* misexpression suppressed the specification of a *GDF7+/WNT1+/LMX1B*+ RP (Fig. 3.7A–E). Interestingly, very small

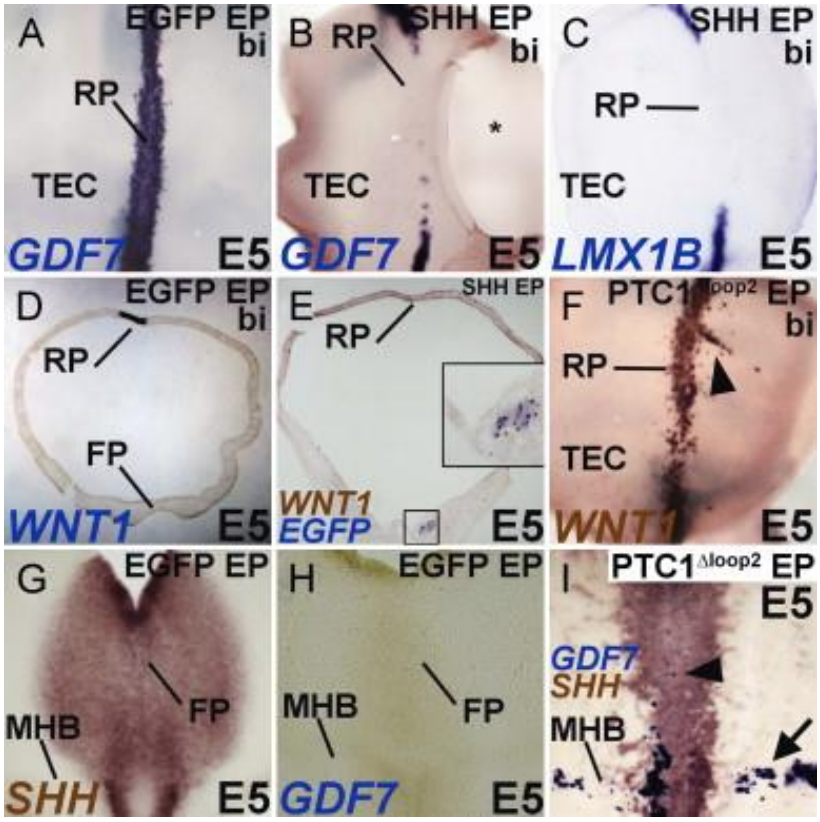

Figure 3.7 FOXA2 and SHH regulate roof plate specification

(A)–(E) Top down (A)–(C) and cross-sectional views (D), (E) demonstrating that compared to EGFP-electroporated controls (A), (D), RP induction is blocked by ventral electroporations of *SHH*. Inset in (E) shows magnified view of the boxed region and demonstrates the location of SHH misexpression by EGFP transgene expression. * in B marks a hole cut in dorsal midbrain for irrigation. (F) Ventral *PTC1*$^{\Delta}$*loop2*misexpression results in ectopic RP induction (arrowhead). (G)–(I) Midbrain flatmounts showing that unlike controls (G), (H), *PTC1*$^{\Delta}$*loop2* misexpression results in reduced *SHH* expression accompanied by ectopic*GDF7* expression in both the ventral midline (arrowhead) and the MHB (arrow).

ventral electroporations of *SHH* were sufficient to non-autonomously suppress RP specification (Fig. 3.7D, E, inset E). Conversely, ventral electroporations of *Ptc1Δloop2* resulted in an expansion and ectopic induction of the midbrain RP, a phenotype similar to the RP expansion noted in Shh−/− mice (Fig. 3.7F; Fogel et al., 2008). Ventral *FOXA2* blockade mimicked the effects of HH blockade by expanding the endogenous midbrain RP and by ectopically inducing RP in dorsal midbrain (Fig. 3.6 K).

Surprisingly, suppression of HH activity along the MHB also resulted in a conversion of the MHB into *GDF7*+ RP cells (Fig. 3.7G–I, arrow in 7I). Together, these results suggest that SHH plays a role in repressing the RP program dorsally and along the MHB. In its absence the RP expands and the MHB and the MFP take on RP identity. These results suggest that HH is required for the specification and/or maintenance of all midbrain signaling centers, including the FP, RP and the MHB.

DISCUSSION

Our results suggest that SHH is both necessary and sufficient for LFP induction, but it is only necessary, and not sufficient for inducing the MFP program (Odenthal et al., 2000; Strähle et al., 2004). By contrast, *FOXA2* is necessary and sufficient to specify the entire FP and does so in a HH-dependent and independent manner (Fig. 3.8). We have also identified a novel function for HH signaling in determining the identity of midbrain signaling centers, with critical consequences for 3-dimensional midbrain patterning and for midbrain and hindbrain identity (Fig. 3.8).

The role of *FOXA2* and *SHH* in FP specification

The role of *SHH* in MFP specification has been difficult to ascertain, with evidence ranging from an absolute requirement for HH signaling in the mouse, to a role

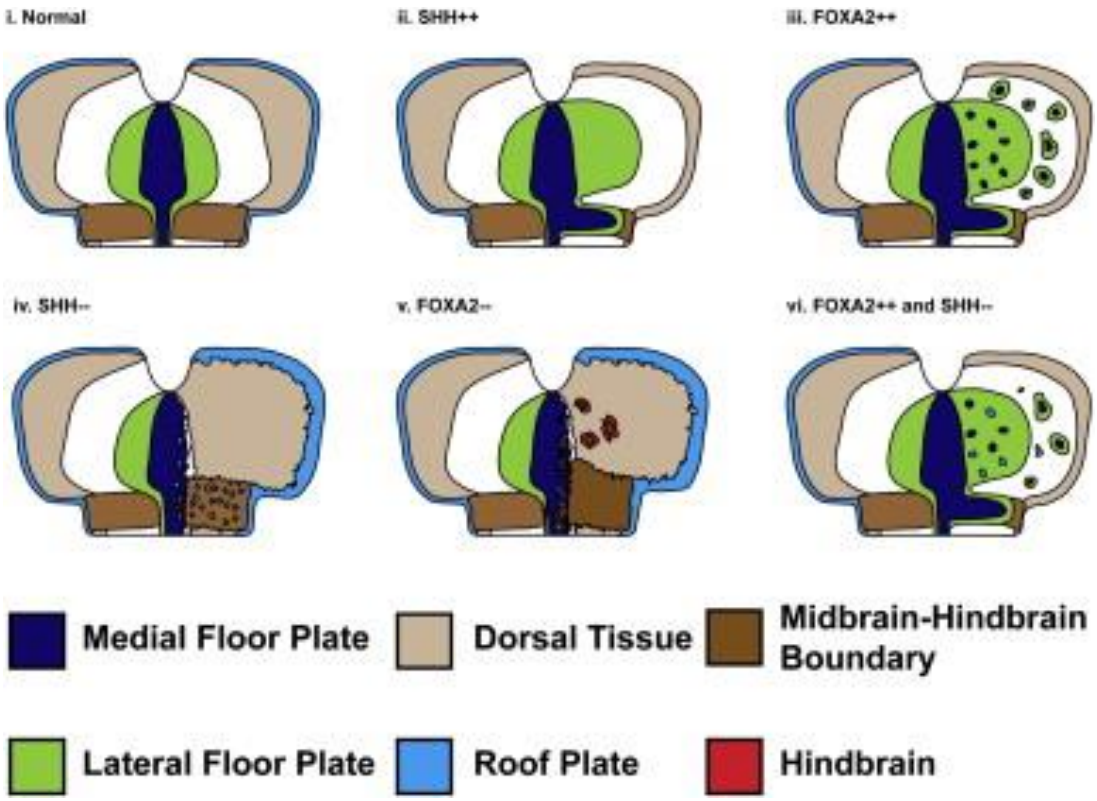

Figure 3.8 Cartoon summarizing the role of SHH and FOXA2 in patterning the MFP, MHB and RP.

(i) Schematic depicting the normal spatial relationships among the RP (light blue), MFP (dark blue), LFP (green), MHB (dark brown) and dorsal midbrain (beige). (ii) Unilateral *SHH* misexpression (right side) ectopically induces LFP and can induce MFP along the MHB while concurrently suppressing MHB fates. Dorsal cell fates, including RP are also suppressed. (iii) Unilateral *FOXA2* misexpression can ectopically induce MFP along the MHB as well as away from the MHB. (iv) In the absence of HH, the MFP can be converted into the MHB or the RP. (v) The loss of *FOXA2* converts the ventral midbrain and the MFP into the MHB. As a consequence of ectopic MHB induction, midbrain fate (*OTX2*+) is suppressed (not shown) and hindbrain fate (*GBX2*+, red) is induced. (vi) *FOXA2* overexpression combined with HH blockade results in ectopic RP induction throughout ventral midbrain.

in MFP maintenance in the fish (Blaess et al., 2006; Fedtsova et al., 2008; Fogel et al., 2008; Odenthal et al., 2000; Perez-Balaguer et al., 2009). In this study, we examined the precise requirement for HH signaling in midbrain MFP specification and show that it is required for ventralizing the MFP by turning on HH pathway and target genes (e.g., SHH, FOXA2, DISP1). However, it is insufficient for executing the full MFP program because it cannot turn on MFP-specific genes such as *DISP1, MN-CAD, LMX1B, LMX1A* and *BMP7*. We also show that HH blockade experiments between H&H 3–21 result in a loss of LFP, but do not eliminate all MFP markers (Bayly et al., 2007). Thus our data suggest that while HH signaling is necessary for MFP and LFP specification, it is only sufficient for LFP, but not MFP specification.

In this and previous work, we have also addressed the issue of the timing and duration of HH requirement (Bayly et al., 2007). Some studies have suggested that FP induction is accomplished at presomitic stages by a brief, but intense pulse of SHH (Patten et al., 2003 and Ribes et al., 2010). Interestingly, we and others have shown that although SHH transcripts are present at the axial midline by H&H 3, the HH signal transduction machinery (*PTC1, PTC2, HHIP, GLI1*) is not present until H&H 5 (Aglyamova and Agarwala, 2007 and Pearse et al., 2001). Surprisingly, the onset of SHH protein expression in the axial midline occurs later, at H&H 8−, when strong *GLI1* and *PTC1*, transcriptional targets and readouts of HH signaling, are also transiently seen at the FP (H&H 8 to <H&H 10; Aglyamova and Agarwala, 2007; Pearse et al., 2001).

This post-somitic expression of SHH proteins in the chick is in contrast to the presomitic SHH expression reported in the mouse, and suggests that HH-mediated FP specification in the midbrain may occur at different time points in these species (Blaess et al., 2006; Fogel et al., 2008; Marti et al., 1995; Placzek and Briscoe, 2005; Ribes et al.,

2010). Furthermore, neither the midbrain FP nor the subjacent notochord expresses the high levels of SHH seen at spinal cord levels (Ribes et al., 2010). However, it is still possible that midbrain FP patterning requires early and low/undetectable levels of the HH signaling emanating from the node or notochord (Jeong and McMahon, 2005; Placzek and Briscoe, 2005). Even so, HH signaling is still only necessary for the induction of HH-target/pathway genes at the ventral midline and not for the induction or blockade of MFP-specific markers such as *LMX1B* and *BMP7*. Thus the principal role of HH signaling in MFP patterning appears to be its ability to ventralize the FP. The precise molecular mechanisms underlying midbrain ventralization have not been extensively studied, but are likely to include the induction of HH pathway genes (*DISP1, PTC1*) and the exclusion of dorsal markers (*PAX7*) from the ventral neural tube (Bayly et al., 2007; Ericson et al., 1997; Fogel et al., 2008).

HH-independent mechanisms in the ventral midbrain patterning have also been noted in the Shh−/− and Smo−/− mice (Fogel et al., 2008). These mutants do not express Gli1 and Ptc1 in the FP and the entire ventral midbrain is dorsalized (Pax7+) by E9 (Blaess et al., 2006; Fogel et al., 2008). Although these results could be interpreted to signify an absolute requirement for HH signaling in the midbrain FP, a Pax7-negative ventral midbrain region is initially specified in the mouse, but it cannot be maintained beyond E9 without HH signaling (Blaess et al., 2006; Chiang et al., 1996; Fedtsova et al., 2008; Fogel et al., 2008). Taken together, these data may reconcile the apparent differences in chick and mouse midbrain FP specification by suggesting that the FP can be initiated in the absence of HH signaling, but requires HH signaling for its ventralization in both amniotes. A full comparison between the chick and mouse FP

however would require knowing whether MFP-specific gene induction also occurs in the Shh−/− and Smo−/− mice, but these data are currently not available.

FOXA2 is both necessary and sufficient for turning on *SHH* in the midbrain, but accomplishes the ventral midline induction of *LMX1B* and *BMP7* in a HH-independent manner. Its ability to induce *LMX1B*, a critical regulator of mDA neuron induction, may account for its greater potency in inducing mDA neurons (Andersson et al., 2006; Lin et al., 2009; Nakatani et al., 2010; Smidt et al., 2000; Yan et al., 2011). Whether *FOXA2* interacts with the Nodal pathway in the chick midbrain is currently under study in our laboratory. Previous studies suggest that joint misexpression of Nodal and *SHH* is sufficient to induce "area a" cells to a FP fate, but whether FP subregions differentially depend upon Nodal and/or *SHH* signaling is not known (Patten et al., 2003). Our preliminary data suggest that multiple TGFß ligands and their essential effectors (phosphorylated SMAD 2, 3) are active throughout the midbrain and are essential early regulators of FOXA2 expression in the FP (Amarnath et al., unpublished observations). Given their widespread distribution, any specific action of Nodal/TGFß signaling within the FP is likely to be mediated via regulation of FOXA2 at the axial midline.

Since *SHH* can induce *FOXA2*, why is *SHH* not as potent as *FOXA2* in MFP induction? One reason for this is that *SHH* protein is not expressed in the axial midline at early stages when *FOXA2* protein expression is clearly detected (this study; Ruiz i Altaba et al., 1993). Since onset of *LMX1B* and *BMP7* mRNA expression at the ventral midline occurs prior to SHH protein expression and *FOXA2* can induce these and other MFP markers in a HH-independent manner, *FOXA2* is likely to initiate the MFP program in the midbrain and not *SHH* (Amarnath et al., unpublished data; Yuan and Schoenwolf, 1999). However, once expressed, *SHH* must rapidly take control of *FOXA2* expression

since cyclopamine-treated explants collected at H&H9, one stage (~90 min) after the onset of SHH protein expression, display severely reduced *FOXA2* (Fig. 3.3F). This short time however is not sufficient to turn down *LMX1B* expression in such explants, despite the critical role of *FOXA2* in its induction (Fig. 3.4A–H).

The role of SHH and FOXA2 in regulating midbrain's signaling centers

Signaling centers that pattern a given tissue are known to cross-regulate each other. Such cross-talk is a key to establishing a 3-dimensionally correct tissue pattern and has been noted between the signaling centers of the limb (Bénazet and Zeller, 2009; Duboc and Logan, 2011). Evidence has also recently accumulated that the modulation of one of midbrain's signaling centers affects the patterning or maintenance of other signaling centers (Aoto et al., 2002; Basson et al., 2008; Blaess et al., 2006, 2011; Fogel et al., 2008).

A clear role for *SHH* in the maintenance of the MHB and suppression of the RP program has been established in the chick and/or mouse (Bayly et al., 2007, Blaess et al., 2006; Fogel et al., 2008). Ventral blockade of *SHH* and *FOXA2* cause an expansion and ectopic induction of RP in dorsal midbrain in both chick and mouse, while their overexpression suppresses RP induction (data not shown; Fogel et al., 2008). Although this could be interpreted as a generic role for SHH in ventralization, our previous data demonstrate specific up and downregulation of dorsal midbrain genes by *SHH* (Fogel et al., 2008). Whether *SHH* regulates RP specification directly or indirectly is not known, although a transient, early wave of *SHH* activity floods and then recedes from the dorsal neural tube, and HH effectors, *GLI1*-*GLI3* are all expressed dorsally (Aglyamova and Agarwala, 2007 and Chamberlain et al., 2008). Finally, multiple HH-binding proteins and

pathway members, which could potentially transduce HH signals (e.g., Megalin, BOC), are also expressed in dorsal midbrain (Aglyamova and Agarwala, 2007).

In this study, we show that ventral midline cells can become MFP or RP, depending on whether HH signaling is present or absent. Why only a handful of MFP cells take on the RP phenotype is not understood. Given the mosaic nature of FP gene expression, one possibility is that only a subset of *LMX1B*+ MFP cells are competent to turn on RP fates in the absence of HH signaling. Alternatively, we and others have noted the scarcity of HH-negative cells at the ventral midline following attempts to block HH signaling in this region (Bayly et al., 2007; Briscoe et al., 2001; Wijgerde et al., 2002). This may be due to the differential cell-affinity based segregation of HH-negative and HH+ cells as noted in the fly (Rodriguez and Basler, 1997). In this scenario, only a few HH-negative cells would remain at the ventral midline, although all of these would turn on RP fates in the absence of HH signaling.

The midbrain–hindbrain boundary

Previous studies suggest that although SHH is not required for MHB induction, it is required for maintaining its spatial coherence and signaling properties (Aoto et al., 2002; Bayly et al., 2007; Blaess et al., 2006, 2008). In the mouse, the absence of SHH results in a progressive loss of FGF8 and a near complete loss of *WNT1* in the MHB by E12.5 (Blaess et al., 2006 and Fogel et al., 2008). Interestingly, *GLI1*-*GLI3* and Megalin are all expressed within the chick MHB at various time points, and MHB regulation by GLI3 has been clearly demonstrated (Aglyamova and Agarwala, 2007, Aoto et al., 2002 and Blaess et al., 2008). Here we extend these observations to show that overexpression of *SHH* blocks MHB induction by converting the MHB into a MFP fate. Together these results show that the MHB is sensitive to both increased and decreased levels of HH

signaling, being converted to MFP in the presence of excess *SHH* and losing its signaling properties when SHH is downregulated.

More surprisingly, the absence of HH signaling can also convert the MFP into the MHB. In such experiments, the MHB can also be converted into a *GDF7*+/*WNT1*+ RP. Fate mapping and lineage analyses suggest a common set of precursors for the MHB and the RP, which might explain their inter-convertibility in our experiments (Alexandre and Wassef, 2003; Zervas et al., 2005). To our knowledge, no common RP/MFP or MFP/MHB precursors have been described. However, as we demonstrate in Fig. 3.1K, L, all 3 signaling centers are physically contiguous and cell exchange among them is therefore feasible. We also note that all midbrain signaling centers express a common set of developmental control genes (*BMP7*, *LMX1B*). Although the significance of BMP7 expression in all 3 signaling centers is not understood, *LMX1B* is clearly involved in FP, MHB and RP specification (Adams et al., 2000; Chizhikov and Millen, 2004; Matsunaga et al., 2002; Millen et al., 2004; O'Hara et al., 2005; Yan et al., 2011). Thus, LMX1B may be a key regulator of midbrain signaling center induction and may specify the MFP, MHB or RP depending upon the specific cellular context. If so, a key component of that cellular context would be the presence or absence of SHH.

Chapter 4: A simple technique for early in vivo electroporation of E1 chick embryos[2]

INTRODUCTION

The introduction of in vivo electroporations to alter gene regulation has revolutionized the use of the chick as an embryonic model system (Itasaki et al., 1999; Voiculescu et al., 2008). This technique involves using small electric shocks to open up transient pores within cell membranes. DNA, RNA interference constructs, or morpholinos can enter the cell through these pores and alter gene function (Sauka-Spengler and Barembaum, 2008). The most common electroporation paradigms involve relatively high voltages (10–25V) and large diameter (~400–500 μm) electrodes held at a fixed distance (Funahashi et al., 1999; Itasaki et al., 1999; Muramatsu et al., 1997; Sakamoto et al., 1998). While such "macroelectroporation" paradigms produce large swaths of transgene expression, they often lead to extensive damage, making them unsuitable for certain types of tissues and experiments (Agarwala et al., 2001).

A few years after the innovation of "macroelectroporation" techniques, "microelectroporation" techniques were introduced, which used lower voltages (~7V) and a small-diameter (40 μm) negative tungsten electrode (Momose et al., 1999a). These authors reported efficient and focal transgene expression along with improved tissue health and embryonic viability (Momose et al., 1999). In previous work, we adapted this

---

[2] These data were published in the following articles:

Brown, C.Y., Eom, D.S., Amarnath, S., and Agarwala, S. (2012a). A simple technique for early in vivo electroporation of E1 chick embryos. Dev. Dyn. *241*, 545–552.

Brown, C.Y., Eom, D.S., Amarnath, S., and Agarwala, S. (2012b). In vivo electroporation of E1 chick embryos. Cold Spring Harb. Protoc.

C.Y. Brown, D.S. Eom and S. Amarnath worked collaboratively to develop this electroporation technique. S. Amarnath provided figure 4.2 E-H. All figures are from C.Y. Brown.

technique to study the morphogenetic function of Sonic Hedgehog (SHH) and created focal sources of SHH in distinct shapes and patterns in the chick midbrain (Agarwala et al., 2001). In recent years, we have successfully microelectroporated ≥HH7 chick midbrains in ovo, although only a small percentage of embryos electroporated at HH7 remained viable and suitable for analyses (Bayly et al., 2007).

In vivo electroporation paradigms targeting ages ≤HH7 have not yet been developed. This is in part due to the tissue damage, dysmorphology, and embryonic lethality associated with the large currents required for such in ovo electroporations (Voiculescu et al., 2008). In addition, many tissues undergoing morphogenesis, e.g., the neural plate, do not yet possess lumina within which the DNA can be injected prior to electroporation. Thus, most experiments requiring E1 electroporations (≥HH3) have employed in vitro paradigms with varying degrees of success (Hatakeyama and Shimamura, 2008; Tanaka et al., 2010; Uchikawa, 2008; Voiculescu et al., 2008). However, many morphogenetic events that occur at E1 (e.g., neural tube closure) involve complex 3-dimensional tissue transformations that would ideally be studied in vivo.

In this study, we report that further modifications of the microelectroporation technique permit the easy in ovo electroporation of E1 embryos as young as HH4. Such electroporations have a reasonable rate of success, and can be focally targeted to specific regions of the neural tube and do not require that the neural tube be closed (Eom et al., 2011, 2012). Furthermore, they do not significantly alter cell-fate specification, 3-dimensional tissue morphology, or size. We have recently successfully used this method to study the early cellular and molecular events involved in midbrain neural tube closure (Eom et al., 2011, 2012).

EXPERIMENTAL PROCEDURES AND RESULTS

Electrode Assembly

A cheap and simple electrode for microelectroporation purposes was devised by Dr. R. Parnaik in Dr. Clifton Ragsdale's laboratory at the University of Chicago and was modified for use in our early electroporations (Parnaik and Ragsdale, unpublished methods). This involved cutting the top and bottom of a cotton swab and using its hollow plastic "sleeve" for insulating the electrode (Fig. 1A). The negative electrode was made from a 25-μm-diameter platinum wire (AM Systems, Carlsborg, WA) wrapped around a "female/socket" gold pin connector (Newark Electronics, Newark, NJ), and then threaded through the plastic sleeve of the cotton swab (Fig. 1A). Approximately 2-mm wire protruded from the plastic sleeve at the electroporating end and was fixed to the sleeve with tacky wax (available at hardware stores; Fig. 1A). The positive electrode was similarly constructed from 50-μm-diameter platinum wire (AM Systems), with approximately 1-cm wire protruding from its front/electroporating end. The protruding length of wire was gently curved at a ~ 130° angle at its approximate midpoint (Fig. 1D–F). This curve allowed for easy insertion underneath the embryo during electroporations, and for reducing the embryo's exposure to an applied electric current. The cables connecting the electrodes to the electroporator (ECM 830; Harvard Apparatus, Holliston, MA, via VWR) were modified by replacing the "micrograbber" alligator clip terminals with "male" gold pin connectors (panels 3–5 in Fig. 1A). The male pins were inserted into the female sockets attached to each electrode to complete the electric circuit. These modifications made the connecting cables lighter and more ergonomic, allowing us to hold the electrodes by hand during long bouts of electroporation.

Since the diameter of each electrode was small, no etching or grinding of the tip was necessary (Agarwala et al., 2001; Momose et al., 1999b). However, we repeatedly cut off the tips of our negative electrodes (~once/12 electroporations) as they became coated with albumen and less able to conduct current. In addition, the exposed portion of the positive electrode was cleaned frequently by gently scraping the wire with forceps to remove any albumen or yolk deposited on its surface. This ensured that the conductivity of the electrodes remained the same over successive electroporations.

In Ovo Electroporation

Egg preparation and the standard electroporation reagents and techniques can be obtained from published protocols and are not described here (Gammill and Krull, 2011; Voiculescu et al., 2008). Eggs were windowed either 4–5 hr after the start of incubation at E0, or just prior to electroporation at E1 using previously established protocols (Agarwala et al., 2001). For electroporations, embryos were irrigated with 2–3 drops of Ringer's solution. A 1-ml tuberculin syringe fitted with a 30-gauge hypodermic needle was filled with 1% India ink (Pelikan, Hamburg, Germany) dissolved in Chick Ringer's solution. The needle was bent at a 130° angle, inserted through area opaca, and positioned underneath the embryonic area targeted for electroporation (Fig. 1B). Since India ink injections were a factor in the embryonic lethality and deformation, only the smallest volume (~ 20 µl) required for visualization was injected, with care taken to prevent any disruption of the yolk (Voiculescu et al., 2008).

Approximately 2 µl of circular plasmid DNA (1 µg/µl) in a 0.1% Fast Green (Sigma, St. Louis, MO) solution in double distilled H2O was front-filled into a glass capillary tube (Sigma) using a vacuum source attached to a picospritzer (World Precision

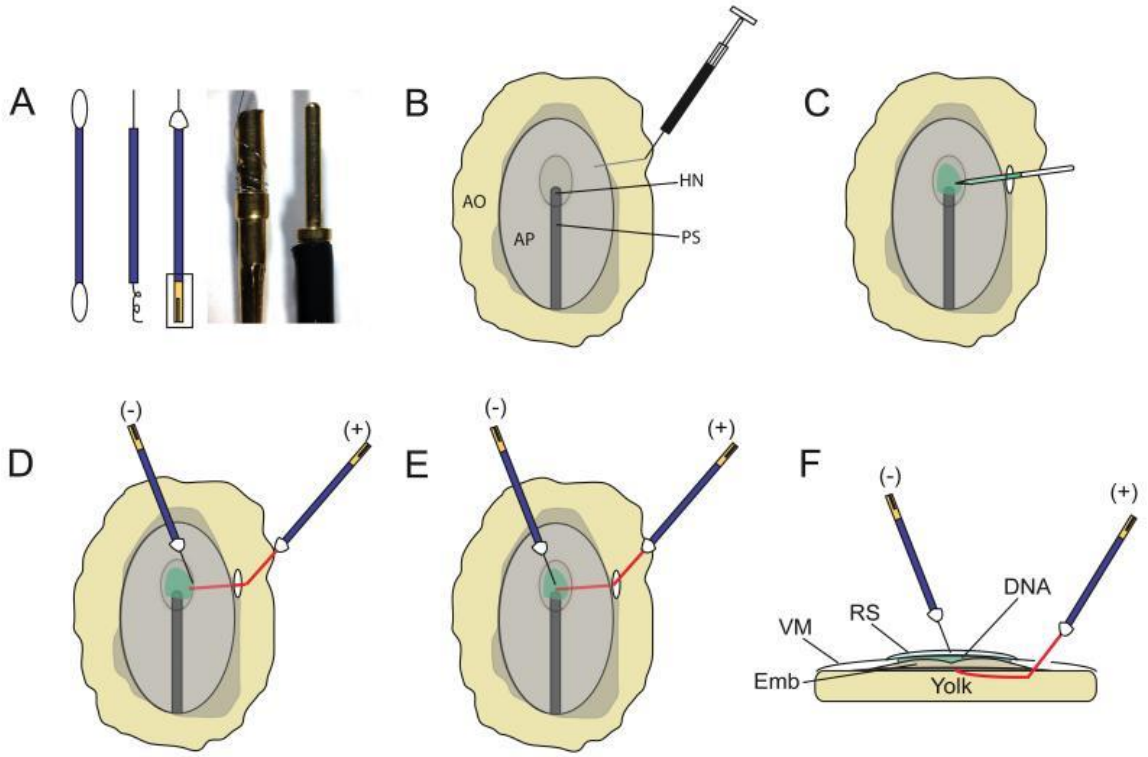

Figure 4.1 The experimental setup for early electroporations

(A) Electrode assembly. Electrodes were made from platinum wire threaded through the hollow plastic sleeve of a cotton swab (panels 1, 2). The wire was fixed to the top of the plastic sleeve with tacky wax (white triangle, panel 3). The bottom end of the wire was wrapped around a "female" socket pin (box, Panel 3). Panel 4 shows a magnified view of the female socket pin, (boxed area in panel 3). A "male" gold pin (panel 5) soldered to the connecting cables (not shown) is inserted into the female pin to complete the circuit. (B-E) Top-down view of HH5 embryo demonstrating the electroporation procedure. (B) India ink injection for visualizing the embryo. **(C)** Injection of the DNA and Fast Green solution between the vitelline membrane and the region (e.g. presumptive midbrain) of the embryo targeted for electroporation. (D-F) Electrode positions for dorsal (D) ventral (E, F) electroporations. A cross-sectional view of E is shown in F. The paler segments of the capillary tube (C) or the positive (+) electrode (D, E) depict the segments of each that lie subjacent to the vitelline membrane and are thus partially obscured from view.

Instruments, Sarasota, FL). This volume of DNA was sufficient to electroporate up to 24 HH4–6 embryos, with each embryo receiving approximately 50–300 nl of the DNA/Fast Green solution.

Prior to electroporation, HH4–6 embryos were re-irrigated with ~10 drops of Ringers' solution. A small incision was made in the vitelline membrane at the area opaca, area pellucida interface with a pair of no. 55 forceps. The DNA-filled capillary tube was inserted via this incision into the space between the vitelline membrane and the target tissue, in our case, the presumptive midbrain neural plate (Fig. 1C; Eom et al., 2011). DNA solution sufficient to cover the entire target region was then expelled from the capillary tube using a picospritzer attached to a foot pedal (Fig. 1C).

Although the incision was made at a distance from the injection site to prevent DNA diffusion, the DNA was not confined within an enclosed space and dispersed rapidly within 0.5–1 min. This required the speedy execution of the subsequent steps. The negative electrode was positioned so that < 1 mm of its tip was submerged in the Ringer's solution previously applied to the vitelline membrane surface. The positive electrode was positioned subjacent to the region to be electroporated, via the incision previously used to introduce DNA. The tip of the positive electrode was directly underneath the target region, while the remaining length of the electrode curved away from this region (Fig. 1D–F). When properly positioned, the 2 electrodes subtended a ~100–110° angle with each other (Fig. 1D–F). Electrodes were held by hand for optimal positioning and care was taken to avoid damage and dysmorphology by preventing the electrodes from coming in contact with one another or the embryo. A foot pedal attached to the electroporator was employed to transfect the DNA using three 50-msec, 5V-pulses, separated by 100-msec interpulse intervals. Following the procedure, the egg was sealed

with polyethylene tape (3M, Austin, Texas) and returned to the incubator until required for further analyses.

Efficacy of Electroporation

Unlike in vitro HH3 manipulations, very few embryos survived in vivo electroporations at HH3 and were not analyzed further (Tanaka et al., 2010). When electroporated at HH4–6, 55.55% embryos (n=40/72) survived until E4. Ten percent of the surviving embryos (n=4/40) were deformed and were excluded from further analyses. Eighty percent of the remaining embryos (n=32/40) displayed robust GFP/RFP expression between 3 hr to 4 days of electroporation (Fig. 2; Eom et al., 2011).

Controlling the Size and Location of the Electroporation

The electroporations could be controlled to produce unilateral or bilateral, broad or focal, dorsal or ventral midbrain transgene misexpression (Fig. 2A–H). The size of the electroporation was controlled by altering the distance between the two electrodes, usually accomplished by regulating the extent to which the negative electrode was submerged in Ringer's solution (compare Fig. 2A, B, and F). To a smaller extent, this could also be accomplished by moving the positive electrode in depth, toward the yolk and away from the embryo. In the latter case, care was taken to prevent disruption of the yolk, as this resulted in reduced embryonic viability. In addition to reducing the size of the electroporation, this also helped minimize damage. Moving the electrodes laterally away from the axial midline produced dorsal or dorsolateral electroporations (Figs. 1D, 2C; see also Fig. 4B). By contrast, moving the electrodes toward the axial midline generally produced ventral electroporations (Figs. 1E, F, 2A, B, D).

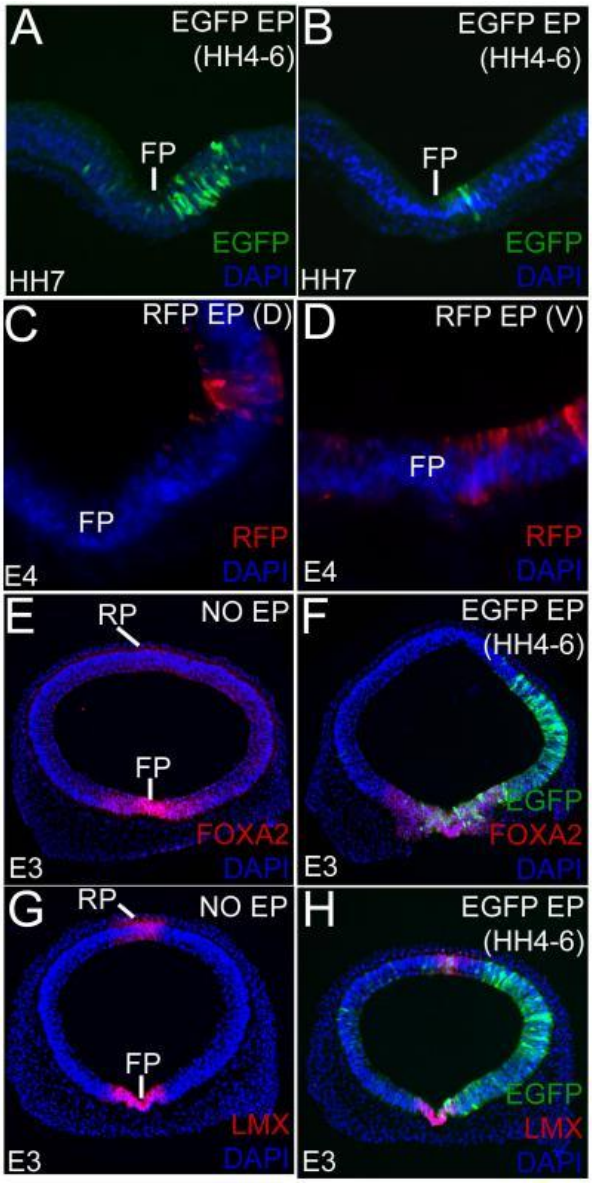

Figure 4.2 Early electroporations can be varied in size and location and do not affect cell fate specification

(A, B) Broad (A) and focal (B) ventral EGFP expression in HH7 midbrains electroporated at HH5. All sections (A-H) are counterstained with DAPI (blue). (C, D) E4 brains showing targeted dorsolateral (C) and ventral (D) RFP electroporations. (E-H) Un-electroporated (E, G) and early-electroporated (F, H) midbrains showing that broad, unilateral EGFP electroporations do not affect FOXA2 and LMX1A/B expression in the floor plate (FP) and roof plate (RP) at E3.

Cell Fate Specification Is Not Affected by E1 Electroporations

To determine whether early electroporations affected midbrain patterning, we compared the FOXA2 and LMX1A/B expression in the control and early-electroporated midbrains at E3 (Fig. 2E–H). No differences in FOXA2 (floor plate) and LMX1A/B (roof plate and floor plate) expression patterns were noted between the un-electroporated controls and the EGFP/RFP electroporated embryos (Fig. 2E–H). Thus, as seen with late-stage electroporations in many studies, early electroporations did not affect cell-fate specification (Bayly et al., 2007; Eom et al., 2011).

Early Electroporations Do Not Affect Midbrain Size or Morphology

We compared the gross morphology of E4 embryos electroporated at HH 4–6 with that of un-electroporated embryos (Figs. 2, 3). In general, the early-electroporated embryos appeared to be slightly smaller, although the differences in their rostrocaudal lengths were not significant (Fig. 3A–C; rostrocaudal length, un-electroporated embryos: 15.55 mm; early-electroporated embryos: 14.27 mm; $P = 0.525$). The cross-sectional morphology and circumference of the HH4–6 electroporated midbrains were also comparable to the un-electroporated controls (Fig. 3D–F; circumference, un-electroporated midbrains: 3.67 mm; early-electroporated midbrains: 3.20 mm; $p = 0.495$). The ventral and dorsal thickness of midbrain neurectoderm also did not differ between un-electroporated controls and early-electroporated embryos at E4 (Fig. 3D, E, G; ventral thickness, controls: 124.38 μm; electroporated: 120.68 μm; $p = 0.798$; dorsal thickness, controls: 79.11 μm; electroporated 79.94 μm; $p = 0.819$). We conclude that early-electroporations do not significantly affect tissue size and morphology.

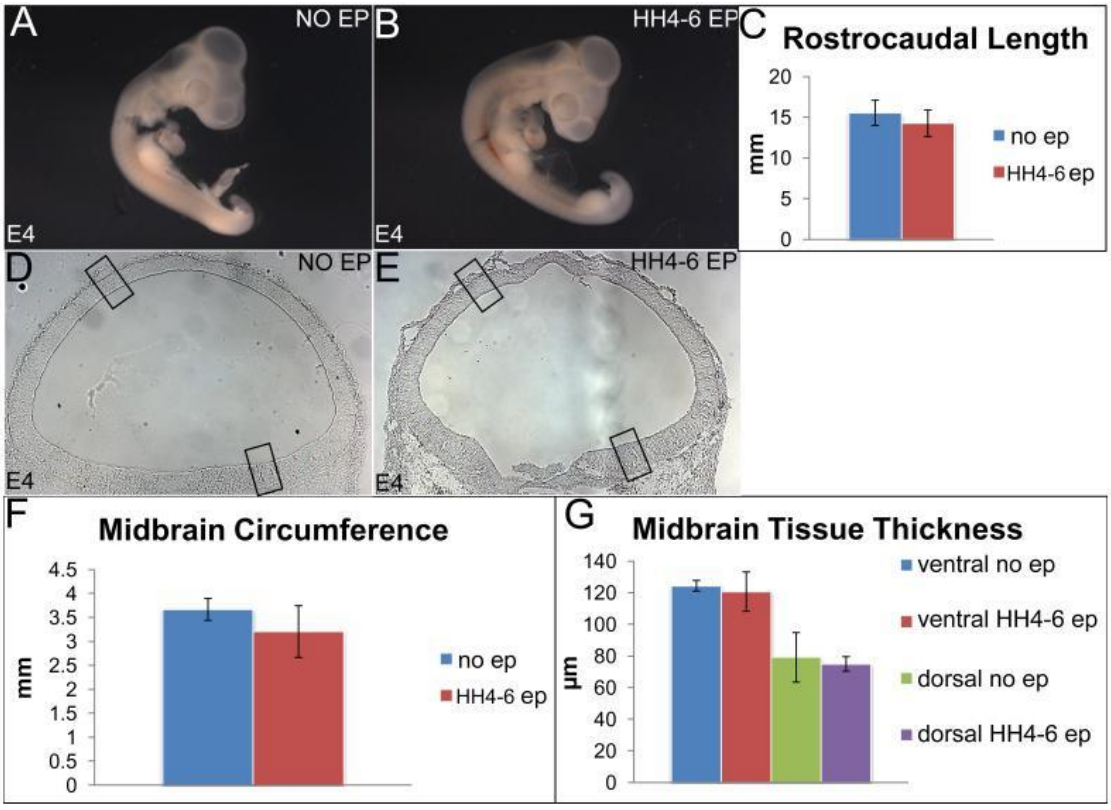

Figure 4.3 Early electroporations do not affect the size of the embryo, midbrain size and morphology

(A-C) Sagittal view of un-electroporated (A) and early-electroporated (B) embryos showing no significant differences in their rostrocaudal length. (C) Quantitation of A, B (rostrocaudal length, un-electroporated: 15.55 +/− 0.525mm; early-electroporated 14.27 +/− 0.945 mm; p=0.525. (D, E) Un-electroporated (D) and early-electroporated midbrains (E) showing similar sizes and tissue morphology. (F, G)Quantitative data demonstrating that midbrain circumference (F) and ventricular-pial thickness (G) do not differ in un-electroporated and electroporated embryos. (Circumference: un-electroporated: 3.67 +/− 0.229 mm; early electroporation: 3.20 +/− 0.540 mm; p= 0.495; ventral thickness: controls 124.38 +/− 3.35 µm; electroporated: 120.68 +/− 12.44 µm; p=0.798; dorsal thickness: controls: 79.11 +/− 15.66 µm; electroporated 79.94 +/− 4.60 µm; p=0.819).

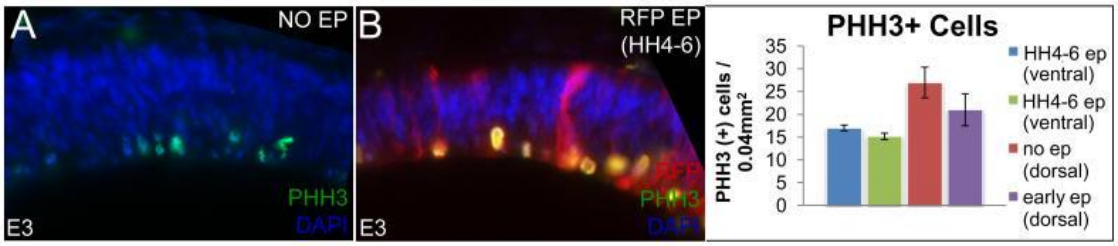

Figure 4.4 Early electroporations do not affect cell proliferation

(A-B) Comparable pHH3 staining in dorsal midbrain in control (A) and early-electroporated (B) embryos. Note that pial is up and ventricular is down in this dorsal section and that PHH3+ cells occur along the ventricular/apical surface lining the lumen of the midbrain. (C)Quantitation of cell proliferation in dorsal and ventral midbrain. (Number of mitotic cells/ 0.04 mm^2: un-electroporated ventral midbrains: 17.00 +/− 0.65 cells; early-electroporated ventral midbrain: 15.16 +/− 0.70 cells; p= 0.168; un-electroporated dorsal midbrains: 27.00 +/− 3.36 cells; early-electroporated dorsal midbrains: 21 +/− 3.51 cells; p= 0.270).

Cell Proliferation Is Not Affected by Early Electroporations

We next compared cell proliferation in ventral and dorsal midbrains at E3 in control and early electroporated embryos and found that the number of pHH3+ cells did not differ between the two groups (Fig. 4A–C; number of pHH3+ mitotic cells/0.04 mm2, un-electroporated ventral midbrain: 17.00 cells; early-electroporated ventral midbrain: 15.16 cells; P = 0.168; un-electroporated dorsal midbrain: 27.00 cells; early-electroporated dorsal midbrain: 21 cells; P = 0.270).

Cell Death and Early Electroporations

Few and variable numbers of activated caspase3+ apoptotic cells were noted in control and electroporated embryos examined at E4 (Fig. 5A–C). Compared to controls, the number of apoptotic cells more than doubled in the early electroporated midbrains (average number of caspase3+ cells/control brain, 4.3; early electroporations, n=10; P = 0.086). However, possibly due their small numbers and the high degree of within-group variability, differences in the numbers of apoptotic cells between un-electroporated and early electroporated were not significant. Similar comparisons of apoptosis between early versus late electroporations were also not significantly different (average number of caspase3+ cells/midbrain early, n=10; late, n=8.67; p = 0.575). Notably, the total number of apoptotic cell/brain in each group was small (< 2 cells/14-μm section). As a result, electroporation-induced apoptosis did not result in altered cell fate specification, cell-proliferation, or in significant differences in midbrain size and morphology (Figs. 2–4).

DISCUSSION

Our study shows that embryos ≥ HH4 can be electroporated in ovo without perturbing overall 3-dimensional morphology, tissue size, cell proliferation, and cell-fate specification. Furthermore, by trapping the DNA between the vitelline membrane and the

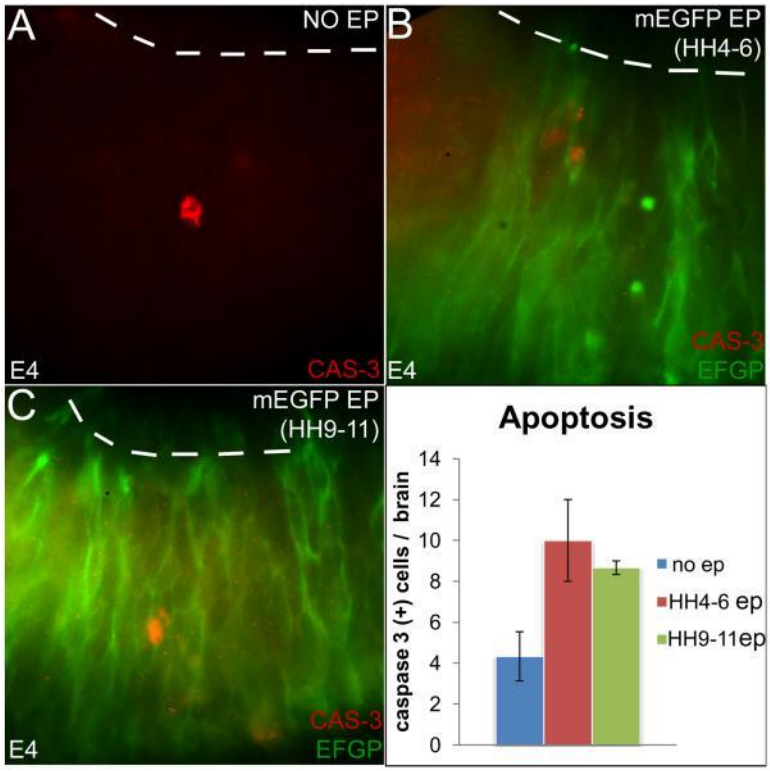

Figure 4.5 The rate of apoptosis does not differ between control, early and late electroporated midbrains

(A-C) Activated cas-3 staining demonstrating apoptosis in control (A), early-(B) and late-electroporated (C) midbrains. (D) Quantitation of apoptosis, showing that cell death does not differ between control and early-electroporated midbrains or between early and late-electroporated midbrains. (Un-electroporated controls: n=4.3 +/− 1.20 cells/midbrain; early electroporations: n=10 +/− 2 cells/midbrain; p=0.086. early electroporations: 10 +/− 2 cells/midbrain; late electroporations: 8.67 cells +/− 0.33 cells/brain; p=0.575).

target tissue, our paradigm obviates the need for confining DNA within an enclosed lumen and can thus be adapted for a wide variety of tissues at many ages. In our hands, the critical parameters involved in successfully electroporating HH4–6 embryos were low voltage and electrode design, diameter and placement. Together, these modifications enabled us to bring the electrodes closer together, giving us the ability to focally electroporate targeted regions of the neural plate without causing damage. While 5V was the lowest voltage that could be applied with the ECM830 electroporator, a smaller voltage/current can potentially be elicited by including a set of resistors in the electric circuit, or utilizing an electroporator capable of applying a lower voltage (e.g., CUY21EX electroporator; Bex Co. Ltd, Tokyo, Japan; Table 1).

As noted by previous studies, an important variable in embryonic viability was the type and amount of India ink used. We had the best viability with the smallest volume (~20 μl/embryo) and lowest concentration (1%) of India ink that permitted good visualization of the embryo (Voiculescu et al., 2008). In addition, the India ink became particulate with age and affected embryonic viability. In our hands, it was best used within 6 months after it was opened and discarded if it became particulate before that.

It is not fully clear to us why HH3 embryos did not survive our electroporations, while a significant number of HH4 embryos did. The survival at HH5–6 was higher still. One possible explanation for this is the progressive epithelialization of the chick neurectoderm over this time period, as also noted in the zebrafish (Dominic and Agarwala, unpublished observations; (Eom et al., 2011, 2012; Hong and Brewster, 2006). The idea is that as the neural plate progresses from a partially to a fully polarized epithelium, it may better withstand the electrical insult imposed by electroporation (Voiculescu et al., 2008). Thus, in vitro paradigms need to be employed until further

innovation makes ≤HH3 in vivo electroporations feasible (Tanaka et al., 2010; Uchikawa, 2008).

Chapter 5: Bone Morphogenetic Proteins (BMPs) regulate neural tube closure by cell cycle dependent mechanisms: a 4D time-lapse analysis

INTRODUCTION

One of the earliest events in neural tube closure is the formation of the median hinge point (MHP) which buckles the developing neural plate at the midline and lifts the neural folds (Smith and Schoenwolf, 1987). Hinge point formation is known to involve stereotypical cell behaviors, including apical constriction, basal nuclear localization and apicobasal shortening (Eom et al., 2011, 2012; Haigo et al., 2003; Jacobson et al., 1986; Schoenwolf, 1985; Smith and Schoenwolf, 1987).

There is evidence that the apical constriction required for hinge point formation is actin cytoskeleton dependent (Haigo et al., 2003; Hildebrand, 2005; Martin and Goldstein, 2014; Nishimura and Takeichi, 2008). These studies suggest that Shroom3 (an adherens junction scaffolding protein) recruits Rho kinase (ROCK) to the adherens junctions where it phosphorylates and activates Myosin II and leads to constriction of the adherens belt (Haigo et al., 2003; Hildebrand, 2005; Nishimura and Takeichi, 2008). Another possible mechanism that has recently been proposed is that planar cell polarity (PCP) dependent junctional remodeling associated with convergent extension results in constriction of the apical surface (Nishimura et al., 2012). However, these models to not take into account the interkinetic nuclear migration (IKNM) of neural progenitors in the amniote which results in only a slender process of each cell contacting the apical surface.

The amniote neurepithelium is pseudostratified and cells are bipolar with cell processes that extend to the apical and basal surfaces (Baye and Link, 2007; Sauer, 1935; Sauer and Walker, 1959). As neural progenitor cells progress through the cell cycle, they undergo IKNM where the cell body/nucleus moves along the apical-basal axis while the

ends of the cell remain in contact with the both the apical and basal surface (Baye and Link, 2007; Sauer, 1935; Sauer and Walker, 1959). Mitotic nuclei are localized to the apical surface, while G1, S and G2 phase nuclei are located throughout the apicobasal thickness of the tissue (Baye and Link, 2007; Guthrie et al., 1991; Kosodo and Huttner, 2009). Since the cell body/nucleus is the widest part of the cell, localization of the nucleus away from the apical surface, as a consequence of IKNM, results in an inherent decrease in apical surface area. This has resulted in controversy in the field as to the contribution of apical constriction (via actin based mechanisms) versus basal nuclear localization in hinge point formation because the apical processes of bipolar cells may be so fine that their constriction is unlikely to substantially reduce apical surface area. In this scenario, only the constriction of apically localized mitotic cells can substantially contribute to the decrease in apical surface area, and the apical constriction and basal localization of nuclei characteristic of hinge point formation could be a result of cell cycle regulation which keeps the cell out of mitosis and the nucleus away from the apical surface (for example, prolongation of G1, S or G2 phase).

Interestingly, BMP signaling is modulated in both a mediolateral and apicobasal, cell cycle dependent manner (Eom et al., 2011, 2012). Mitotic cells exhibit high levels of BMP signaling (as evidenced by high pSMAD1,5,8) while cells in other phases of the cell cycle have relatively low BMP signaling activation by comparison (Eom et al., 2011, 2012). BMP signaling is also regulated along the mediolateral axis of the neural plate where there is low BMP signaling in the MHP and increasing amounts of BMP signaling in more lateral tissues (Eom et al., 2011, 2012). In addition to having low levels of signaling at the endogenous MHP, our lab has shown that BMP blockade is sufficient to

induce ectopic hinge points that mimic the endogenous MHP based on morphology and cell behaviors.

It is also known that BMP signaling can regulate cell cycle kinetics. For example, BMP blockade in neural crest cells has been shown to block the G1 to S transition (Burstyn-Cohen and Kalcheim, 2002; Burstyn-Cohen et al., 2004). In addition, BMP misexpression has been shown to decrease the number of BrdU+ nuclei after pulse labeling (Ille et al., 2007). Since BMP signaling regulates HP formation and cell cycle kinetics, it is possible that signaling controls IKNM and cell cycle regulation in order to localize the nuclei basally, contributing to HP formation. To adequately test this hypothesis, we must visualize cell cycle dynamics in real time. In this study, we use Noggin mediated ectopic hinge points as a model by which to elucidate the mechanisms of MHP formation. We utilize a novel organotypic explant system to visualize hinge point formation in real time and study the cellular mechanisms involved. Here we find that BMP signaling regulates HP formation by altering cell cycle kinetics in a phase dependent way such that the cells stay in interphase and away from the nucleus.

RESULTS

WT MHP cells exhibit decreased and sub-apical mitosis

To explore whether there are alterations in mitosis at the MHP we used phosphohistone H2 (PHH3) to study the number and localization of mitotic cells. We found that the number of mitotic cells at the ventral midline decreases as the MHP forms. At HH4-5 before the midline buckles, there are 4.17 ± 0.31 (n=6) mitotic cells at the midline, but at HH6-7 there are 0.5 ± 0.22 (n=6) mitotic cells in the, now forming, MHP,

indicating a significant decrease in mitotic index at the MHP ($p=2.2 \times 10^{-6}$; Figure 5.1A-D). This decrease in the number of mitotic cells makes sense in the context of apical constriction and basal nuclear localization. Since the cell nucleus is the widest part of the cell and mitosis occurs at the apical surface, decreasing the number of mitotic cells would inherently lead to a reduction in the apical surface area of this tissue. In addition, since cells are only at the apical surface for mitosis, a decrease in mitosis also corresponds with basal nuclear localization since non-mitotic cells are localized more basally. A subset of the cells that do undergo mitosis at the MHP do so sub-apically (n=3); Figure 5.1C, E), which again, supports the idea that regulation of mitosis coordinates with the cell behaviors necessary for HP formation.

Ectopic hinge points induced by BMP blockade display reduced mitotic index and sub-apical mitosis similar to the endogenous MHP

Previous data in the lab have shown that BMP signaling occurs in a gradient with high levels of signaling at the neural folds and low levels of signaling at the MHP (Figure 5.1F; Eom et al., 2012, 2011). However, at the MHP where BMP signaling is low overall, signaling is high in mitotic cells and low in the more basally localized interphase cells suggesting that BMP signaling is coordinated with cell cycle phase (Figure 5.1F). In addition, BMP blockade induces effects on mitotic index and localization, as shown below (Figure 5.1E, G-J).

Alterations in BMP signaling result in mislocalization of mitotic nuclei. Under normal circumstances, non-HP cells undergo mitosis at the apical surface and then move basally, away from the apical surface (Figure 5.1A, E, J, Figure 2 C-C'''). However, BMP blockade results in sub-apical mitosis (Figure 5.1G-H, J). Although not all mitotic nuclei are sub-apical, on average, Noggin electroporated, PHH3+ mitotic nuclei are more

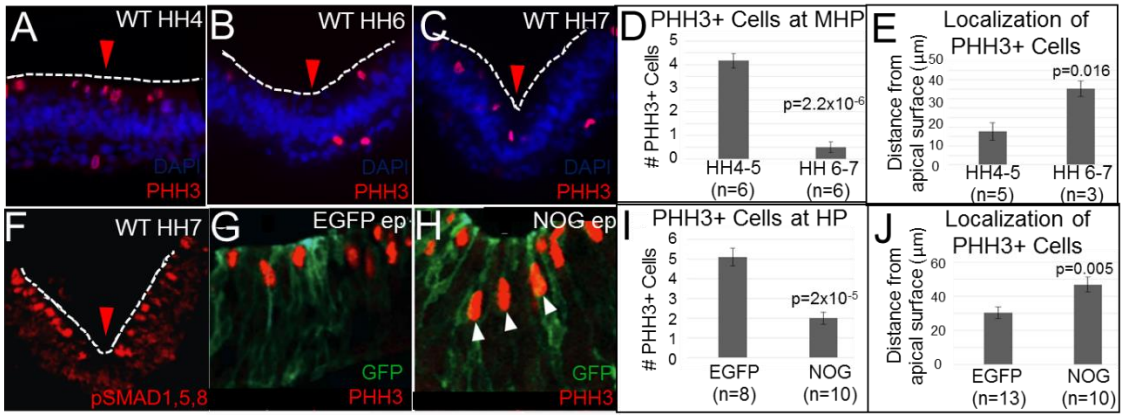

Figure 5.1 BMP blockade mimics MHP behaviors

A-C) Neural plate sections showing Phosphohistone H3 (PHH3) positive mitotic cells (arrowheads denote ventral midline; dotted line denotes apical surface). A) WT HH4 neural plate showing mitotic cells at the ventral midline. B) WT HH6 neural plate showing reduced mitosis at developing MHP. There are so few mitotic nuclei at the MHP that some sections have no mitotic cells in the MHP C) WT HH7 neural plate showing mitosis at MHP occurs subapically. D) Quantitation showing number of PHH3+ cells at the ventral midline/MHP (HH4-5 4.17±0.31 cells, n=6; HH6-7 0.5±0.22, n=6; $p=2.2x10^{-6}$). E) Quantitation of PHH3+ mitotic cell localization showing distance from the apical surface is increased in the HH6-7 MHP versus the HH4-5 ventral midline (HH4-5 16.48±4.38 n=5; HH6-7 39.87±5.62 p=0.016). F) Phosphorylated SMAD 1,5,8 (pSMAD1,5,8) expression in HH7 neural plate showing high BMP activity in apically localized mitotic cells and low signaling in interphase cells. G-H) PHH3+ mitotic cells in EGFP control (G) or Noggin (NOG) (H) electroporated cells. Arrowheads denote subapical mitosis. I) Quantitation showing # of PHH3+ cells in EGFP versus NOG induced ectopic hinge points (EGFP 5.11±0.45; NOG 2.0±0.30 $p=2.0x10^{-5}$) (J) Quantitation of PHH3+ mitotic cell localization showing distance from the apical surface is increased in Noggin electroporated cells versus EGFP electroporated cells (EGFP 30.37±3.38; NOG 46.82±4.49 p=0.005). Significance for all statistics was determined via student's two-tailed t test.

than twice as far away from the apical surface versus controls (Figure 5.1G-H, J). Together, with the fact that BMP blockade decreases mitosis (Figure 5.1I and data not shown), these data suggest that BMP may induce HPs via cell cycle modulation. By reducing the number of apically localized mitotic cells, BMP blockade is, in effect, inducing basal nuclear localization and causes a resulting decrease in apical surface area.

Explant system allows real time analysis of cell behaviors during MHP formation

To explore the role of cell cycle modulation on HP formation, we developed a 3D explant system by which we can visualize cell cycle dynamics in real time. We developed an organotypic midbrain explant culture where the embryo is electroporated at HH4-6 and the midbrain is explanted at HH9-11 (Figure 5.2A). This novel system allows us to image cells in the apicobasal axis as they undergo IKNM and proceed through the cell cycle for the first time (Figure 5.2B-C'''). As seen in Figure 5.2C, cells move to the apical surface where they divide and then begin to move basally after mitosis is complete. This system also allows us to visualize gross morphogenetic tissue movements, including the formation of hinge points (Figure 5.2D-O). As previously described, BMP blockade using Noggin misexpression, induces the formation of ectopic hinge points which mimic the endogenous MHP (Figure 5.1; Eom et al., 2012, 2011). This culture system allows us to visualize the formation of these ectopic hinge points in real time for >7hrs, a timeline which matches that for endogenous MHP formation in WT brains (Figure 5.2D-O; Hamburger and Hamilton, 1951). Therefore, this system allows us to use Noggin misexpression as a model for MHP formation and visualize the cellular mechanisms involved in MHP formation in a closed neural tube, precluding the dysmorphology associated with open neural tube explants.

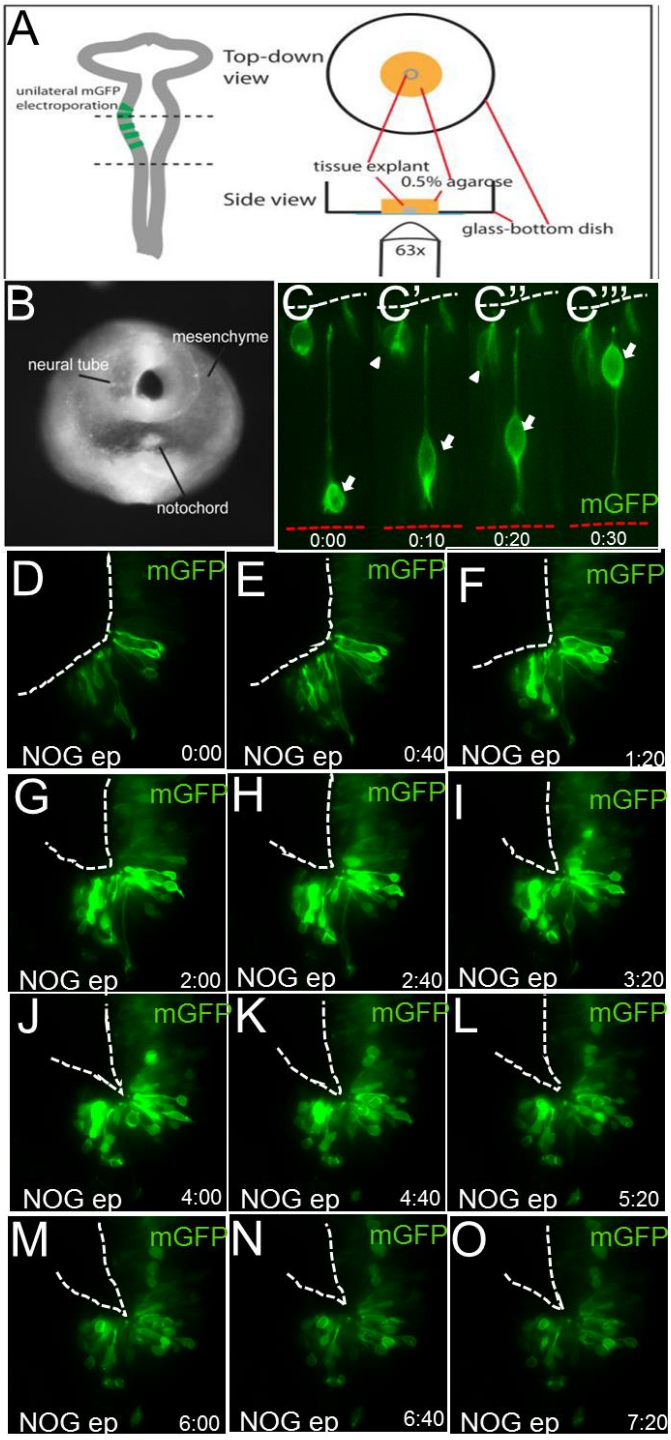

Figure 5.2 3D explant culture paradigm and HP formation in vitro

Figure 5.2 3D explant culture paradigm and HP formation in vitro

A) Schematic showing explant paradigm. Electroporated midbrain is excised (dotted lines) and embedded cut side down in agarose. Tissue is imaged through a glass bottom dish. B) Low power image of explant. C-C’’’) mGFP electroprated cells undergo IKNM (arrow) in the explant system, with mitosis occurring at the apical surface (arrowhead; white line denotes apical surface, red line denotes basal surface). D-O) Noggin electroporated explant showing HP formation over >7 hrs (dashed line denotes apical surface).

BMP signaling alters mitotic localization and cleavage angle, not mitotic duration

Since BMP signaling alters mitotic localization and mitotic index (Figure 5.1G-J), we next asked whether it regulates other aspects of mitosis. In the WT MHP, cells mitotic cells divide with a cleavage plane that is parallel to the apical surface, while ventral midline cells prior to HP formation divide perpendicular to the apical surface (Figure 5.3A-C; HH4 91.1˚± 5.89˚; HH6-7 10.9˚± 2.53˚ p=0.0002). Therefore, we examined cleavage angle at the BMP blockade mediated ectopic hinge points and found that, like the endogenous HP, BMP blockade alters cleavage angle in mitotic cells. However, it only does so in cells that divide sub-apically. In control and apically dividing Noggin electroporated cells, on average, cells divided with the average cleavage plane perpendicular to the apical surface (Figure 5.3D, F). However, sub-apical mitotic cells divide parallel to the apical surface (Figure 5.3E-F; Control 61.48˚± 11.68˚; Noggin (apical) 47.44˚± 11.45˚ p=0.347; Noggin (sub-apical) 11.39˚± 5.90˚ p=0.001). Although the mechanism by which this occurs is not understood, this may be another mechanism by which BMP blockade exaggerates HP formation. Since these cells divide with the average cleavage plane parallel to the apical surface, the mitotic nuclei take up less lateral space which may allow for decreased apical surface area.

Next we looked at whether BMP blockade affects mitotic duration. It is plausible that the decrease in PHH3+ mitotic nuclei seen in fixed tissue is actually the result of a decreased duration of mitosis (Figure 5.1D). To test this, cells were co-electroporated with membrane tagged EGFP (mEGFP) and Importin-RFP, to visualize the nuclear membrane (Figure 5.3G-H). Breakdown of the Importin-labeled nuclear envelope was used to mark the beginning of mitosis, and cytokinesis (two visible daughter cells, separated by membrane, with Importin-labeled nuclear envelope beginning to re-form)

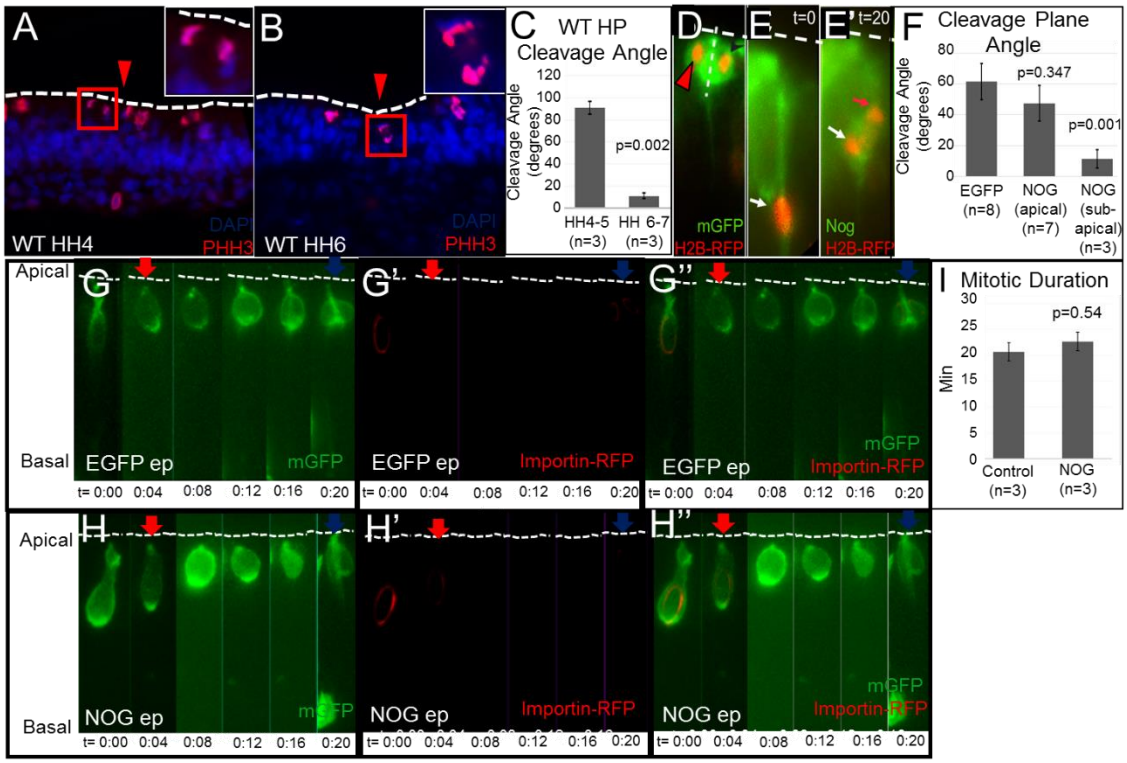

Figure 5.3 BMP signaling regulates mitotic cleavage angle but not mitotic duration

Figure 5.3 BMP signaling regulates mitotic cleavage angle but not mitotic duration.

A-B) Neural plate sections showing PHH3+ mitotic cells (arrowheads denote ventral midline; dotted line denotes apical surface; insets high power of red boxes) A) WT HH4 mitotic cell divides with perpendicular cleavage plane. B) WT HH6 mitotic cell divides with parallel cleavage plane. C) Quantitation showing that the mitotic cleavage plane is perpendicular prior to MHP formation and parallel after MHP formation (HH4 91.1˚± 5.89˚; HH6-7 10.9˚± 2.53˚ p=0.0002). D-E') Cells expressing mGFP or Noggin and Histone 2B-RFP (H2B-RFP) to visualize the nucleus. D) mGFP electroporated cells divided with a cleavage plane perpendicular to the apical surface. E-E') Noggin electroporated subapical mitotic cells divided with a cleavage plane parallel to the apical surface. F) Quanititation of cleavage angle (Control 61.48˚± 11.68˚; Noggin (apical) 47.44˚± 11.45˚ p=0.347; Noggin (sub-apical) 11.39˚± 5.90˚ p=0.001). G-H'') Cells electroporated with mGFP to visualize cell outlines and Importin-RFP to visualize the nuclear envelope. Mitosis was defined to start when Importin-RFP is no longer visible, indicating nuclear envelope break down, and end when two daughter cells (separated by mGFP-labeled membrane) are visible and the Importin-RFP labeled nuclear envelope begins to reform, indicating cytokinesis has occurred. Dashed line indicates apical surface. Red arrow indicates start of mitosis. Blue arrow indicates end of mitosis. I) Quantitation of mitotic duration (Control 20.67 ± 3.06min, n=3; Noggin 22.67 ± 4.16, p=0.54, n=3). Significance for all statistics was determined via student's two-tailed t test.

was used to mark the end of mitosis. Based on a student's t-test, we found no significant difference in mitotic duration after Noggin misexpression (Figure 5.2G-I; Control 20.67 ± 3.06min, n=3; Noggin 22.67 ± 4.16, p=0.54, n=3). This suggests that although BMP signaling regulates mitotic index, mitotic localization and cleavage plane angle (which all keep the nucleus away from the apical surface), it does not affect mitotic duration. However, additional experiments must be performed to conclude this with certainty. However, the trend we see with this limited number of ns suggests that BMP signaling is regulating cell cycle dynamics prior to or after mitosis.

BMP signaling regulates G1 duration

We next analyzed duration of G1. After mitosis, the cell enters G1 and begins to move away from the apical surface (Figure 1C). Membrane targeted RFP (mRFP) was used to visualize the cell outline, and PCNA-GFP was used to analyze cell cycle phase (Figure 5.4A-B). During G1 and G2 phase, PCNA appears equally distributed throughout the nucleus. However, upon entering S phase, PCNA begins to appear punctate. These puncta increase in size and decrease in number in late S phase before disappearing upon entering G2 (Leonhardt et al., 2000; Leung et al., 2011). We used this cell cycle dependent visualization of PCNA-GFP to determine the length of G1 phase.

We found that Noggin misexpression leads to a doubling of G1 duration (Figure 5.4A-C; Control 7.33 ± 0.567hr, n=6; Noggin 14.11 ± 0.873hr, p=0.003, n=3). This is consistent with the basal nuclear localization seen in HP formation and supports the idea Noggin regulates HP formation via cell cycle modulation. By regulating G1, the nucleus is kept away from the apical surface for a longer period of time, thus inducing the basal nuclear localization characteristic of HP formation.

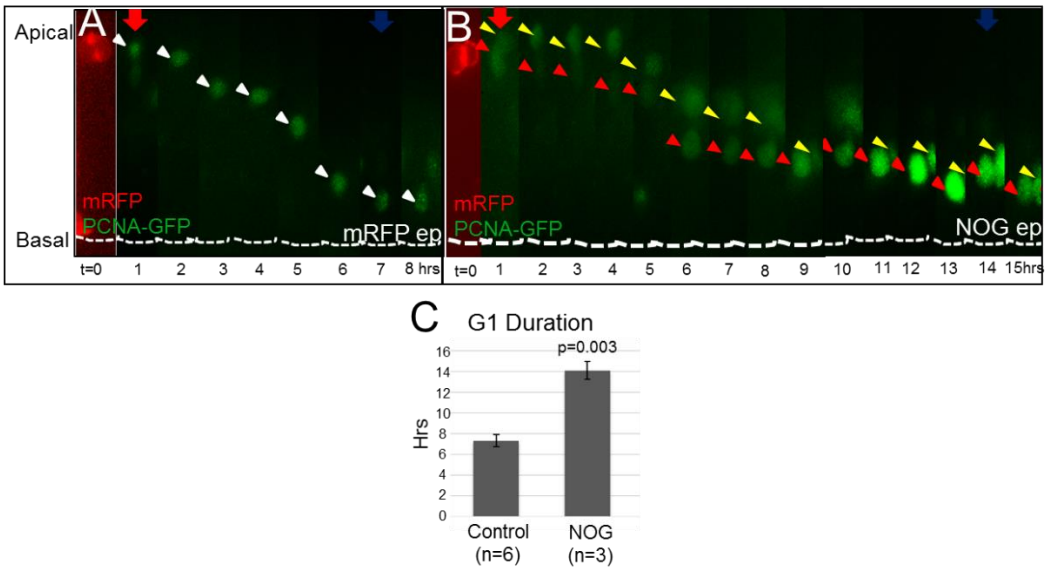

Figure 5.4 BMP blockade increases G1 duration.

A-B) Cells electroporated with mRFP and PCNA-GFP to visualize the start of S phase. RFP channel was removed after t=0 for visual clarity. The start of G1 was defined as the first visualization of PCNA-GFP after cytokinesis and the end of G1 was considered the visualization of PCNA-GFP puncta, which indicates the beginning of S phase (arrowheads denote individual cells tracked over time; dashed line denotes basal surface). A) Control cell in G1 for 8hrs. B) Noggin misexpression through G1 visualized for 15 hrs. Red arrow indicates start of mitosis. Blue arrow indicates end of mitosis. C) Quantitation of G1 duration in mRFP and Noggin electroporated brains (Control 7.33 ± 0.567hr, n=6; Noggin 14.11 ± 0.873hr, p=0.003, n=3). Significance for all statistics was determined via student's two-tailed t-test.

BMP blockade regulates S phase duration

After beginning to move away from the apical surface during G1, during S phase, the nucleus may be distributed throughout the apicobasal thickness of the tissue (Baye and Link, 2007). However, cells in S phase are typically localized basally (Figure 5.5A), and an increase in S phase duration, similar to an increase in G1, would also effectively keep the nucleus away from the apical surface for a greater percentage of time. This is what we see in Noggin misexpressed brains. A 30 min BrdU pulse showed that there was a significant increase in BrdU+ cells in the Noggin electroporated brain (Figure 5.5A-C; Control 30.02 ± 1.92, n=3; Noggin 42.4 ± 1.62, n=3; p=0.007). We next confirmed that this increase in BrdU is due to an increase in S phase duration via timelapse studies using PCNA-GFP to identify S phase cells. We see that BMP blockade leads to a significant increase in S phase duration (Figure 5.5D-F; Control 2.93 ± 0.59hrs; Noggin 5.85 ± 2.44hrs, p=0.01), which is consistent with the idea that basal nuclear localization necessary for Noggin mediated hinge point formation.

BMP signaling results in premature exit of G2 in a subset of cells

G2 phase is relatively quick when compared to G1 and S phase (Figure 5.4C, 5.5F, 5.6C), and duration does not appear to be altered by BMP blockade or (Figure 5.6A-C; Control 0.87 ± 0.18hrs; Noggin 1.04 ± 0.21hrs, p=0.099). However, a subset of Noggin missexpressed cells exit G2 prior to reaching the apical surface and enter mitosis ectopically (Figure 5.6D-D''). In these cells, the nucleus begins to travel toward the apical surface, but stops abruptly, and undergoes mitosis at a sub-apical location (Figure 5.5D, 1E-G). This premature exit of mitosis may explain the basal localization of mitotic cells seen in Noggin electroporated cells (Figure 5.1G-H,J),

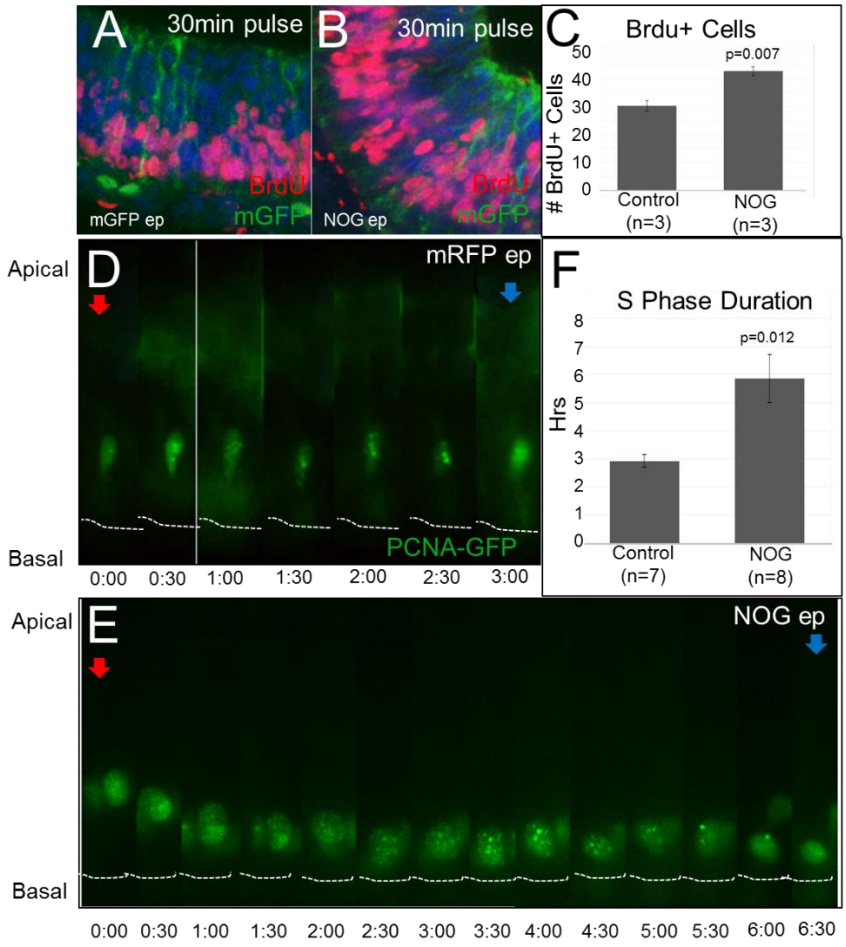

Figure 5.5 BMP blockade increases S phase duration.

A-B) NT electroporated at HH9-10 with mGFP or Noggin. Tissue was collected at HH11-12 following a 30min BrdU pulse. A) mGFP electroporated NT showing BrdU+ cells mainly near the basal surface. B) Noggin electropoated NT showing increased BrdU+ cells. C) Quantitation showing a significantly increased number of BrdU+ S phase cells in Noggin electroporated cells. D-E) Timelapse analysis of S phase. mRFP control or Noggin electroporated cells coexpressing PCNA-GFP to visualize S phase. S phase was considered to start when PCNA-GFP puncta become visible and end when puncta are replaced by diffuse labeling (dashed line denotes basal surface; red arrow indicates start of S phase; blue arrow indicates end of S phase). D) Control S phase cell visualized for 3 hours. E) Noggin electroporated S phase cell over 6.5 hrs. F) Quantitation of S phase duration showing a significant increase in S phase duration in Noggin electroporated cells. Significance for all statistics was determined via student's two-tailed t test

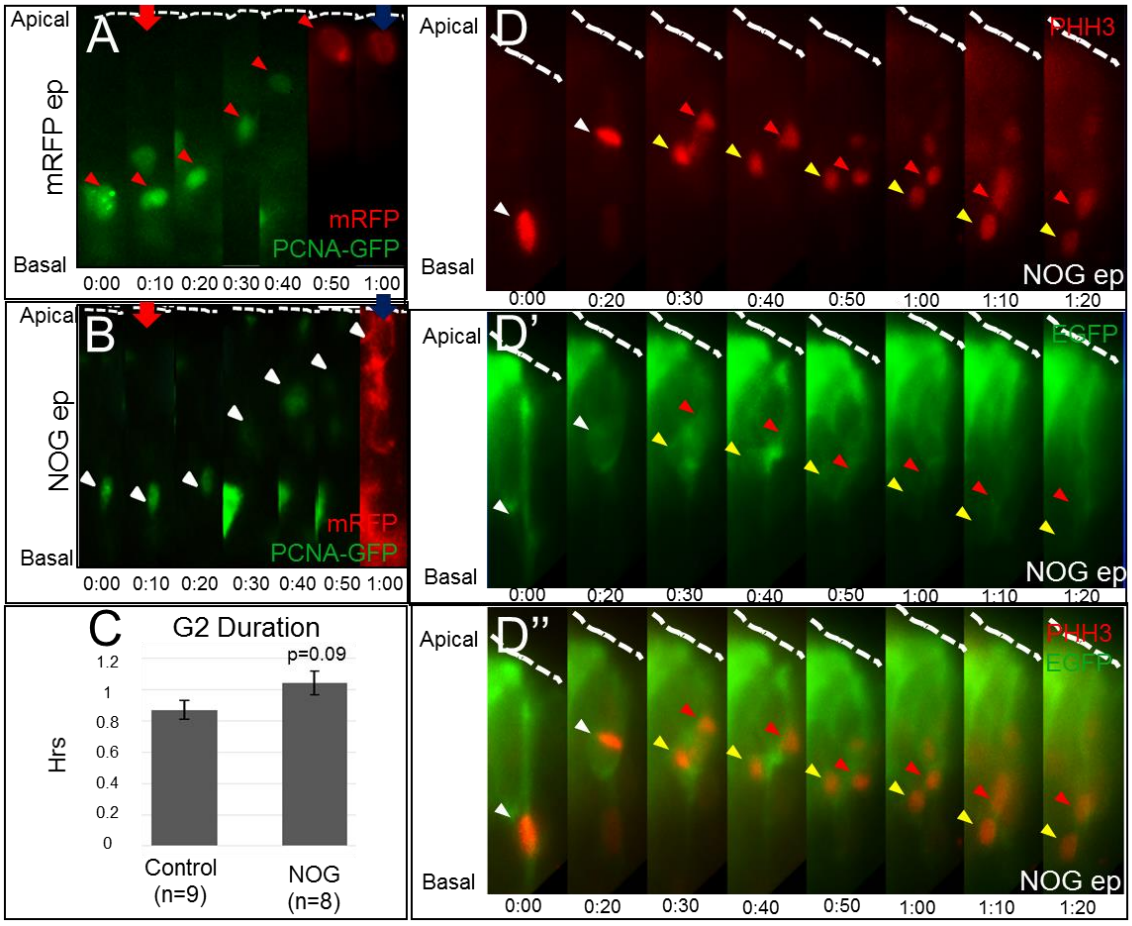

Figure 5.6 BMP causes a subset of cells to prematurely exit G2 resulting in subapical mitosis.

A-B) Control or Noggin electroporated cells coexpressing PCNA-GFP to visualize the end of S phase. G2 was considered to start when PCNA-GFP puncta were no longer visible and end when PCNA-GFP expression disappeared and the cell rounded for mitosis. mRFP channel was removed from early time points for clarity of PCNA visualization (arrows denote individual cells; dashed line denotes apical surface; red arrow indicates start of S phase; blue arrow indicates end of S phase). C) Quantitation of G2 duration showing no alteration in G2 length in Noggin electroporated cells. D-D'') Noggin electroporated cell moves apically, but stalls and undergoes mitosis before reaching the apical surface (0:30). The daughter cells then proceed to move back toward the basal surface (white arrow denotes mother cell; red and yellow arrows denote daughter cells; dashed line denotes apical surface).

and again, shows that subapical mitosis is due to a lack of migration to the apical surface, not a basal migration away from the apical surface.

DISCUSSION

In this study, we have shown that BMP signaling regulates HP formation via modulation of cell cycle kinetics. BMP blockade results in an increase in the overall length of interphase (specifically increasing G1 and S phase), a decrease in mitotic index and the subapical localization of mitotic cells (Figure 5.7). These cell cycle modulations work together to effectively keep the nucleus away from the apical surface, resulting in the overall nuclear basal shift associated with HP formation.

Cell-cell variability

Although both BMP blockade and BMP overexpression result in a significant number of subapically localized mitotic cells, there are also a large number of cells that continue to divide apically. It is possible that the cells that divide apically versus cells that divide subapically differ in the timing misexpression of Noggin or BMP4 expression vectors. Since misexpression was performed via electroporation, each cell that was electroporated was in a different phase of the cell cycle when the expression vector was introduced, and it takes approximately 3 hours for the vectors to be expressed at levels sufficient for visualization. Therefore, individual cells will receive different levels of BMP signaling at different cell cycle phases resulting in significant cell-cell variability. Although the exact mechanism by which BMP signaling modulates the cell cycle remains unclear, but our lab has shown that both the levels and the subcellular localization of BMP effectors changes in a cell cycle dependent manner (Eom et al., 2012, 2011,

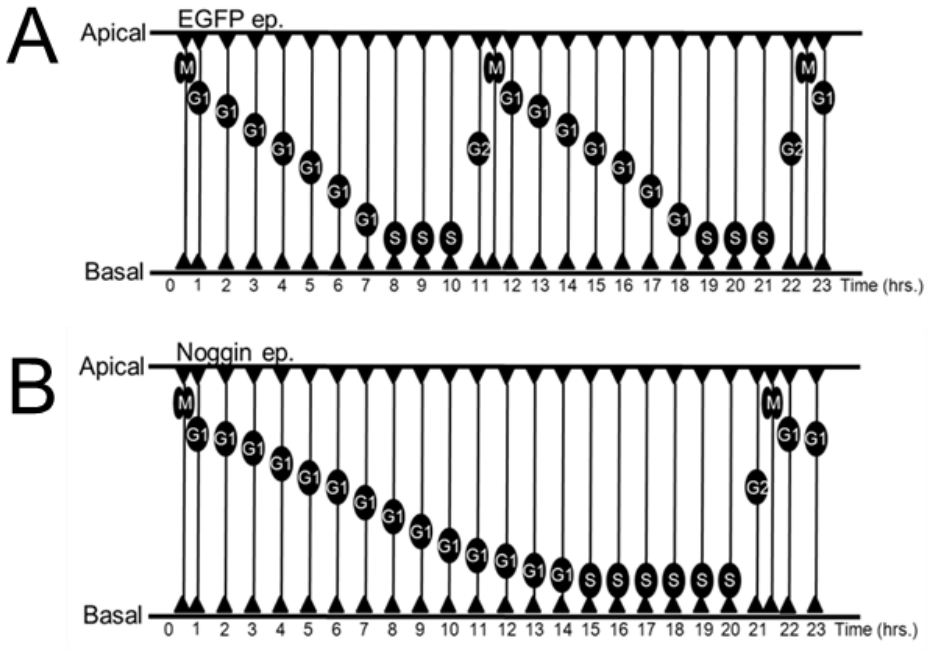

Figure 5.7 BMP blockade induces basal nuclear migration by increasing G1 and S phases.

A) Schematic representing cell cycle in control cells. Cells undergo mitosis at the apical surface, move basally during G1 and return to the apical surface during G2. B) Schematic representing cell cycle in Noggin electroporated cells. Noggin misexpression induces basal nuclear localization by increasing G1 and S phase duration which keep the nucleus away from the apical surface for a greater percentage of time.

Amarnath et al., unpublished) so it is likely that misexpression must occur at a specific cell cycle phase in order for these effects to occur.

Apical constriction versus basal nuclear localization

There is evidence that the apical constriction required for hinge point formation is actin cytoskeleton dependent (Haigo et al., 2003; Hildebrand, 2005; Martin and Goldstein, 2014; Nishimura and Takeichi, 2008). However, the amniote neurepithelium is pseudostratified and cells are bipolar with cell processes that extend to the apical and basal surfaces (Baye and Link, 2007; Sauer, 1935; Sauer and Walker, 1959). As discussed above, these cells undergo interkinetic nuclear migration, during which the nucleus moves along the apicobasal axis as it progresses through the cell cycle. Mitotic nuclei are localized to the apical surface, while G1, S and G2 phase nuclei are located throughout the apicobasal thickness of the tissue (Baye and Link, 2007; Guthrie et al., 1991). Since the cell body/nucleus is the widest part of the cell, localization of the nucleus away from the apical surface, as a consequence of interkinetic nuclear migration, results in an inherent decrease in apical surface area. This has resulted in controversy in the field as to the contribution of apical constriction (via actin based mechanisms) versus basal nuclear localization in hinge point formation because the apical processes of bipolar cells may be so fine that their constriction is unlikely to substantially reduce apical surface area. In this scenario, only the constriction of apically localized mitotic cells can substantially contribute to the decrease in apical surface area. In this view, hinge point formation in pseudostratified tissues likely occurs as a consequence of basal nuclear localization rather than actomyosin constriction. Our data seems to support this model whereby cell cycle regulation modulates nuclear localization and thereby induces HP

formation. However, further studies must be performed to adequately determine if actomyosin constriction of the apically localized mitotic cells plays a role in HP formation in the amniote.

Subapical mitosis may result from regulation of cell polarity

Our lab has previous shown that BMP effectors biochemically interact with apicobasal polarity proteins at the apical junctions and that BMP blockade regulates these polarity complexes via endocytosis (Eom et al., 2012). It is possible that this is the mechanism by which BMP signaling is also regulating cell cycle kinetics. Studies have shown that downregulation of apical junctional polarity proteins results in disorganization of cell polarity and a resulting displacement of centrosomes from the apical surface (Imai et al., 2006; Liu et al., 2010; Tamai et al., 2007). When the centrosome arrives at the nucleus, the nuclear envelope begins to breakdown and the cell proceeds into mitosis subapically (Cappello et al., 2006; Imai et al., 2006). In addition, in the mouse neocortex, downregulation of centrosomal proteins Hook3 and PCM1 results in decreased anchorage of microtubules to the centrosome and results in impairment of IKNM (Ge et al., 2010). Therefore, it is possible that regulation of mitotic localization is a result of centrosomal mislocalization due to altered apicobasal polarity, and should be further explored.

Chapter 6: Future Directions

INTRODUCTION

FOXA2 plays roles in both the cell fate specification and morphogenesis of the midbrain ventral midline. As discussed in Chapter 3, FOXA2 is capable of inducing FP cell fate specification. However, less explored is the role it plays in the induction of the associated HPs (Figure 3.5B'). In the future, the studies from Chapter 3 will merge with those in Chapter 5 to study the role of FOXA2 in HP formation and the interactions between FOXA2 and the BMP signaling pathways to regulate HP formation. In addition, the exact mechanism by which BMP signaling alters cell cycle dynamics and/or IKNM should be explored.

FOXA2-BMP-TGFB INTERACTIONS

In addition to inducing FP cell fate specification, we have shown that FOXA2 is also capable of inducing the morphological properties of the FP (Figure 3.5B'). When misexpressed in lateral midbrain, FOXA2 is sufficient to induce ectopic HPs similar to those seen at the endogenous MHP and in BMP blockade experiments (Figure 3.5B'; 5.2D-O; data not shown). Interestingly, our data shows that FOXA2 is capable of upregulating *BMP7* and *NOGGIN* transcription (data not shown), suggesting that FOXA2 has the potential to interact with both BMP and TGFβ signaling cascades, which function antagonistically to regulate HP formation (Figure 5.2D-O; Amarnath and Agarwala, in review). Further analyses as to which BMP and TGFβ ligands, effectors, and antagonists are regulated by FOXA2 should be performed. In addition, a more specific analyses as to the effects of nuclear versus cytoplasmic FOXA2 with respect to BMP and TGFβ signaling should also be performed. It is possible that FOXA2 transcriptionally regulates

BMP and TGFβ pathway members, but it is also possible that these pathways interact with FOXA2 in a cytosolic location.

Data in the lab has shown that FOXA2 biochemically interacts with the apical polarity complex PAR3 (Amarnath and Agarwala, unpublished observations). Since PAR3 also biochemically interacts with SMAD proteins, it is possible that FOXA2 interacts with BMP and TGFβ effector proteins at the apical junctions and acts via these pathways in order to regulate apicobasal polarity and tissue shape changes. More specifically, FOXA2 may induce MHP formation via regulation of BMP and TGFβ signaling.

NUCLEAR VERSUS CYTOPLASMIC ROLE OF FOXA2

FOXA2 has been identified as a pioneer transcription factor. It has been shown to bind to the genome before activation and before the binding of other factors (Zaret and Carol, 2011). The FOXA family of proteins has been shown to bind particularly tightly to chromatin and is capable of remaining bound even during mitosis (Sekiya et al., 2009; Yan et al., 2006; Zaret et al., 2011; Zaret and Carol, 2011). However, as mentioned above, the role of FOXA2 in the nucleus is not the only possible mechanism by which it can function. Studies involving insulin secreting pancreatic cells have shown nucleo-cytoplasmic shuttling of FOXA2. In these cells, the shuttling of FOXA2 out of the nucleus leads to a reduction in its transcriptional activity and lowers insulin secretion, and data in the lab suggests that similar nucleo-cytoplasmic shuttling occurs in midbrain FP cells (Wolfrum et al., 2003; Amarnath and Agarwala, unpublished observations). This shuttling may passively reduce the transcriptional role of FOXA2, but nucleo-cytoplasmic shuttling may also play an active role in tissue morphogenesis by allowing FOXA2 interaction with apical proteins.

No direct cytoplasmic function has been attributed to FOXA2, however, studies have shown that FOXA2 regulates polarized cellular events, and data in our lab indicates that FOXA2 biochemically interacts with the apical polarity protein, PAR3 in the cytoplasm (Burtscher and Lickert, 2009; Amarnath and Agarwala, unpublished observations). This suggests that FOXA2 may play a cytoplasmic as well as nuclear role in midbrain development. To test this hypothesis, mutated forms of FOXA2 which exclusively localize to the nucleus or cytoplasm can be misexpressed in FP and lateral neural plate and then analyzed for changes in cell fate specification (i.e. FP specification) and tissue morphogenesis (i.e. HP formation).

THE CELLULAR BASIS OF HP FORMATION

Identification of pSMAD interacting partners

As discussed previously, upon activation, BMP receptors phosphorylate downstream receptor SMADs (SMAD 1, 5, or 8) which then bind to SMAD 4. This pSMAD1,5,8-SMAD4 complex translocates into the nucleus to regulate gene transcription (Figure 1.3; Liu and Niswander, 2005). Studies from our lab have shown that the nuclear or cytoplasmic localization of pSMAD 1,5,8 is cell cycle dependent and this study has shown that BMP signaling regulates HP formation in a cell cycle dependent manner (Chapter 5; Amarnath and Agarwala, in review). However, the molecular mechanisms by which BMP signaling regulates cell cycle progression remains unknown. Performing a ChIP-seq analysis would allow us to determine the pSMAD interacting partners and gain further insight into how BMP signaling alters cell cycle progression.

Role of nuclear localization in HP formation

Our data suggests that BMP signaling regulates HP formation via cell cycle modulations which localize the nuclei basally. However, we have not yet confirmed that the basal localization of nuclei alone is sufficient to induce HP formation. In order to test this, we must independently manipulate nuclear localization.

Multiple mechanisms for how the nucleus moves during IKNM have been proposed, but it is generally accepted in the field that basal to apical translocation during G2 requires the microtubule-dependent mechanisms (Gambello et al., 2003; Hebbar et al., 2008; Tsai et al., 2005). The minus ends of microtubules attach to the apically localized centrosomes, and evidence suggests that the cell nucleus is moved along these microtubules via dynein motor proteins (Cappello et al., 2011; Kosodo, 2012; Norden et al., 2009; Tsai et al., 2005). LIS1 and NUDC, members of the dynein motor complex, are required for the G2 movement of the nucleus to the apical surface for mitosis. Disruption of LIS1 has been shown to inhibit this apical migration and results in nuclei being basally localized (Assadi et al., 2003; Cappello et al., 2011; Faulkner et al., 2000; Gambello et al., 2003; Hebbar et al., 2008; Smith et al., 2000; Tsai et al., 2005).

Evidence in the rat brain suggests that apical to basal migration is mediated by an unconventional kinesin motor protein called KIF1A (Tsai et al., 2010). Similar to dynein, kinesins are motor proteins that move cargo along microtubules (Hirokawa et al., 2010). Knockdown of KIF1A via siRNA results in the inhibition of basal migration and a resulting apical localization of nuclei (Tsai et al., 2010).

It should be noted that LIS1 manipulations have been tested in the lab and were not found to cause significant effects on nuclear localization in our system (data not

shown). However, manipulations of other dynein motor complex proteins (such as NUDC) may prove more fruitful and should be tested. If our hypothesis is correct, basal localization of nuclei due to inhibition of the dynein motor complex in lateral neural plate, should result in the formation of ectopic hinge points. Conversely, apical localization of nuclei due to inhibition of KIF1A at the endogenous NP, should result in flattening or potentially reversing the endogenous MHP.

Cell cycle manipulations

Although our data suggests that BMP mediated cell cycle modulations result in HP formation, we are unable to definitively differentiate whether the alterations in cell cycle progression mediate HP formation or are a consequence of HP formation. In order to address this issue, targeted cell cycle manipulations which elongate G1 or S phase could be performed.

Various molecules in vitro are known to prevent G1/S transition. Including Mimosine which upregulates $p27^{kip1}$ and results in inhibition of G1/S transition (Wang et al., 2000; Burstyn-Cohen and Kalcheim, 2002) and AG5555, which functions by blocking the activation of the cyclin-dependent kinase cdk-2 (Kleinberger-Doron et al., 1998; Burstyn-Cohen and Kalcheim, 2002).

Unfortunately, in vivo cell cycle manipulations may be difficult. Since cells are executing IKNM in coordination with cell cycle progression, unlinking these two processes may be difficult. Particularly when considering that both IKNM and mitosis utilize microtubule dynamics. Therefore, any cell cycle inhibitor which uses a microtubule based mechanism to inhibit cell cycle progression will also likely inhibit IKNM, making the results uninterpretable. Burstyn-Cohen and Kalcheim successfully utilized MyoD to block G1/S transition in chick neurepithelium (Burstyn-Cohen and

Kalcheim, 2002). If our hypothesis is correct, this manipulation should result in the stalling of cells in G1 phase and induce ectopic HP formation.

Electroporation Alternatives

Until this point, all of our BMP manipulations have been performed via electroporation. However, with this technique, there is approximately 3 hour lag time between when the plasmid constructs are introduced and when protein expression becomes visible. As discussed in Chapter 5, each cell may receive varying amounts of plasmid and the plasmid will be introduced to individual cells at various stages of the cell cycle. In order to reduce the uncertainty associated with the concentration and timing of the electroporation paradigm, we could perform bead experiments where a protein coated bead is introduced into the explant system. This would ensure an immediate source of protein and that all the cells are exposed to the protein at the same time.

In order for these experiments to be successful, the embryos must still be electroporated in order to introduce the fluorescent markers that are utilized to visualize cell movements and cell cycle progression (mGFP, PCNA-GFP, etc). The embryos should be electroporated at HH5-6, incubated until HH9 and explanted according to the established protocol. Just prior to the start of imaging, a NOGGIN soaked bead would be placed directly adjacent to the explant. Bead placement and protein concentration may be critical, and due to the large size of the bead as compared to the developing neural tube, the bead must be placed in such a way as to minimize physical interference with the tissue.

Another possible alternative to electroporation of Noggin would be the use of small molecule inhibitors of BMP signaling. These small molecule inhibitors such as K02288, which inhibits the BMP receptor kinase ALK2, or DMH1, which mimics

Noggin phenotypes, could be added directly to the culture media (Neely et al., 2012; Sanvitale et al., 2013). This would allow for an immediate and consistent introduction of BMP blockade. However, universal BMP blockade may result in gross tissue dismorphology, making results difficult to interpret.

Chapter 7: Conclusions

In this study, we analyzed the specification and morphogenesis of the midbrain ventral midline in the amniote. We show that, similar to the fish, the amniote anterior neural plate can be divided into MFP and LFP subdivisions which differentially require SHH and FOXA2 for their specification. More specifically, SHH is capable of inducting LFP, but not MFP while FOXA2 is sufficient to induce the entire midbrain FP pattern. In addition, we find that all three midbrain signaling centers (FP, RP and MHB) are physically continuous and their identities are interconvertible, based on exposure to SHH signaling.

We next analyzed the morphogenesis of the ventral midline which is the site of MHP formation. In order to study early morphogenetic events in the midbrain, we developed an early electroporation technique which allowed us to electroporate embryos in vivo as early as HH4, before the MHP is formed. Here, we showed that this novel technique allows electroporations at ≥HH4 without perturbing overall 3-dimensional morphology, tissue size, cell proliferation, or cell-fate specification.

We then utilized this technique to develop a 3D explant paradigm with which to study HP formation in real time. Here, we utilized BMP blockade induced ectopic HPs as a model for MHP formation. This allowed us to analyze the cell cycle kinetic and cell behaviors involved in MHP formation. We found that BMP signaling regulates cell cycle dynamics is specific ways in order to regulate basal nuclear localization and therefore HP formation. BMP blockade results in an increase in the overall length of interphase by increasing the duration of G1 and S phase. It also causes a reduction in mitotic index, and a subset of cells prematurely exit the cell cycle and undergo sub-apical G2-M transition. This is similar to what is seen in the MHP where there is reduced mitotic index and cells

undergo mitosis sub-apically. These cell cycle modulations work together to effectively keep the nucleus away from the apical surface, resulting in the overall nuclear basal shift associated with HP formation.

References

Adams, K., Maida, J., Golden, J., and RD, R. (2000). The transcription factor Lmx1b maintains Wnt1 expression within the isthmic organizer. Development *127*, 1857–1867.

Agarwala, S., and Ragsdale, C.W. (2002). A role for midbrain arcs in nucleogenesis. Development *129*, 5779–5788.

Agarwala, S., Sanders, T.A., and Ragsdale, C.W. (2001). Sonic hedgehog control of size and shape in midbrain pattern formation. Science *291*, 2147–2150.

Aglyamova, G. V, and Agarwala, S. (2007). Gene expression analysis of the hedgehog signaling cascade in the chick midbrain and spinal cord. Dev. Dyn. *236*, 1363–1373.

Alexandre, P., and Wassef, M. (2003). The isthmic organizer links anteroposterior and dorsoventral patterning in the mid/hindbrain by generating roof plate structures. Development *130*, 5331–5338.

Altaba, A.R. i, Jessell, T.M., and Roelink, H. (1995). Restrictions to Floor Plate Induction by hedgehog and Winged-Helix Genes in the Neural Tube of Frog Embryos. Mol. Cell. Neurosci. *6*, 106–121.

Andersson, E., Tryggvason, U., Deng, Q., Friling, S., Alekseenko, Z., Robert, B., Perlmann, T., and Ericson, J. (2006). Identification of intrinsic determinants of midbrain dopamine neurons. Cell *124*, 393–405.

Ang, S.-L., and Rossant, J. (1994). HNF-3β is essential for node and notochord formation in mouse development. Cell *78*, 561–574.

Aoto, K., Nishimura, T., Eto, K., and Motoyama, J. (2002). Mouse GLI3 Regulates Fgf8 Expression and Apoptosis in the Developing Neural Tube, Face, and Limb Bud. Dev. Biol. *251*, 320–332.

Assadi, A.H., Zhang, G., Beffert, U., McNeil, R.S., Renfro, A.L., Niu, S., Quattrocchi, C.C., Antalffy, B.A., Sheldon, M., Armstrong, D.D., et al. (2003). Interaction of reelin signaling and Lis1 in brain development. Nat. Genet. *35*, 270–276.

Bai, C.B., Stephen, D., and Joyner, A.L. (2004). All Mouse Ventral Spinal Cord Patterning by Hedgehog Is Gli Dependent and Involves an Activator Function of Gli3. Dev. Cell *6*, 103–115.

Basson, M.A., Echevarria, D., Ahn, C.P., Sudarov, A., Joyner, A.L., Mason, I.J., Martinez, S., and Martin, G.R. (2008). Specific regions within the embryonic midbrain and cerebellum require different levels of FGF signaling during development. Development *135*, 889–898.

Baye, L.M., and Link, B.A. (2007). Interkinetic nuclear migration and the selection of neurogenic cell divisions during vertebrate retinogenesis. J. Neurosci. *27*, 10143–10152.

Baye, L.M., and Link, B.A. (2008). Nuclear migration during retinal development. Brain Res. *1192*, 29–36.

Bayly, R.D., Ngo, M., Aglyamova, G. V, and Agarwala, S. (2007). Regulation of ventral midbrain patterning by Hedgehog signaling. Development *134*, 2115–2124.

Bénazet, J.-D., and Zeller, R. (2009). Vertebrate limb development: moving from classical morphogen gradients to an integrated 4-dimensional patterning system. Cold Spring Harb. Perspect. Biol. *1*, a001339.

Blaess, S., Corrales, J.D., and Joyner, A.L. (2006). Sonic hedgehog regulates Gli activator and repressor functions with spatial and temporal precision in the mid/hindbrain region. Development *133*, 1799–1809.

Blaess, S., Stephen, D., and Joyner, A.L. (2008). Gli3 coordinates three-dimensional patterning and growth of the tectum and cerebellum by integrating Shh and Fgf8 signaling. Development *135*, 2093–2103.

Blaess, S., Bodea, G.O., Kabanova, A., Chanet, S., Mugniery, E., Derouiche, A., Stephen, D., and Joyner, A.L. (2011). Temporal-spatial changes in Sonic Hedgehog expression and signaling reveal different potentials of ventral mesencephalic progenitors to populate distinct ventral midbrain nuclei. Neural Dev. *6*, 29.

Briscoe, J., Chen, Y., Jessell, T.M., and Struhl, G. (2001). A Hedgehog-Insensitive Form of Patched Provides Evidence for Direct Long-Range Morphogen Activity of Sonic Hedgehog in the Neural Tube. Mol. Cell *7*, 1279–1291.

Brown, C.Y., Eom, D.S., Amarnath, S., and Agarwala, S. (2012a). A simple technique for early in vivo electroporation of E1 chick embryos. Dev. Dyn. *241*, 545–552.

Brown, C.Y., Eom, D.S., Amarnath, S., and Agarwala, S. (2012b). In vivo electroporation of E1 chick embryos. Cold Spring Harb. Protoc. *2012*, pdb.prot069708 – .

Burstyn-Cohen, T., and Kalcheim, C. (2002). Association between the Cell Cycle and Neural Crest Delamination through Specific Regulation of G1/S Transition. Dev. Cell *3*, 383–395.

Burstyn-Cohen, T., Stanleigh, J., Sela-Donenfeld, D., and Kalcheim, C. (2004). Canonical Wnt activity regulates trunk neural crest delamination linking BMP/noggin signaling with G1/S transition. Development *131*, 5327–5339.

Cappello, S., Attardo, A., Wu, X., Iwasato, T., Itohara, S., Wilsch-Bräuninger, M., Eilken, H.M., Rieger, M.A., Schroeder, T.T., Huttner, W.B., et al. (2006). The Rho-GTPase cdc42 regulates neural progenitor fate at the apical surface. Nat. Neurosci. *9*, 1099–1107.

Cappello, S., Monzo, P., and Vallee, R.B. (2011). NudC is required for interkinetic nuclear migration and neuronal migration during neocortical development. Dev. Biol. *357*, 326–335.

Catala, M., Ziller, C., Lapointe, F., and Le Douarin, N.M. (2000). The developmental potentials of the caudalmost part of the neural crest are restricted to melanocytes and glia. Mech. Dev. *95*, 77–87.

Chamberlain, C.E., Jeong, J., Guo, C., Allen, B.L., and McMahon, A.P. (2008). Notochord-derived Shh concentrates in close association with the apically positioned basal body in neural target cells and forms a dynamic gradient during neural patterning. Development *135*, 1097–1106.

Charrier, J.-B., Lapointe, F., Le Douarin, N.M., and Teillet, M.-A. (2002). Dual origin of the floor plate in the avian embryo. Development *129*, 4785–4796.

Charron, F., Stein, E., Jeong, J., McMahon, A.P., and Tessier-Lavigne, M. (2003). The Morphogen Sonic Hedgehog Is an Axonal Chemoattractant that Collaborates with Netrin-1 in Midline Axon Guidance. Cell *113*, 11–23.

Chiang, C., Litingtung, Y., Lee, E., Young, K.E., Corden, J.L., Westphal, H., and Beachy, P.A. (1996). Cyclopia and defective axial patterning in mice lacking Sonic hedgehog gene function. Nature *383*, 407–413.

Chizhikov, V. V, and Millen, K.J. (2004). Control of roof plate development and signaling by Lmx1b in the caudal vertebrate CNS. J. Neurosci. *24*, 5694–5703.

Colas, J.F., and Schoenwolf, G.C. (2001). Towards a cellular and molecular understanding of neurulation. Dev. Dyn. *221*, 117–145.

Copp, A.J., Greene, N.D.E., and Murdoch, J.N. (2003). The genetic basis of mammalian neurulation. Nat. Rev. Genet. *4*, 784–793.

Dal-Pra, S., Thisse, C., and Thisse, B. (2011). FoxA transcription factors are essential for the development of dorsal axial structures. Dev. Biol. *350*, 484–495.

Darnell, D., Stark, M., and Schoenwolf, G. (1999). Timing and cell interactions underlying neural induction in the chick embryo. Development *126*, 2505–2514.

Dodd, J. (1998). NEUROSCIENCE:The When and Where of Floor Plate Induction. Science (80-.). *282*, 1654–1657.

Duboc, V., and Logan, M.P.O. (2011). Regulation of limb bud initiation and limb-type morphology. Dev. Dyn. *240*, 1017–1027.

Dubreuil, V., Marzesco, A.-M., Corbeil, D., Huttner, W.B., and Wilsch-Bräuninger, M. (2007). Midbody and primary cilium of neural progenitors release extracellular membrane particles enriched in the stem cell marker prominin-1. J. Cell Biol. *176*, 483–495.

Echelard, Y., Epstein, D.J., St-Jacques, B., Shen, L., Mohler, J., McMahon, J.A., and McMahon, A.P. (1993). Sonic hedgehog, a member of a family of putative signaling molecules, is implicated in the regulation of CNS polarity. Cell *75*, 1417–1430.

Eom, D.S., Amarnath, S., Fogel, J.L., and Agarwala, S. (2011). Bone morphogenetic proteins regulate neural tube closure by interacting with the apicobasal polarity pathway. Development *138*, 3179–3188.

Eom, D.S., Amarnath, S., Fogel, J.L., and Agarwala, S. (2012). Bone morphogenetic proteins regulate hinge point formation during neural tube closure by dynamic modulation of apicobasal polarity. Birth Defects Res. A. Clin. Mol. Teratol. *94*, 804–816.

Ericson, J., Rashbass, P., Schedl, A., Brenner-Morton, S., Kawakami, A., van Heyningen, V., Jessell, T.., and Briscoe, J. (1997). Pax6 Controls Progenitor Cell Identity and Neuronal Fate in Response to Graded Shh Signaling. Cell *90*, 169–180.

Faulkner, N.E., Dujardin, D.L., Tai, C.Y., Vaughan, K.T., O'Connell, C.B., Wang, Y., and Vallee, R.B. (2000). A role for the lissencephaly gene LIS1 in mitosis and cytoplasmic dynein function. Nat. Cell Biol. *2*, 784–791.

Fedtsova, N., Quina, L.A., Wang, S., and Turner, E.E. (2008). Regulation of the development of tectal neurons and their projections by transcription factors Brn3a and Pax7. Dev. Biol. *316*, 6–20.

Ferri, A.L.M., Lin, W., Mavromatakis, Y.E., Wang, J.C., Sasaki, H., Whitsett, J.A., and Ang, S.-L. (2007). Foxa1 and Foxa2 regulate multiple phases of midbrain dopaminergic neuron development in a dosage-dependent manner. Development *134*, 2761–2769.

Fogel, J.L., Chiang, C., Huang, X., and Agarwala, S. (2008). Ventral specification and perturbed boundary formation in the mouse midbrain in the absence of Hedgehog signaling. Dev. Dyn. *237*, 1359–1372.

Funahashi, J., Okafuji, T., Ohuchi, H., Noji, S., Tanaka, H., and Nakamura, H. (1999). Role of Pax-5 in the regulation of a mid-hindbrain organizer's activity. Dev. Growth Differ. *41*, 59–72.

Gambello, M.J., Darling, D.L., Yingling, J., Tanaka, T., Gleeson, J.G., and Wynshaw-Boris, A. (2003). Multiple Dose-Dependent Effects of Lis1 on Cerebral Cortical Development. J. Neurosci. *23*, 1719–1729.

Gammill, L.S., and Krull, C.E. (2011). Embryological and genetic manipulation of chick development. Methods Mol. Biol. *770*, 119–137.

Ge, X., Frank, C.L., Calderon de Anda, F., and Tsai, L.-H. (2010). Hook3 interacts with PCM1 to regulate pericentriolar material assembly and the timing of neurogenesis. Neuron *65*, 191–203.

Goodrich, L. V. (1997). Altered Neural Cell Fates and Medulloblastoma in Mouse patched Mutants. Science (80-.). *277*, 1109–1113.

Gray, S.D., and Dale, J.K. (2010). Notch signalling regulates the contribution of progenitor cells from the chick Hensen's node to the floor plate and notochord. Development *137*, 561–568.

Grosse, S.D., Waitzman, N.J., Romano, P.S., and Mulinare, J. (2005). Reevaluating the benefits of folic acid fortification in the United States: economic analysis, regulation, and public health. Am. J. Public Health *95*, 1917–1922.

Guthrie, S., Butcher, M., and Lumsden, A. (1991). Patterns of cell division and interkinetic nuclear migration in the chick embryo hindbrain. J. Neurobiol. *22*, 742–754.

Haigo, S.L., Hildebrand, J.D., Harland, R.M., and Wallingford, J.B. (2003). Shroom Induces Apical Constriction and Is Required for Hingepoint Formation during Neural Tube Closure. Curr. Biol. *13*, 2125–2137.

Hamburger, V., and Hamilton, H.L. (1951). A series of normal stages in the development of the chick embryo. J. Morphol. *88*, 49–92.

Hatakeyama, J., and Shimamura, K. (2008). Method for electroporation for the early chick embryo. Dev. Growth Differ. *50*, 449–452.

Hatta, K., Kimmel, C.B., Ho, R.K., and Walker, C. (1991). The cyclops mutation blocks specification of the floor plate of the zebrafish central nervous system. Nature *350*, 339–341.

Hebbar, S., Mesngon, M.T., Guillotte, A.M., Desai, B., Ayala, R., and Smith, D.S. (2008). Lis1 and Ndel1 influence the timing of nuclear envelope breakdown in neural stem cells. J. Cell Biol. *182*, 1063–1071.

Hildebrand, J.D. (2005). Shroom regulates epithelial cell shape via the apical positioning of an actomyosin network. J. Cell Sci. *118*, 5191–5203.

Hinds, J.W., and Ruffett, T.L. (1971). Cell proliferation in the neural tube: An electron microscopic and Golgi analysis in the mouse cerebral vesicle. Zeitschrift F�r Zellforsch. Und Mikroskopische Anat. *115*, 226–264.

Hirokawa, N., Niwa, S., and Tanaka, Y. (2010). Molecular motors in neurons: transport mechanisms and roles in brain function, development, and disease. Neuron *68*, 610–638.

Hirota, T., Kunitoku, N., Sasayama, T., Marumoto, T., Zhang, D., Nitta, M., Hatakeyama, K., and Saya, H. (2003). Aurora-A and an Interacting Activator, the LIM Protein Ajuba, Are Required for Mitotic Commitment in Human Cells. Cell *114*, 585–598.

Hong, E., and Brewster, R. (2006). N-cadherin is required for the polarized cell behaviors that drive neurulation in the zebrafish. Development *133*, 3895–3905.

Hynes, M., Ye, W., Wang, K., Stone, D., Murone, M., Sauvage, F. d, and Rosenthal, A. (2000). The seven-transmembrane receptor smoothened cell-autonomously induces multiple ventral cell types. Nat. Neurosci. *3*, 41–46.

Ille, F., Atanasoski, S., Falk, S., Ittner, L.M., Märki, D., Büchmann-Møller, S., Wurdak, H., Suter, U., Taketo, M.M., and Sommer, L. (2007). Wnt/BMP signal integration

regulates the balance between proliferation and differentiation of neuroepithelial cells in the dorsal spinal cord. Dev. Biol. *304*, 394–408.

Imai, F., Hirai, S., Akimoto, K., Koyama, H., Miyata, T., Ogawa, M., Noguchi, S., Sasaoka, T., Noda, T., and Ohno, S. (2006). Inactivation of aPKClambda results in the loss of adherens junctions in neuroepithelial cells without affecting neurogenesis in mouse neocortex. Development *133*, 1735–1744.

Imamura, T., Takase, M., Nishihara, A., Oeda, E., Hanai, J., Kawabata, M., and Miyazono, K. (1997). Smad6 inhibits signalling by the TGF-beta superfamily. Nature *389*, 622–626.

Incardona, J., Gaffield, W., Kapur, R., and Roelink, H. (1998). The teratogenic Veratrum alkaloid cyclopamine inhibits sonic hedgehog signal transduction. Development *125*, 3553–3562.

Itasaki, N., Bel-Vialar, S., and Krumlauf, R. (1999). "Shocking" developments in chick embryology: electroporation and in ovo gene expression. Nat. Cell Biol. *1*, E203–E207.

Jackman, M., Lindon, C., Nigg, E.A., and Pines, J. (2003). Active cyclin B1-Cdk1 first appears on centrosomes in prophase. Nat. Cell Biol. *5*, 143–148.

Jacobson, A.G., Oster, G.F., Odell, G.M., and Cheng, L.Y. (1986). Neurulation and the cortical tractor model for epithelial folding. J Embryol Exp Morphol *96*, 19–49.

Jeong, J., and McMahon, A.P. (2005). Growth and pattern of the mammalian neural tube are governed by partially overlapping feedback activities of the hedgehog antagonists patched 1 and Hhip1. Development *132*, 143–154.

Joksimovic, M., Anderegg, A., Roy, A., Campochiaro, L., Yun, B., Kittappa, R., McKay, R., and Awatramani, R. (2009). Spatiotemporally separable Shh domains in the midbrain define distinct dopaminergic progenitor pools. Proc. Natl. Acad. Sci. U. S. A. *106*, 19185–19190.

Keller, R. (2002). Shaping the vertebrate body plan by polarized embryonic cell movements. Science *298*, 1950–1954.

Kingsbury, B.F. (1920). The extent of the floor-plate of his and its significance. J. Comp. Neurol. *32*, 113–135.

Kittappa, R., Chang, W.W., Awatramani, R.B., and McKay, R.D.G. (2007). The foxa2 gene controls the birth and spontaneous degeneration of dopamine neurons in old age. PLoS Biol. *5*, e325.

Kosodo, Y. (2012). Interkinetic nuclear migration: beyond a hallmark of neurogenesis. Cell. Mol. Life Sci. *69*, 2727–2738.

Kosodo, Y., and Huttner, W.B. (2009). Basal process and cell divisions of neural progenitors in the developing brain. Dev. Growth Differ. *51*, 251–261.

Kosodo, Y., Suetsugu, T., Suda, M., Mimori-Kiyosue, Y., Toida, K., Baba, S.A., Kimura, A., and Matsuzaki, F. (2011). Regulation of interkinetic nuclear migration by cell cycle-coupled active and passive mechanisms in the developing brain. EMBO J. *30*, 1690–1704.

Lawrence, P.A. (1997). Developmental biology. Straight and wiggly affinities. Nature *389*, 546–547.

Lawson, A., Colas, J.F., and Schoenwolf, G.C. (2001). Classification scheme for genes expressed during formation and progression of the avian primitive streak. Anat. Rec. *262*, 221–226.

Leonhardt, H. (2000). Dynamics of DNA Replication Factories in Living Cells. J. Cell Biol. *149*, 271–280.

Leung, L., Klopper, A. V, Grill, S.W., Harris, W.A., and Norden, C. (2011). Apical migration of nuclei during G2 is a prerequisite for all nuclear motion in zebrafish neuroepithelia. Development *138*, 5003–5013.

Lin, W., Metzakopian, E., Mavromatakis, Y.E., Gao, N., Balaskas, N., Sasaki, H., Briscoe, J., Whitsett, J.A., Goulding, M., Kaestner, K.H., et al. (2009). Foxa1 and Foxa2 function both upstream of and cooperatively with Lmx1a and Lmx1b in a feedforward loop promoting mesodiencephalic dopaminergic neuron development. Dev. Biol. *333*, 386–396.

Liu, A., and Niswander, L.A. (2005). Bone morphogenetic protein signalling and vertebrate nervous system development. Nat. Rev. Neurosci. *6*, 945–954.

Liu, A., Losos, K., and Joyner, A. (1999). FGF8 can activate Gbx2 and transform regions of the rostral mouse brain into a hindbrain fate. Development *126*, 4827–4838.

Liu, X., Hashimoto-Torii, K., Torii, M., Ding, C., and Rakic, P. (2010). Gap junctions/hemichannels modulate interkinetic nuclear migration in the forebrain precursors. J. Neurosci. *30*, 4197–4209.

Marti, E., Takada, R., Bumcrot, D., Sasaki, H., and McMahon, A. (1995). Distribution of Sonic hedgehog peptides in the developing chick and mouse embryo. Development *121*, 2537–2547.

Martin, A.C., and Goldstein, B. (2014). Apical constriction: themes and variations on a cellular mechanism driving morphogenesis. Development *141*, 1987–1998.

Matise, M., Epstein, D., Park, H., Platt, K., and Joyner, A. (1998). Gli2 is required for induction of floor plate and adjacent cells, but not most ventral neurons in the mouse central nervous system. Development *125*, 2759–2770.

Matsunaga, E., Katahira, T., and Nakamura, H. (2002). Role of Lmx1b and Wnt1 in mesencephalon and metencephalon development. Development *129*, 5269–5277.

Millen, K.J., Millonig, J.H., and Hatten, M.E. (2004). Roof plate and dorsal spinal cord dl1 interneuron development in the dreher mutant mouse. Dev. Biol. *270*, 382–392.

Momose, T., Tonegawa, A., Takeuchi, J., Ogawa, H., Umesono, K., and Yasuda, K. (1999a). Efficient targeting of gene expression in chick embryos by microelectroporation. Dev. Growth Differ. *41*, 335–344.

Momose, T., Tonegawa, + Akane, Takeuchi, J., Ogawa, H., Umesono, K., and Yasuda, K. (1999b). Efficient targeting of gene expression in chick embryos by microelectroporation. Dev. Growth Differ. *41*, 335–344.

Muramatsu, T., Mizutani, Y., Ohmori, Y., and Okumura, J. (1997). Comparison of three nonviral transfection methods for foreign gene expression in early chicken embryos in ovo. Biochem. Biophys. Res. Commun. *230*, 376–380.

Nakamura, T., Takio, K., Eto, Y., Shibai, H., Titani, K., and Sugino, H. (1990). Activin-binding protein from rat ovary is follistatin. Science (80-.). *247*, 836–838.

Nakatani, T., Kumai, M., Mizuhara, E., Minaki, Y., and Ono, Y. (2010). Lmx1a and Lmx1b cooperate with Foxa2 to coordinate the specification of dopaminergic neurons and control of floor plate cell differentiation in the developing mesencephalon. Dev. Biol. *339*, 101–113.

Nishimura, T., and Takeichi, M. (2008). Shroom3-mediated recruitment of Rho kinases to the apical cell junctions regulates epithelial and neuroepithelial planar remodeling. Development *135*, 1493–1502.

Nishimura, T., Honda, H., and Takeichi, M. (2012). Planar cell polarity links axes of spatial dynamics in neural-tube closure. Cell *149*, 1084–1097.

Norden, C., Young, S., Link, B.A., and Harris, W.A. (2009). Actomyosin is the main driver of interkinetic nuclear migration in the retina. Cell *138*, 1195–1208.

Norton, W.H., Mangoli, M., Lele, Z., Pogoda, H.-M., Diamond, B., Mercurio, S., Russell, C., Teraoka, H., Stickney, H.L., Rauch, G.-J., et al. (2005). Monorail/Foxa2 regulates floorplate differentiation and specification of oligodendrocytes, serotonergic raphé neurones and cranial motoneurones. Development *132*, 645–658.

O'Hara, F.P., Beck, E., Barr, L.K., Wong, L.L., Kessler, D.S., and Riddle, R.D. (2005). Zebrafish Lmx1b.1 and Lmx1b.2 are required for maintenance of the isthmic organizer. Development *132*, 3163–3173.

Odenthal, J., van Eeden, F.J., Haffter, P., Ingham, P.W., and Nüsslein-Volhard, C. (2000). Two distinct cell populations in the floor plate of the zebrafish are induced by different pathways. Dev. Biol. *219*, 350–363.

Ono, Y., Nakatani, T., Sakamoto, Y., Mizuhara, E., Minaki, Y., Kumai, M., Hamaguchi, A., Nishimura, M., Inoue, Y., Hayashi, H., et al. (2007). Differences in neurogenic potential in floor plate cells along an anteroposterior location: midbrain dopaminergic neurons originate from mesencephalic floor plate cells. Development *134*, 3213–3225.

Oshimori, N., and Fuchs, E. (2012). Paracrine TGF-β signaling counterbalances BMP-mediated repression in hair follicle stem cell activation. Cell Stem Cell *10*, 63–75.

Patten, I., Kulesa, P., Shen, M.M., Fraser, S., and Placzek, M. (2003). Distinct modes of floor plate induction in the chick embryo. Development *130*, 4809–4821.

Pearse, R. V, Vogan, K.J., and Tabin, C.J. (2001). Ptc1 and Ptc2 transcripts provide distinct readouts of Hedgehog signaling activity during chick embryogenesis. Dev. Biol. *239*, 15–29.

Perez-Balaguer, A., Puelles, E., Wurst, W., and Martinez, S. (2009). Shh dependent and independent maintenance of basal midbrain. Mech. Dev. *126*, 301–313.

Peyrot, S.M., Wallingford, J.B., and Harland, R.M. (2011). A revised model of Xenopus dorsal midline development: differential and separable requirements for Notch and Shh signaling. Dev. Biol. *352*, 254–266.

Placzek, M., and Briscoe, J. (2005). The floor plate: multiple cells, multiple signals. Nat. Rev. Neurosci. *6*, 230–240.

Portch, P.A., and Barson, A.J. (1974). Scanning electron microscopy of neurulation in the chick. J. Anat. *117*, 341–350.

Postigo, A.A. (2003). Opposing functions of ZEB proteins in the regulation of the TGFbeta/BMP signaling pathway. EMBO J. *22*, 2443–2452.

Rastegar, S., Albert, S., Le Roux, I., Fischer, N., Blader, P., Müller, F., and Strähle, U. (2002). A floor plate enhancer of the zebrafish netrin1 gene requires Cyclops (Nodal) signalling and the winged helix transcription factor FoxA2. Dev. Biol. *252*, 1–14.

Ribes, V., Balaskas, N., Sasai, N., Cruz, C., Dessaud, E., Cayuso, J., Tozer, S., Yang, L.L., Novitch, B., Marti, E., et al. (2010). Distinct Sonic Hedgehog signaling dynamics specify floor plate and ventral neuronal progenitors in the vertebrate neural tube. Genes Dev. *24*, 1186–1200.

Rodriguez, I., and Basler, K. (1997). Control of compartmental affinity boundaries by hedgehog. Nature *389*, 614–618.

Ruiz i Altaba, A., Prezioso, V.R., Darnell, J.E., and Jessell, T.M. (1993). Sequential expression of HNF-3β and HNF-3α by embryonic organizing centers: the dorsal lip/node, notochord and floor plate. Mech. Dev. *44*, 91–108.

Sakamoto, K., Nakamura, H., Takagi, M., Takeda, S., and Katsube, K. (1998). Ectopic expression of lunatic Fringe leads to downregulation of Serrate-1 in the developing chick neural tube; analysis using in ovo electroporation transfection technique. FEBS Lett. *426*, 337–341.

Sasaki, H., and Hogan, B. (1993). Differential expression of multiple fork head related genes during gastrulation and axial pattern formation in the mouse embryo. Development *118*, 47–59.

Sasaki, H., and Hogan, B.L.M. (1994). HNF-3β as a regulator of floor plate development. Cell *76*, 103–115.

Sasaki, H., Hui, C., Nakafuku, M., and Kondoh, H. (1997). A binding site for Gli proteins is essential for HNF-3beta floor plate enhancer activity in transgenics and can respond to Shh in vitro. Development *124*, 1313–1322.

Sauer, F.C. (1935). Mitosis in the neural tube. J. Comp. Neurol. *62*, 377–405.

Sauer, F.C. (1936). The interkinetic migration of embryonic epithelial nuclei. J. Morphol. *60*, 1–11.

Sauer, M.E., and Walker, B.E. (1959). Radioautographic Study of Interkinetic Nuclear Migration in the Neural Tube. Exp. Biol. Med. *101*, 557–560.

Sauka-Spengler, T., and Barembaum, M. (2008). Gain- and loss-of-function approaches in the chick embryo. Methods Cell Biol. *87*, 237–256.

Schauerte, H., van Eeden, F., Fricke, C., Odenthal, J., Strahle, U., and Haffter, P. (1998). Sonic hedgehog is not required for the induction of medial floor plate cells in the zebrafish. Development *125*, 2983–2993.

Schoenwolf, G.C. (1985). Shaping and bending of the avian neuroepithelium: Morphometric analyses. Dev. Biol. *109*, 127–139.

Schoenwolf, G., and Smith, J. (1990a). Mechanisms of neurulation: traditional viewpoint and recent advances. Development *109*, 243–270.

Schoenwolf, G.C., and Franks, M. V. (1984). Quantitative analyses of changes in cell shapes during bending of the avian neural plate. Dev. Biol. *105*, 257–272.

Schoenwolf, G.C., and Sheard, P. (1990). Fate mapping the avian epiblast with focal injections of a fluorescent-histochemical marker: ectodermal derivatives. J. Exp. Zool. *255*, 323–339.

Schoenwolf, G.C., and Smith, J.L. (1990b). Mechanisms of neurulation: traditional viewpoint and recent advances. Development *109*, 243–270.

Smart, H.I. (1972). Proliferative characteristis of the ependymal layer during the early development of the spinal cord in the mouse. J. Anat. *111*, 365–380.

Smidt, M.P., Asbreuk, C.H., Cox, J.J., Chen, H., Johnson, R.L., and Burbach, J.P. (2000). A second independent pathway for development of mesencephalic dopaminergic neurons requires Lmx1b. Nat. Neurosci. *3*, 337–341.

Smith, J. (1997). Neurulation: coming to closure. Trends Neurosci. *20*, 510–517.

Smith, J.L., and Schoenwolf, G.C. (1987). Cell cycle and neuroepithelial cell shape during bending of the chick neural plate. Anat. Rec. *218*, 196–206.

Smith, D.S., Niethammer, M., Ayala, R., Zhou, Y., Gambello, M.J., Wynshaw-Boris, A., and Tsai, L.H. (2000). Regulation of cytoplasmic dynein behaviour and microtubule organization by mammalian Lis1. Nat. Cell Biol. *2*, 767–775.

Spear, P.C., and Erickson, C.A. (2012). Apical movement during interkinetic nuclear migration is a two-step process. Dev. Biol. *370*, 33–41.

Strahle, U., Blader, P., Henrique, D., and Ingham, P.W. (1993). Axial, a zebrafish gene expressed along the developing body axis, shows altered expression in cyclops mutant embryos. Genes Dev. *7*, 1436–1446.

Strähle, U., Blader, P., and Ingham, P.W. (1996). Expression of axial and sonic hedgehog in wildtype and midline defective zebrafish embryos. Int. J. Dev. Biol. *40*, 929–940.

Strähle, U., Lam, C.S., Ertzer, R., and Rastegar, S. (2004). Vertebrate floor-plate specification: variations on common themes. Trends Genet. *20*, 155–162.

Streit, A., and Stern, C.D. (1999). Neural induction: a bird's eye view. Trends Genet. *15*, 20–24.

Streit, A., Stern, C., Thery, C., Ireland, G., Aparicio, S., Sharpe, M., and Gherardi, E. (1995). A role for HGF/SF in neural induction and its expression in Hensen's node during gastrulation. Development *121*, 813–824.

Tamai, H., Shinohara, H., Miyata, T., Saito, K., Nishizawa, Y., Nomura, T., and Osumi, N. (2007). Pax6 transcription factor is required for the interkinetic nuclear movement of neuroepithelial cells. Genes Cells *12*, 983–996.

Tanaka, J., Harada, H., Ito, K., Ogura, T., and Nakamura, H. (2010). Gene manipulation of chick embryos in vitro, early chick culture, and long survival in transplanted eggs. Dev. Growth Differ. *52*, 629–634.

Tsai, J.-W., Chen, Y., Kriegstein, A.R., and Vallee, R.B. (2005). LIS1 RNA interference blocks neural stem cell division, morphogenesis, and motility at multiple stages. J. Cell Biol. *170*, 935–945.

Tsai, J.-W., Lian, W.-N., Kemal, S., Kriegstein, A.R., and Vallee, R.B. (2010). Kinesin 3 and cytoplasmic dynein mediate interkinetic nuclear migration in neural stem cells. Nat. Neurosci. *13*, 1463–1471.

Uchikawa, M. (2008). Enhancer analysis by chicken embryo electroporation with aid of genome comparison. Dev. Growth Differ. *50*, 467–474.

Voiculescu, O., Papanayotou, C., and Stern, C.D. (2008). Spatially and temporally controlled electroporation of early chick embryos. Nat. Protoc. *3*, 419–426.

Vrijens, K., Lin, W., Cui, J., Farmer, D., Low, J., Pronier, E., Zeng, F.-Y., Shelat, A.A., Guy, K., Taylor, M.R., et al. (2013). Identification of small molecule activators of BMP signaling. PLoS One *8*, e59045.

Wallingford, J.B., Fraser, S.E., and Harland, R.M. (2002). Convergent Extension. Dev. Cell *2*, 695–706.

Weinstein, D.C., Ruiz i Altaba, A., Chen, W.S., Hoodless, P., Prezioso, V.R., Jessell, T.M., and Darnell, J.E. (1994). The winged-helix transcription factor HNF-3β is required for notochord development in the mouse embryo. Cell *78*, 575–588.

Wijgerde, M., McMahon, J.A., Rule, M., and McMahon, A.P. (2002). A direct requirement for Hedgehog signaling for normal specification of all ventral progenitor domains in the presumptive mammalian spinal cord. Genes Dev. *16*, 2849–2864.

Yan, C.H., Levesque, M., Claxton, S., Johnson, R.L., and Ang, S.-L. (2011). Lmx1a and lmx1b function cooperatively to regulate proliferation, specification, and differentiation of midbrain dopaminergic progenitors. J. Neurosci. *31*, 12413–12425.

Ybot-Gonzalez, P., Cogram, P., Gerrelli, D., and Copp, A.J. (2002). Sonic hedgehog and the molecular regulation of mouse neural tube closure. Development *129*, 2507–2517.

Ye, W., Shimamura, K., Rubenstein, J.L.., Hynes, M.A., and Rosenthal, A. (1998). FGF and Shh Signals Control Dopaminergic and Serotonergic Cell Fate in the Anterior Neural Plate. Cell *93*, 755–766.

Yuan, S., and Schoenwolf, G.C. (1999). The spatial and temporal pattern of C-Lmx1 expression in the neuroectoderm during chick neurulation. Mech. Dev. *88*, 243–247.

Zervas, M., Blaess, S., and Joyner, A.L. (2005). Classical embryological studies and modern genetic analysis of midbrain and cerebellum development. Curr. Top. Dev. Biol. *69*, 101–138.